



HAL
open science

Biological dose estimation in hadrontherapy using the GATE Monte Carlo simulation platform

Yasmine Ali

► **To cite this version:**

Yasmine Ali. Biological dose estimation in hadrontherapy using the GATE Monte Carlo simulation platform. Physics [physics]. Université de Lyon, 2021. English. NNT : 2021LYSE1329 . tel-03783569

HAL Id: tel-03783569

<https://theses.hal.science/tel-03783569>

Submitted on 22 Sep 2022

HAL is a multi-disciplinary open access archive for the deposit and dissemination of scientific research documents, whether they are published or not. The documents may come from teaching and research institutions in France or abroad, or from public or private research centers.

L'archive ouverte pluridisciplinaire **HAL**, est destinée au dépôt et à la diffusion de documents scientifiques de niveau recherche, publiés ou non, émanant des établissements d'enseignement et de recherche français ou étrangers, des laboratoires publics ou privés.



N°d'ordre NNT :
2021LYSE1329

THESE de DOCTORAT DE L'UNIVERSITE DE LYON

opérée au sein de
l'Université Claude Bernard Lyon 1

Ecole Doctorale ED52
Physique & Astrophysique de Lyon

Spécialité de doctorat : Physique médicale
Discipline : Physique

Soutenue publiquement le 14/12/2021, par :
Yasmine ALI

Biological dose estimation in hadrontherapy using the GATE Monte Carlo simulation platform

Devant le jury composé de :

Nom, prénom	grade/qualité	établissement/entreprise	Président(e)
GEORG Dietmar,	Professeurs des universités,	Medical University of Vienna	Rapporteur
BALDACCHINO Gérard,	Chercheur, Ingénieur	CEA, CEA Paris Saclay	Rapporteur
THARIAT Juliette,	Professeur des Universités,	IN2P3/ENSICAEN/CNRS	Examinatrice
CHIAVASSA Sophie,	Physicienne,	ICO Nantes René Gauducheau	Examinatrice
ABDOUL-CARIME Hassan,	Maitre de Conférences,	IP2I	Examineur
LETANG Jean-Michel,	Maitre de Conférences,	Université de Lyon	Examineur
BEUVE Michaël,	Professeur des Universités,	Université Claude Bernard Lyon 1	Directeur de thèse
MAIGNE Lydia,	Maitre de Conférences,	Université Clermont Auvergne	Co-directrice de thèse
ETIENNE Testa,	Maitre de Conférences,	Université Claude Bernard Lyon 1	Invité

Résumé

Un des challenges en hadronthérapie est l'estimation de la dose biologique. Les systèmes de planification de traitement (TPS) doivent optimiser les faisceaux de traitement en prenant en compte la prédiction de la dose biologique en plus de la prédiction de la dose physique. Pour estimer la dose biologique, des modèles biophysiques ont été développés tels que les modèles mMKM et NanOx. Les paramètres d'entrée de ces modèles peuvent être estimés grâce à des codes de calculs Monte Carlo en structure de trace. Nous utilisons les codes Geant4-DNA et LPCHEM et les comparons pour évaluer leurs différences. Les deux codes peuvent simuler les radiations ionisantes jusqu'à l'eV ainsi que la production d'espèces radiolytiques suite à la radiolyse de l'eau entre la picoseconde et la microseconde. Les modèles biophysiques permettent des calculs de dose complexes à l'échelle du voxel en les couplant à des codes de calcul Monte Carlo. Nous avons développé un outil pour la plateforme de calcul Monte Carlo GATE, le "biodose actor", dans le but d'estimer la dose biologique pour des pics de Bragg étalés issus de lignes cliniques et précliniques, irradiant avec les faisceaux de protons, d'ions hélium et d'ions carbone. Nous avons comparé les codes Geant4-DNA et LPCHEM pour la simulation de spectres nanodosimétriques dans le cœur de trace d'ion et la production d'espèce radiolytiques dans l'eau par des particules chargées (10 MeV protons). Les spectres totaux d'énergie spécifique dans des cibles nanométriques ainsi que les rendements d'espèces radiolytiques pour les deux codes sont en bon accord. En plus de l'implémentation du BioDose actor dans GATE, l'outil a été testé et validé avec des données expérimentales de survie cellulaire obtenues grâce à différents pics de Bragg étalés. Cet outil facilitera les comparaisons et évaluation des différents modèles biophysiques.

Abstract

One of the current challenges in hadrontherapy is the evaluation of the biological effects due to microscopic pattern of energy deposition of ions. Treatment Planning Systems (TPS) should optimize beam parameters taking into account their predictions through the calculation of the biological dose in addition to the physical dose. To estimate the biological dose, biophysics models have been developed such as the mMKM and NanOx models. Some input parameters of the models are generally estimated with Monte Carlo Track Structure Codes such as Geant4-DNA and LPCHEM codes. Both codes are able to perform the simulation of ion and electron transport in water down to some eV as well as the evaluation of the chemical species generated during water radiolysis between 10^{-12} and 10^{-6} s. In this work, we first compared the outcome of LPCHEM and Geant4-DNA in terms of specific energy in nano and micro targets as well as yields of chemical species (input of the biophysical models). Then, we enhanced the GATE Monte Carlo simulation platform by creating a “Biodose actor” in order to estimate the biological dose for different clinical Spread-out Bragg Peaks (SOBP) with hydrogen, helium and carbon ion beams. We performed the first comparison between the LPCHEM and Geant4-DNA codes for the simulation of nanodosimetry spectra in the track core and the production of chemical species yields for water irradiations with charged particles (10 MeV protons). The total specific energy spectra in nanometric targets and the chemical yields predicted by the two codes are in good agreement. Besides the implementation of the BioDose actor in GATE has been tested and validated with comparison against experimental cell survival obtained in several SOBP. This tool paves the way of facilitated benchmarking between different models and evaluation approaches.

Table des matières

Chapter 1	12
Biological dose prediction in hadrontherapy	12
1.1. Introduction	12
1.2. Cancer treatments using hadrons	12
1.2.1. Principles of hadrontherapy	13
1.2.2. Irradiations techniques	14
1.2.3. Why considering biological dose?	16
1.3. Biophysical models.....	20
1.3.1. The Local Effect Model (LEM)	21
1.3.2. The modified microdosimetric model (mMKM)	23
1.3.3. The NanOx model	26
1.4. Biological dose evaluation through Monte Carlo treatment planning systems	29
1.4.1. Monte carlo codes used in biophysical models	29
1.4.2. FLUKA	31
1.4.3. TOPAS.....	35
1.5. Conclusion.....	38
Chapter 2	39
Monte Carlo simulations of nanodosimetry and radiolytic species production for monoenergetic proton and electron beams. Benchmarking of GEANT4-DNA and LPCHEM codes.	39
2.1. Introduction	39
2.2. Material and methods	42
2.2.1. Simulation of nanodosimetry spectra	42
2.2.2. Radiolytic species production.....	44

2.2.3. Computing time	45
2.3. Results	46
2.3.1. Nanodosimetry spectra	46
2.3.2. Radiolytic species yields.....	50
2.3.3. Radical yields comparison against experimental data for 1 MeV electrons	50
2.3.4. Radical yields simulation for 10 MeV protons	51
2.3.5. Computing time	53
2.4. Discussion.....	54
2.4.1. Nanodosimetry spectra (physical stage)	55
2.4.2. Radiolytic yields at 10^{-12} s (physico-chemical stage)	55
2.4.3. Evolution of the radiolytic yields up to 10^{-6} s (chemical stage)	57
2.4.4. Computing time	58
2.5. Conclusion.....	58
Chapter 3	60
Cell survival predictions using mMKM and NanOx models.....	60
3.1. Introduction	60
3.2. Materials and Methods	61
3.2.1. NanOx parameters for HSG cell line.....	62
3.2.2. mMKM parameters for HSG cell line	62
3.3.3. Figure of merit	67
3.3. Results	67
3.4. Discussion.....	69
3.4.1. Validation of the mMKM input parameters for HSG cell line.....	69
3.4.2. Comparison of α values estimated with NanOx and mMKM using LPCHEM and Geant4-DNA.....	70

3.4.3. Comparison of α values with the literature	71
3.5. Conclusion	72
Chapter 4	73
Estimate of the biological dose in hadrontherapy with GATE: development and validation of the BioDose actor	73
4.1. Introduction	73
4.2. Material and methods	73
4.2.1. Implementation of the BioDose actor	74
4.2.2. Validation tests	77
4.2.3. Estimate of cell survival fractions, biological doses and RBE for carbon and helium beam lines using GATE.....	81
4.3. Results	87
4.3.1. Cell survival fractions, biological doses and RBE of carbon and helium beam lines in HIMAC AND HIMBC.....	87
4.3.2. ARRONAX preclinical line.....	90
4.4. Discussion.....	92
4.4.1. Validation tests	92
4.4.2. Estimate of cell survival fractions, biological doses and RBE for carbon and helium beam lines.....	93
4.5. Conclusion.....	94
General conclusion.....	95
Curriculum vitae of this thesis	98
References	Erreur ! Signet non défini.
Appendix	109

General Introduction

Hadrontherapy is a technique that uses high-energy ions in order to irradiate tumors. The biological and ballistic properties of ions involve a better selectivity by delivering high radiation dose concentrations in the tumor volume while the organs at risk receive as low dose concentration as possible. Regarding these advantages, it is mandatory for the treatment planning systems to determine optimized irradiation solutions that takes into account the biological consequences of the ions. The RBE (relative biological effectiveness) has been defined as a quantity to characterize the effectiveness of the ions compared to photons and lead to the estimation of the biological dose for treatment planning.

The estimation of the RBE has been challenging. As few experimental data was available, little was known on the effect of the ions on the irradiated cells, which led to oversimplifications and practical solutions to start the treatment in the nineties. In 1994, started the first carbon ion trials at the NIRS (National Institute of Radiological Sciences). At that moment, RBE was estimated by taking into account its LET dependency, leaving the other parameters as open questions. It is in 2000 that the use of biophysical models for the estimation of the RBE in clinical settings emerges at the GSI (German Heavy Ion Research Center, Germany) with the implementation of the LEM (Local Effect model) in the Trip98 TPS, a model proposed by Scholtz and Kraft ¹. Then followed with the development of the mMKM (Modified Microkinetic model) in 2006 by the researchers at the NIRS ² and its implementation in the HIPLAN TPS later in 2015 ³. Both models led to estimating the survival fraction using the specific energy distribution at a micrometric scale. However, due to different mathematical formalisms, approximations within the models and even different irradiation techniques between the NIRS and GSI, disparities in the predictions of the RBE were observed. It gives room to the development of new biophysical models, proposing new approaches and frameworks, such as the NanOx model that has been developed starting 2009 by the researchers of the IP2I Laboratory in Lyon ⁴. In the NanOx model, the survival fraction does not only rely on the specific energy deposition but on the oxidative stress caused by the radical species generated by the irradiation as well. However, even though more experiments have been performed with the development of biophysics models, the few collected data to this day and their large uncertainties make it difficult to classify models in term of accuracy.

RBE estimation is not the only concern in a TPS but the accuracy of the estimation of the physical dose has also been raised. Indeed, TPS uses analytical algorithms, which gives fast computing advantages. However, heterogeneities are known to lead to uncertainties in the dose prediction with such analytical algorithms. In hadrontherapy, due to the ion beam characteristics, these uncertainties can lead to even more biological consequences. Therefore, the gold standard Monte Carlo codes are considered interesting supports for hadrontherapy clinical activity. Monte Carlo toolkits for medical applications have been developed along with user friendly interfaces to offer an accessible framework to the medical professionals. Consequently, methodologies for the coupling of biophysical models to Monte Carlo codes have been explored, with the challenge of optimizing their computing time. In this PhD work, our interest has focused on the open-source GATE Monte Carlo platform (www.opengatecollaboration.org), based on the Geant4 toolkit (geant4.cern.ch) and dedicated to medical physics, from PET, SPECT and CT imaging to radiation therapy applications. GATE benefits from a large and active community of users but also developers, which makes the platform constantly evolving to propose advanced functionalities. For now, no tool has been developed in the platform to estimate the biological dose. Therefore, the goal of this PhD work is the implementation of a BioDoseActor, that will calculate the RBE and the biological dose using validated biophysical models. We decided to couple the NanOx model, developed at IP2I, and the mMKM model as it's already been used in clinics.

The objectives to tackle in this PhD were :

1. to benchmark the Monte Carlo Track Structure (MCTS) codes LPCHEM and Geant4-DNA for the simulation of the physico, physico-chemical and chemical stages for the production of the specific energy distributions and radiolytic species in nanometric targets. Those quantities are used as input parameters in the mMKM and the NanOx models.
2. to produce databases of cell survival fraction coefficients using the mMKM and NanOx models for the HSG cell line irradiated with hydrogen, helium, carbon and oxygen ions. These databases will be used as input to the BioDoseActor in the GATE platform.
3. to develop and implement the BioDoseActor in the GATE platform.
4. to validate the BioDoseActor for the prediction of the survival fraction, the RBE and the biological dose for helium and carbon ions for pre-clinical and clinical beams.

This thesis is composed of four chapters. The first chapter describes the features of hadrontherapy along with the motivations for the estimation of the biological dose in treatment planning. Then, the mathematical formalisms of three biophysical models, the LEM, the mMKM and the NanOx models are described. Finally, a review of Monte Carlo frameworks predicting the biological dose through the implementation of biophysical models is proposed.

Then, in the second chapter, are benchmarked two MCTS: LPCHEM and Geant4-DNA. These codes are used to calculate specific energies in nanometric and micrometric targets as well as the physicochemical and chemical reactions resulting from the water radiolysis caused by proton and electron irradiations; these quantities are then used in the mathematical formalism of the biophysical models to predict the biological dose. We argued about their differences concerning physical processes that led to specific energy spectra in nanometric targets, as well as differences in simulating physico-chemical and chemical stages that led to radiolytic species production. Finally, we explained the consequences of variations in specific energy at nanometric scale on radiolytic species diffusion.

The third chapter explains the choice and optimization of the input parameters for the mMKM and the NanOx models for the estimation of cell survival fraction coefficients for the HSG cell line. We then compare the saturation corrected dose mean specific energies and the dose at 10% of survival, calculated with LPCHEM and Geant4-DNA Monte Carlo codes, before estimating the α coefficient in function of the LET for the mMKM and the NanOx models. We included also comparisons with the PIDE database along with mMKM predictions performed by other authors in the literature.

The fourth chapter details the methodology of the implementation of the BioDoseActor in GATE, along with its models and approximations. The technical validation of the BioDoseActor is performed and recommendations to the users are given. For the validation of this tool, the modeling of the pre-clinical ARRONAX beam line (67.8 MeV/n helium ions), in Nantes, and the clinical HIMAC/HYOGO beam lines (320 MeV/n carbon ions), in Chiba in Japan, is detailed. Finally, the biological dose, the survival fraction and the RBE are calculated and compared.

Chapter 1

Biological dose prediction in hadrontherapy

1.1. Introduction

Hadrontherapy using protons or carbon ions are considered very adapted to the treatment of radioresistant tumors. The greater radiobiological efficacy of light ion beam therapy compared to photons has been shown in numerous clinical trials. This feature is especially due to the high LET of the particles compared to photons. Computer based predictive tools are being implemented to tackle the biological dose delivered to tumoral tissues and organ at risks during treatments. In this chapter, after explaining the typology of cancer treatments using hadrons, we present biophysical models developed in the objective of predicting the survival of cells in clinical conditions; some of them, like LEM I and mMKM are already implemented in clinical treatment planning systems. From a decade, they have been implemented also in Monte Carlo frameworks to offer the most accurate predictive dosimetry.

1.2. Cancer treatments using hadrons

The goal of radiation therapy is not only to kill the tumoral cells but to stop their proliferation. In radiotherapy, to measure the ability of cells to proliferate after irradiation, the quantity that is estimated is the cell survival.

Many models have been developed in order to describe the cell survival, but the most used is the LQ model (Linear quadratic model). It has been established by Chadwick and Leenhouts in 1981⁵ and relies on the following hypothesis:

- The integrity of the nuclear DNA molecules is essential for the normal propagation of the cell;
- The DNA double strand break is the most critical radiation-induced lesion and cause lethal lesions to the cell;
- The radiation can cause sub-lethal lesions that can be repaired and the effects of the radiation can vary depending on that.

The curves of cell survival rates as a function of absorbed dose can be fitted using:

$$S(D) = e^{-\alpha D + \beta D^2} \quad (1)$$

Several interpretations have been suggested to link the model to radiobiological phenomena. One proposed by Kellerer and Rossi ⁶, commonly adopted by the scientific community, is the following:

- the α parameter expresses the lethal damages that can't be repaired;
- the β parameter expresses the sub-lethal damages that could either be repaired or multiple-hit cell death resulting from the interaction of damage from different radiation tracks.

Though, many different mechanisms can lead to the death of the cells, mechanisms that are molecular and can also happen at different times of the cell cycle. These mechanisms will also vary depending on the type of the cells and their inactivation also depend on the type of cells as well.

1.2.1. Principles of hadrontherapy

Radiotherapy is one of the most important techniques used for cancer treatment. The aim of radiotherapy is to shrink tumors with the use of ionizing radiations. High radiation dose concentrations are reached in the tumor volume while the healthy tissues and organs at risk receive as low dose concentration as possible. Along the years, a strong improvement of the treatment delivery could be managed thanks to the evolution of imagery modalities, delivery systems and even software in order to maximize the dose to the tumors and spare of the organs. ⁷ One of the results of this technical improvement is the IMRT (Intensity modulated radiation therapy) technique. Though, despite the improvement of selectivity provided by the IMRT technique, more limitations remain such as the resistance of tumoral cells. Indeed, targeted tumoral cells might not respond to the radiations as expected. Many different mechanisms can lead to the death of the cells, mechanisms that are molecular and happen at different times of the cell cycle. These mechanisms and their timings will also vary depending on the type of the cells. For example, for cells that proliferate rapidly such as lymphomas cells, cell death may occur within hours post irradiation and appear particularly responsive to irradiation. However, it is not the case for solid tumor.

Therefore, another possibility to treat cancers while overcoming the selectivity and tumor resistance limits of radiotherapy is hadrontherapy.

Hadrontherapy is a radiation therapy modality that uses ions. The modality has been shown to reduce the dose delivered to surrounding normal tissues. With their physical characteristics, ions can penetrate through the tissues with a low-dose plateau region followed by a dose increase near the end of the ion range (Bragg peak). Therefore, maximum of the dose is deposited within the Bragg peak and energy deposited through the patient's body within the organ at risk before the tumor localization, is lower compared to photons⁸. The ions also have a well-defined fall off which is the region of the Bragg peak where the dose decreases drastically, from 80% to 20%, which also preserves the organs after the tumor localization by having a low exit dose compared to radiotherapy. The local control of the tumor is better.

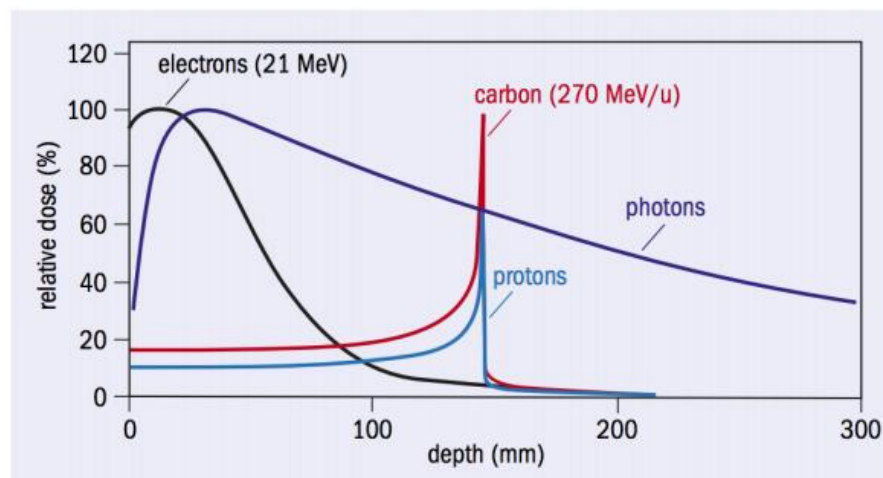


Figure 1 - Comparison between the relative dose deposition in depth for electron beam (black), carbon ion beam (red), photon beam (dark blue) and proton beam (light blue).

1.2.2. Irradiations techniques

In order to guarantee a homogeneous dose distribution, the ion beams have to be adapted regarding their energy and shape. Two irradiation techniques have been developed and used in hadrontherapy : the passive irradiation and the active irradiation (or scanning irradiation). Passive irradiation has been performed since 1994 for the first clinical trials using carbon ions for HIMAC (Heavy-Ion Medical Accelerator in Chiba) at the NIRS (National Institute of Radiological Sciences) in Japan. Meanwhile scanning irradiation has been initiated in 2000 at the GSI (German Heavy Ion Research Center, Germany) in Germany¹.

With passive irradiation, the beam is first spread in order to properly cover the tumor. A modulator is then used on several mono-energetic single Bragg peaks in order to super-impose them into a SOBP (spread-out Bragg Peak).

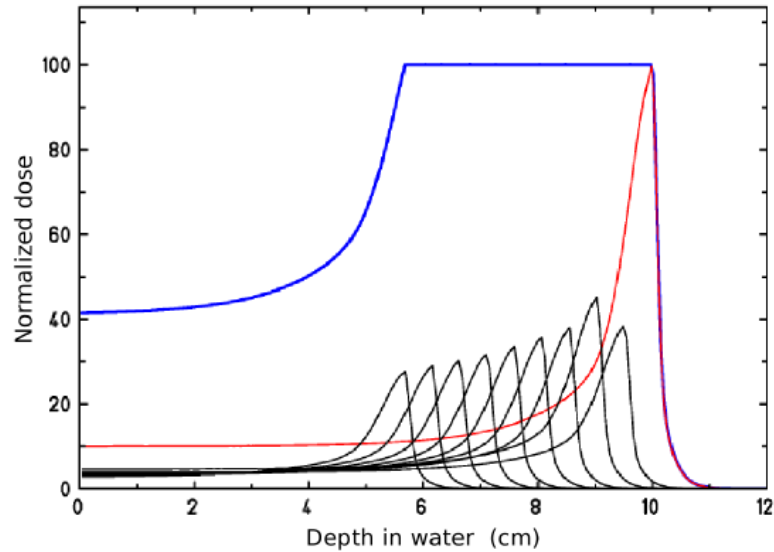


Figure 2 – Example SOBP with the superposition of several Bragg peaks of different energies.

With a SOBP, shows in Figure 2, we obtain a plateau of homogenous dose corresponding to the maximum of the thickness of the target volume. In order to spare the healthy tissues and organs at risk, the beam is collimated. Finally, in order to conform to the shape of the target volume, the beam goes through a compensator, as shown in Figure 3.

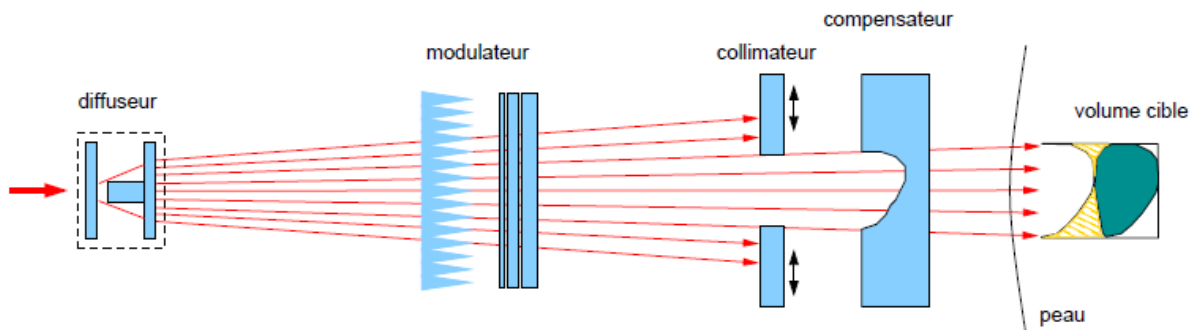


Figure 3 – Representation of the passive irradiation technique.

Nowadays, most hadrontherapy centers implemented the pencil beam technique. For this technique, spot scanning beams have the ability to modulate energy as well as intensity without the use of collimators and compensators.

The beam is directly used to irradiate the target volume that is segmented in iso energetic slices. The energy is set thanks to a degrader in order to cover each slice successively. The beam is then guided thanks to magnets, as shown in Figure 4.

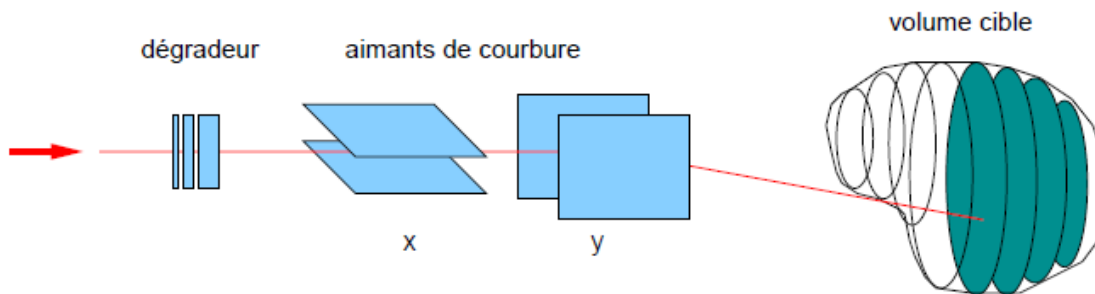


Figure 4 - Representation of the active irradiation technique

In dosimetry, the active technique has been acknowledged as more interesting than the passive technique. Indeed, with a passive technique, the healthy tissues located before the target volume receive too much dose, meanwhile with the active technique, as the energy is adapted to each slice, notably for the most distal ones, the dose imparted to healthy tissues located in the beam path are spared more efficiently.

1.2.3. Why considering biological dose?

The spatial and energy distributions of the ions are different than the photons which leads to differences in the survival rates. X-rays produce a low density of ionization meanwhile the ion beams are proven to be biologically more effective if the same absorbed dose is applied, due to the charged particles characterized by a high local ionization density. Therefore, the survival probability of the cells irradiated by ions for the same dose is lower than the one observed with X rays. Even between ions we observe differences in energy distributions. Indeed, the heavier an ion is, the higher its local ionization density is, as shown in Figure 5 with the comparison between a proton (left) and a carbon ion track segment (right) with same length ($1\mu\text{m}$) and same energy (1 MeV/u).

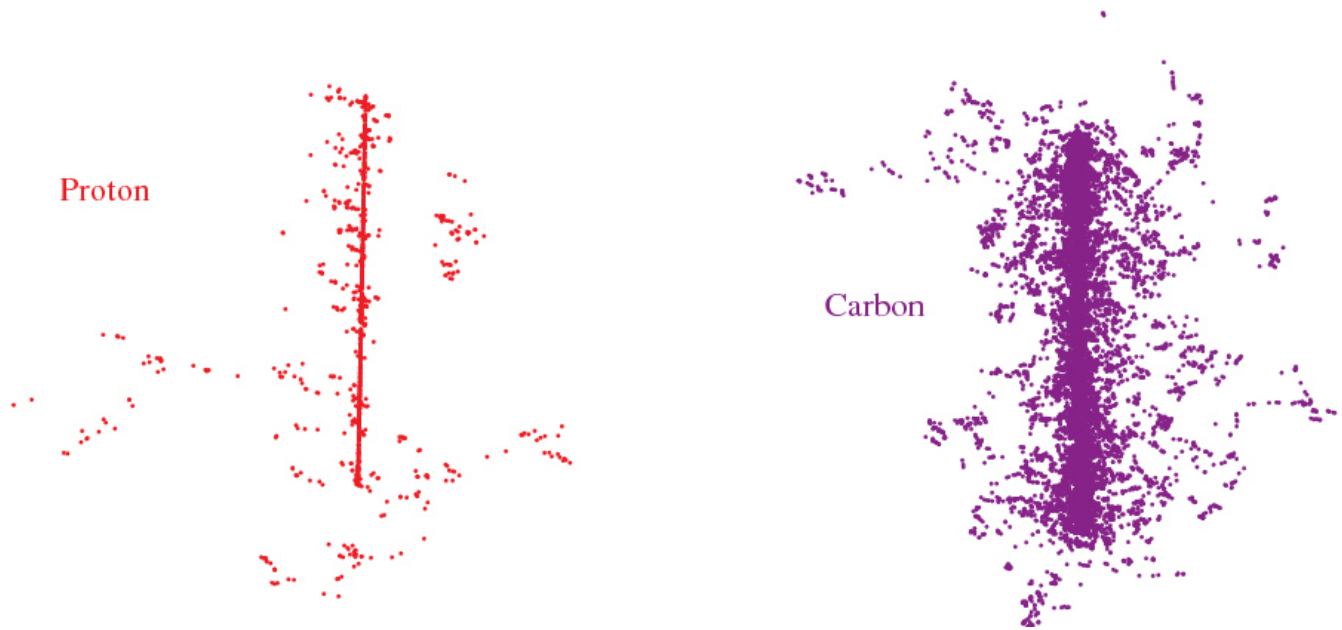


Figure 5 - Proton (left) and carbon (right) ion track segments of 1 μm length for 1 MeV/u particles.

Experimental measurements of survival rates were done with both X-rays and various ion beams, like in the work of Kagawa et al. ⁹. In this work, the surviving rates for HSG (Human submandibular gland) cells irradiated with 4 MV X-ray (X4), 190 MeV/u protons ions for a dose of 3.3 Gy and 320 MeV/u carbon ion for a dose of 2.4 Gy at the isocenter are shown in Figure 6. Different LET values lead to different types of damage and therefore to a different capacity of the cell to repair. For high LET ions, strand breaks are more concentrated in space and the associated damage is less likely to be repaired which leads to survival rates that decreases significantly. This is observed as the X rays display higher surviving rate values than both protons and carbon ions. We then observe that carbon ions, being heavier, display lower surviving rates than protons as well as higher RBE values.

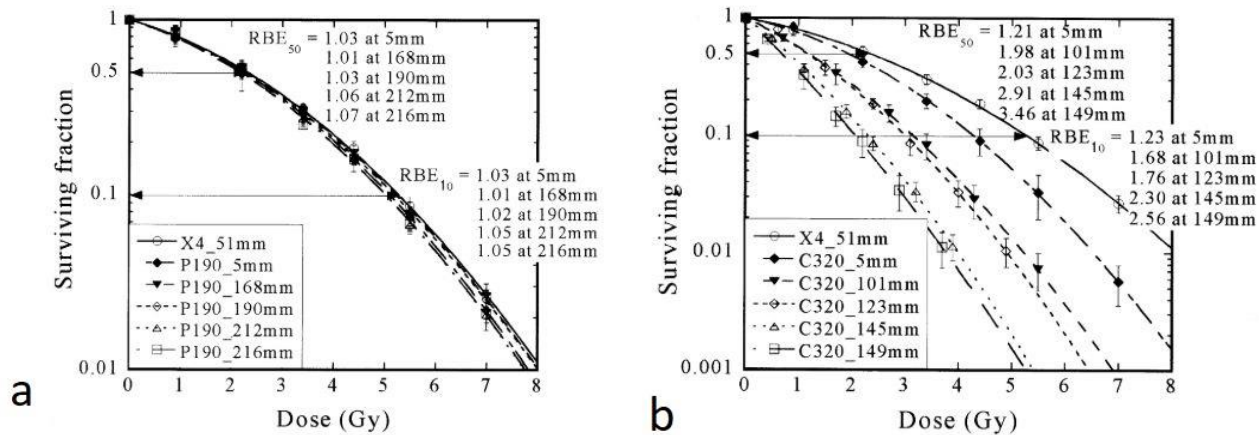


Figure 6 - Cell survival curves of X4 and 190 MeV/u protons for a 6cm SOBP (a). Cell survival curves of X4 and 190 MeV/u protons for a 6cm SOBP (a).

The survival probability depends also on the cell type. In the work of Weyrather et al.¹⁰ is compared the survival curves for different cell lines (CHO-K1 (Chinese hamster Ovary) and V79 (Chinese hamster lung fibroblast)) irradiated with carbon ions of different energies (4.2 MeV/u, 11.0 MeV/u, 18.0 MeV/u, 76.9 MeV/u, 266.4 MeV/u).

As for high LET ions, damage is less likely to be repaired which leads to lower survival rates. This is observed in Figure 7 for ions with highest LET and an energy of 4.2 MeV/u displaying lowest surviving rates values for both CHO-K1 (Chinese hamster Ovary) and V79 (Chinese hamster lung fibroblast) cell lines. The opposite conclusion is made for ions of the lowest LET for an energy of 266.4 MeV/u, displaying the highest surviving rates values.

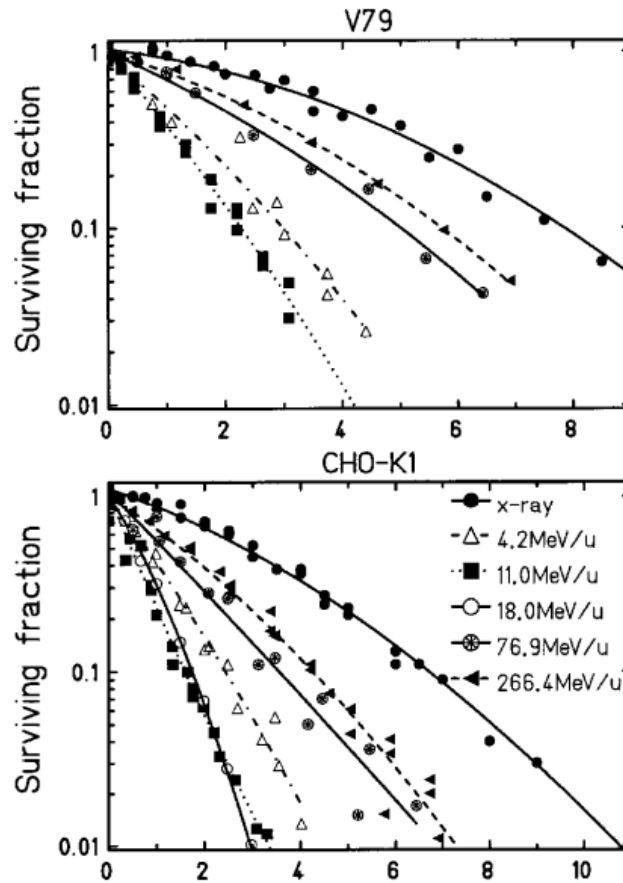


Figure 7 - Measured survival curves for CHO-K1 (Chinese hamster Ovary) and V79 (Chinese hamster lung fibroblast) cell lines for 250 keV X rays and carbon mono-energetic beams ¹⁰

In order to account for differences in energy deposition patterns in hadrontherapy, quantities such as the RBE (relative biological effectiveness) and biological dose have been introduced to establish a relation between reference radiation (photons) and ion beam irradiation.

According to the ICRU 40 report, the definition of the RBE (equation 2) is the ratio of a reference dose administered by X-rays D_{Ref} and a given dose D leading to the same biological effect under identical conditions. Because the RBE depends on the photon reference radiation, the reference has to be stated when reporting RBE values.

$$RBE = \frac{D_{Ref}}{D} \quad (2)$$

The RBE is not a constant term but a complex quantity that depends on many factors regarding the radiation and cell types. It is then postulated that:

- The RBE-LET relation differs with the ion type. ¹¹
- The RBE differs with the cell type. ¹²

Not only the RBE can quantify damage of ions compared to photons, it is also used to calculate the biological dose D_{Bio} (equation 3), with D the absorbed dose.

$$D_{Bio} = D \times RBE \quad (3)$$

Biological doses in hadrontherapy are prescribed as Gy (RBE) to reflect that the absorbed dose D is multiplied by a RBE value.

1.3. Biophysical models

Biophysical models have been developed through different approaches explored along the years in order to estimate the biological impact of radiation, in treatment facilities such as the NIRS in Japan ¹³ and the GSI in Germany ¹. For both institutions, clinical trials have started in the late 1990s and have led to the development and use of biophysical models such as the LEM (Local effect model) I ¹ and the mMKM (modified microkinetic model) ². Clinical trials at the GSI center in Germany started in 2000 ¹. The irradiation technique was based on an active energy variation of the beam to shape the tumor: the pencil beam scanning technique. With several beam positions, several intensities and 3D intensity modulation, new ways to estimate the RBE had to be proposed. Scholtz and Kraft ¹⁴ proposed the LEM I model to predict the RBE. LEM I was incorporated into the treatment planning system for ion therapy TRiP and uses the radial dose calculated by Kiefer–Chatterjee amorphous track structure model ¹. Nowadays, the LEM I is still used in European TPS.

In 2011, the NIRS acquired an active beam scanning system and chose to use the MKM model presented by Hawkins in 1993 ¹⁵ to estimate the cell survival fraction after the exposure to heavy ion beams relying on the estimation of micrometric quantities. The model was modified by Kase et al. in 2006 ² by adding

the saturation correction to take into account the overkill effect of the ions and was then implemented by Inaniwa et al. in 2010¹⁶ in the HIMAC TPS.

Even though these models have been implemented and used in TPS, it does not mean there is no room for improvement. Indeed, the clinical applications of the models also came with limitations and had to rely on approximations and hypotheses that were conditioned by the complexity of the radiobiological damage. As the status of the knowledge in hadrontherapy and radiobiology is evolving along the years, new models are still currently being developed. LEM I evolved through LEM II¹⁴, LEM III¹⁷ and LEM IV¹⁸ since the implementation of its first version in 2000. New models are developed with the purpose of covering the shortcomings of the already existing ones such as the mMKM² and the NanOx model^{4,19}.

1.3.1. The Local Effect Model (LEM)

The local effect model was developed by Kraft and Scholz from the GSI in Germany in its first version, LEM I²⁰ and has been updated into the LEM II, III and IV. In this work, we will describe the main principles and the formalism in a simplified manner. The aim of the LEM in its original version was to predict the effect of the ions using the knowledge of the corresponding biological effect for X rays. It was based on the fact that damage to cells were the same whatever incoming radiation type, the DNA strand breaks resulted from the secondary electrons actions released in the medium. Therefore, the basic principle of the model is that the local biological effect is determined by the energy deposition in micrometric cellular sub-volume and is independent of the radiation type. However, the acknowledged difference between photons and ions was their spatial distribution in these micrometric sub-volumes. Meanwhile the energy deposition from X rays is constant in the sub-volumes, the energy deposition from the ions depends on their traversal positions.

$$D(r) = \begin{cases} \lambda \text{LET}_{\infty} \frac{1}{r_{min}^2} & r < r_{min} \quad (4) \\ \lambda \text{LET}_{\infty} \frac{1}{r^2} & r_{min} \leq r \leq r_{max} \quad (5) \\ 0 & r > r_{max} \quad (6) \end{cases}$$

Where λ is a normalization constant, which ensures that the total deposition equals the LET.

$$\lambda = \frac{1}{r\pi(1 + \ln\left(\frac{r_{max}^2}{r_{min}^2}\right))} \quad (7)$$

In the LEM, each ion traversing the sub volumes cause ionizations in the volume that are described by an average local dose deposition $d(r)$ depending on r the radial distance from the track axis. r_{min} is the core region of the track where the dose is constant. In the LEM I version of the model, r is defined with a fixed value of 10 nm in order to take into account the diffusion of free radicals. Though in the LEM III, this value has been re-defined as a velocity-dependent radius. Indeed, the core radius isn't constant on 10 nm but its extension increases with the velocity of the primary particle.

$$r_{min} = \beta \cdot r_c \quad (8)$$

with $\beta = v/c$, and r_c is the largest extension of the track core in the limit $v = c$.

Meanwhile, r_{max} is the maximum radial distance travelled by the δ -electrons with the highest energy. It depends on the ion energy E expressed in MeV/u.

$$r_{max} = \gamma \cdot E^\delta \quad (9)$$

where γ and δ are coefficients.

$$\gamma = 0.062 \frac{\mu m}{\left(\frac{MeV}{u}\right)^\delta} \quad \delta = 1.7 \quad (10)$$

After calculating both r_{min} and r_{max} , it is possible to calculate the dose deposition D and therefore the surviving probability for ions irradiation. The surviving fraction S_{ion} is defined as:

$$S_{ion} = e^{-N_{ion}(D)} \quad (11)$$

With N_{ion} the average number of lethal events induced per cell by ion irradiation.

$$N_{ion} = \int v(d(x, y, z)) dV_{Nucleus} = \int \frac{-\ln(S_x(d(x, y, z)))}{V_{Nucleus}} dV_{Nucleus} \quad (12)$$

N_{ion} can be calculated by integration of the local density $v(d(x, y, z))$ for the production of lethal events that is assumed to be the same for ions and for photons. The estimation of this surviving

probability depends on the known surviving probability to photons irradiation for the same cell line $S_X(D)$.

$$S_X(D) = e^{-N_X(D)} \quad (13)$$

When the model has been upgraded to the LEM IV ²¹, a different approach has been used. The probability of cell survival after ion irradiation has been re-focused on the DNA damage distribution induced by the radiation. In accordance to other existing models, the microdosimetric spatial distribution of the DNA damage (such as the DSB) has become the main element to measure the probability of cell survival.

In each sub volume of the cell nucleus, the mean number of DSB is determined. If only one DSB is found in the sub volume, it is called an isolated DSB (iDSB), if two or more DSB are found in the sub volume, it is called a clustered DSB (cDSB). A mean complexity C of the induced damage is derived from equation 14:

$$C = \frac{N_{cDSB}^{Ion}}{N_{cDSB}^{Ion} + N_{iDSB}^{Ion}} \quad (14)$$

With N_{iDSB}^{Ion} the number of sub-volumes and N_{cDSB}^{Ion} the number of subvolumes with clustered DSB resulting from a single particle traversal. In the line of the previous LEM versions, the ion-induced damage is then related to the photon-induced damage by considering the photon dose that would lead to the same level of complexity of DSB.

After this change of approach, there has been a comparison between the four versions of the LEM for RBE-weighted dose predictions along different carbon SOBPs. Indeed, even though the LEM IV has been given a better description of in-vitro data compared to other versions, it had yet to be compared in detail with clinical results of the LEM I that was already used in clinical settings.

The difference in RBE-weighted dose predictions between LEM I and LEM IV for typical tumor has been determined to be less than 10%. Therefore, the transition to LEM IV in treatment facilities wasn't expected to lead to significant differences as compared to the LEM I. ²²

1.3.2. The modified microdosimetric model (mMKM)

The MKM and mMKM models have been developed respectively by Hawkins et al. (original version) ^{23, 24} and by Kase et al. and Inaniwa et al. from NIRS (modified version) ^{2, 25, 16}. As the models have

already been described in details by these authors, we will describe the main principles and the formalism in a simplified manner. We only briefly describe the MKM in order to set the origins of the model to then focus on the mMKM.

The MKM model was inspired by the TDRA model ⁶. The TDRA model determines the lethal events by dividing the nucleus into sub microscopic structures called “sites”. The site concept is taken up by Hawkins et al. to be applied to ion beams. In the MKM model, the sites are called “domains” and are all considered of the same mass m and diameter d . If the population of cells is irradiated with a microscopic dose D , the dose absorbed by each domain will depend on the statistical distribution of energy imparted to the domains: the specific energy z . The specific energy varies from one domain to another, and so the average of specific energy z over the entire population of cells is equal to the macroscopic dose D .

Two types of damage are described:

- Lethal lesions

The first type of damage corresponds to lethal lesions. These lesions are not reparable and mainly consist in several DNA damages such as double strand breaks (DSB) leading to the death of the cell. The probability of a lethal lesion is assumed to be proportional to the specific energy z absorbed by a domain d .

- Sub-lethal lesions

The second type of damage corresponds to sub-lethal lesions. These lesions are reparable and, when alone, non-lethal to the cell. But, when combined to another sub lethal lesion, it can form a lethal unrepeatable lesion. Its probability of occurrence is proportional to the square of the specific energy deposited in that domain.

For low LET ions, the lethal lesions distribution is assumed to be a Poisson distribution among the cells. The survival fraction is given by a linear quadratic relation. The survival fraction S (equation 15) and the number of lethal events L_n (equation 16 and 17) are calculated as follows:

$$S = e^{-(L_n)} \quad (15)$$

$$L_n = \alpha_d z d + \beta_d z d^2 \quad (16)$$

$$L_n = (\alpha_0 + \beta z_{1d}) D + \beta D^2 \quad (17)$$

with:

- L_n is the average number of lethal lesions in a nucleus,
- D is the absorbed dose (Gy),
- z_{1D} is the mean specific energy deposited during single energy deposition events in a domain (Gy),
- α_0 corresponds to the proportionality coefficient (between L_n and D) in the limit of LET equal to zero (Gy^{-1}),
- β corresponds to the LQ model coefficient and is assumed to be independent of the radiation type and is fixed to the coefficient obtained with the photon radiation (Gy^{-2}).

At first, the assumption of a Poisson distribution is also considered valid for both low LET and high LET ions. However, in 2003, Hawkins added a non-Poisson correction to the model as it was postulated that a high LET causes deviation from the Poisson distribution ¹⁵

In 2006, after the high LET non-Poisson distribution postulated by Hawkins et al., Kase et al. ² modified the MKM model by adding a saturation correction (z_0) to the domain-specific energy in order to take into account the overkilling effect of the ions. The modification then led to rename the model into the Modified MKM (mMKM). The number of lethal events L_n is now expressed with a saturation corrected mean specific energy (z_{1d}^*):

$$\langle L_n \rangle \geq (\alpha_0 + \beta z_{1d}^*)D + \beta D^2 \quad (18)$$

$$z_{1d}^* = \frac{l}{m} \frac{y_0^2 \int_0^\infty \left(1 - e^{-\left(\frac{y}{y_0}\right)^2}\right) f_1(y) dy}{\int_0^\infty y f_1(y) dy} \quad (19)$$

with:

- l , the mean cord length of the domain
- m , the mass of the domain
- $f_1(z)$, the probability density of the specific energy z deposited by a single energy-deposition event in the domain
- z_0 , the saturation coefficient

$$y_0 = \frac{\rho\pi R_n R_d^2}{\sqrt{\beta(R_d + R_n^2)}} \quad (20)$$

The coefficient of saturation z_0 is calculated with R_n the radius of the cell nucleus (μm) and R_d the radius of the domain (μm).

1.3.3. The NanOx model

NanOx is a model that has been developed in 2017 by Beuve et al. ⁴ We will not address the full complexity of NanOx in this section as the model has already been described in the work of Cunha et al. ⁴ and Monini et al. ²⁶. We will describe the main features, the principles as well as the formalism in a simplified manner.

Like mMKM, NanOx is a multiscale model taking into account the stochastic nature of radiation. However, NanOx does not only consider the energy transfer points at micrometric and nanometric scales. NanOx also considers the physicochemical and chemical consequences of the radiation at such scales by evaluating the oxidative stress undergone by cells during water radiolysis.

The average cell survival probability is estimated over all the irradiation configurations. For a given radiation type and energy, a configuration (C_k) is : “a set of parameters that describe the radiation impact k totally or partially inside the volume of influence, including for instance the spatial distribution of energy-transfer points and the resulting physicochemical events at a given time.” ⁴ The volume of influence is defined as a volume large enough that an impact of a particle outside this volume leads to a negligible transfer of energy into the sensitive volumes associated with local and non-local lethal events.

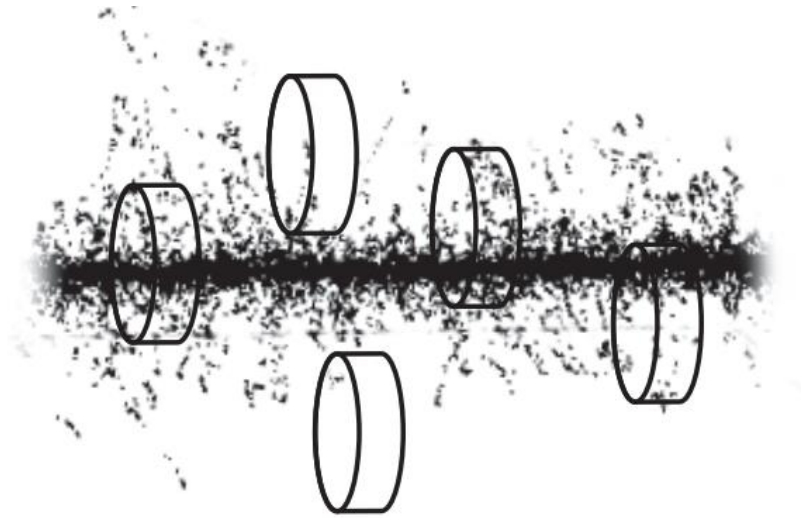


Figure 8 - Schematic illustration of a configuration of an irradiation of cells by a given radiation impact. ⁴

The average survival probability in function of dose is calculated as follows: (equation 21).

$$S(D) = \sum_{k=0}^{k=\infty} P(K, D) \cdot \langle {}^{CK}S \rangle_{C_k} \quad (21)$$

where $P(K, D)$ is the probability to have a number K of impacts in the volume of influence with a dose D and $\langle {}^{CK}S \rangle_{C_k}$ is the mean survival probability over all the configurations C_k .

The cell death and survival are resulting from two types of biological events taking place at two scales: the local events taking place at a nanometric scale and the non-local events taking place at a micrometric scale. Therefore, in the NanOx model are defined two sensitive volume sizes associated to both types of events.

- Local lethal events

The local lethal events depend on biological events caused by physicochemical processes in a nanodosimetric sensitive volume smaller than 100 nm ²⁷. These events alone can lead to the death of cells due to the severe and unrepaired DNA damage such as DSB (double strand break). In the sensitive volume are defined cylindrical local targets of 10 nm to match approximatively the expense of DNA DSB ²⁷. The inactivation of one of the local targets is enough to cause the death of the cell.

- Non local lethal events

One non-local lethal event leads to cell damage without involving a cell death. It is similar to the sub-lethal lesions described in the MKM or the mMKM. The non-local lethal events can correspond to reparable DNA damage such as single strand breaks (SSBs) or even a state of oxidative stress in the cell. The accumulation and the interaction between several non-local lethal events at the micrometric scale can cause the cell death.

Therefore, the probability of cell survival ${}^{C_k}S$ (equation 14) can be expressed by the local lethal events ${}^{C_k}S_L$ and the non-local events ${}^{C_k}S_{NL}$. The probabilities ${}^{C_k}S_L$ and ${}^{C_k}S_{NL}$ are independent and can be calculated separately.

$${}^{C_k}S = {}^{C_k}S_L \times {}^{C_k}S_{NL} \quad (22)$$

For the cell survival due to local events, an effective lethal function (F) is calculated at the nanometric scale. This function characterizes the effect of a given radiation quality in a local target.

In equation 23 is defined the effective lethal function F:

$$F(z) = \frac{h}{2} \left[1 + \operatorname{erf} \left(\frac{z - z_0}{\sigma} \right) \right] \quad (23)$$

The three parameters, z_0 (the threshold), σ (the width of the increase), h (the height of the response) are obtained via the fit of measured α values of a specific cell line irradiated by photons and at least two monoenergetic ion beams characterized by intermediate and high LET values. These three parameters are explained and their calculation is developed in details in the work of Monini et al.¹⁹

The probability of cell survival to a local lethal event will be the probability that no local target is inactivated, for a given configuration of radiation impacts C_K for one local targets C_i . We can use the local lethal function to express the action of local lethal events ${}^{C_k}S_L$.

$${}^{C_k}S_L = \prod_{K=1}^K \exp(-\langle F(C_i, C_k Z) \rangle_{C_i}) \quad (24)$$

For the cell survival to non-local events, the action of non-local lethal events ${}^{C_k}S_{NL}$ are represented by global events due to the production of chemical reactive species that induce DNA sub lethal damage and

participate to the oxidative cell stress²⁸. To characterize the radiation consequences at this scale, the model introduces the relative chemical effectiveness (RCE).

The RCE is the ratio of the specific energies deposited by the reference radiation and an ion responsible for the same level of oxidative stress. Together with the RCE, can be calculated the chemical specific energy $C_K Z$, for a configuration of radiation impacts C_k (equation 25). Both quantities are estimated at T_{RCE} , the time when the yield of the reactive chemical species of interest is calculated. T_{RCE} is 10^{-11} s and the chemical species considered is the hydroxyl radical $\cdot\text{OH}$.

$$C_K Z = \sum_{k=1}^K C_k RCE \times C_K Z \quad (25)$$

The cell survival of the non-local events can be expressed as a Linear Quadratic expression:

$$C_K S_G = C_{norm} \times (-\alpha_G \times C_K \tilde{Z} - \beta_G \times C_K \tilde{Z}^2) \quad (26)$$

with C_{norm} as : “ factor ensuring that the average of cell survival over all irradiation configurations leads to the experimental probability of cell survival to an irradiation with a reference radiation characterized by the coefficients α_r and β_r of the respective LQ fit”.⁴ The photons emitted from a ^{60}Co source as reference radiation. For now, the α_G coefficient is set to 0 and β_G is the coefficient from the linear quadratic fit of cell survival for the reference radiation.

1.4. Biological dose evaluation through Monte Carlo treatment planning systems

1.4.1. Monte carlo codes used in biophysical models

For treatment planning in radiation therapy, the TPS uses pencil beam algorithms. This type of algorithms is fast and accurate in homogeneous mediums. This is not true for heterogeneous mediums, such as the interfaces between bone and soft tissue for example, which can lead to uncertainties in the treatment planning²⁹ with the particles depositing dose to normal tissues and compromising the homogeneity of the dose inside the tumoral target volume. In hadrontherapy, due to the ion beam characteristics, these uncertainties can have even more severe biological consequences than in radiotherapy.

Indeed, anatomical heterogeneities in the ion beams path, the Bragg peak region of the ions is degraded which leads to changes in the energy spectrum of the ions. Consequently, we observe the attenuation of the primary beam, the production of secondary fragments, an alteration of the three-dimensional spread of the beam and an alteration of the fall-off width. Unlike the analytical algorithms, the Monte Carlo method is capable of taking into account these consequences, and therefore has been chosen as the gold standard for calculations in medical physics.³⁰ Several Monte Carlo codes have been developed for radiation transport calculation, which have then been used in medical physics, such as MCNP, GEANT4 and FLUKA.

Not only Monte Carlo codes offer a higher accuracy, they also offer tools that make Monte Carlo codes appear useful to support clinical activity. Indeed, regarding complex delivery systems, Monte Carlo dose calculation is often based on a complete simulation of the treatment geometry and the spread-out Bragg peaks to deliver the treatment. Using blueprints and information of the delivery systems, the geometrical and material information to the machines can be modeled to sharpen the accuracy of the predictions. Therefore, in last decades several Monte Carlo toolkits have been developed and are used for simulation of linear accelerators and dose calculation in the patient.

Among the existing toolkits, our interest goes to GATE is an open-source software based on the Geant4 toolbox, developed by the OpenGATE collaboration since 2001. The platform is used to perform simulations for applications such as Emission Tomography, Transmission Tomography, Radiotherapy, Optical Imaging and Hadrontherapy³¹ Being an open-source code with yearly releases, GATE now has a wide community of users and developers. Gate is also user-friendly, therefore for treatment devices modeling, geometries can be easily designed and controlled using a macro file system without any coding knowledge. From a developer point of view, Gate is a layer structure code in C++ as a set of classes that defines the features available in GATE. Therefore, as developers, we can add the required classes to Gate source code for an implemented tool to then be used by GATE users. In GATE's nomenclature, the tools which allow to interact with the simulations are called "actors". The actors can collect information during the simulation, such as energy deposit, number of particles created in a given volume, etc. The actors lead to output files from the simulation that are the collected information.

Gate appears as an interesting software for the implementation of a tool for the calculation of biological quantities for hadrontherapy in the context of this PhD work as for now, only a tool leading to the calculation of the physical dose has been implemented and validated in the toolkit.

It is known though that simulations relying fully on Monte Carlo techniques are computationally intensive both in time and memory space requirements. Especially if the estimation of the biological dose rely on biophysics models that perform calculation micrometric and nanometric scales. Therefore approaches have been explored in order to : benefit of the biophysics models for the estimation of the biological dose, rely on the Monte Carlo codes accuracy and keep the computation times to the minimum.

1.4.2. FLUKA

The Monte Carlo code FLUKA ³² has been coupled with the LEM in the work of Mairani et al. in 2010 ³³ and is now adopted at the HIT (Heidelberg Ion-Beam center) in Germany and CNAO (National Center for Oncological Hadrontherapy) in Italy in Pavia ³⁴. FLUKA has then been coupled with the mMKM model in 2017 and described in Magro et al. ³⁵. The methodology concerning the coupling between the code and the models was established by Mairani et al. ³³ has shown in Figure 9 and the same methodology was then used in the work of Magro et al ³⁵. The method consists in first using the Monte Carlo code to estimate the input parameters of the biophysics models. The biophysics models are then used to calculate the cell survival coefficients and stored in databases. These databases are then the input for biological calculations in a MC framework or an analytical TPS.

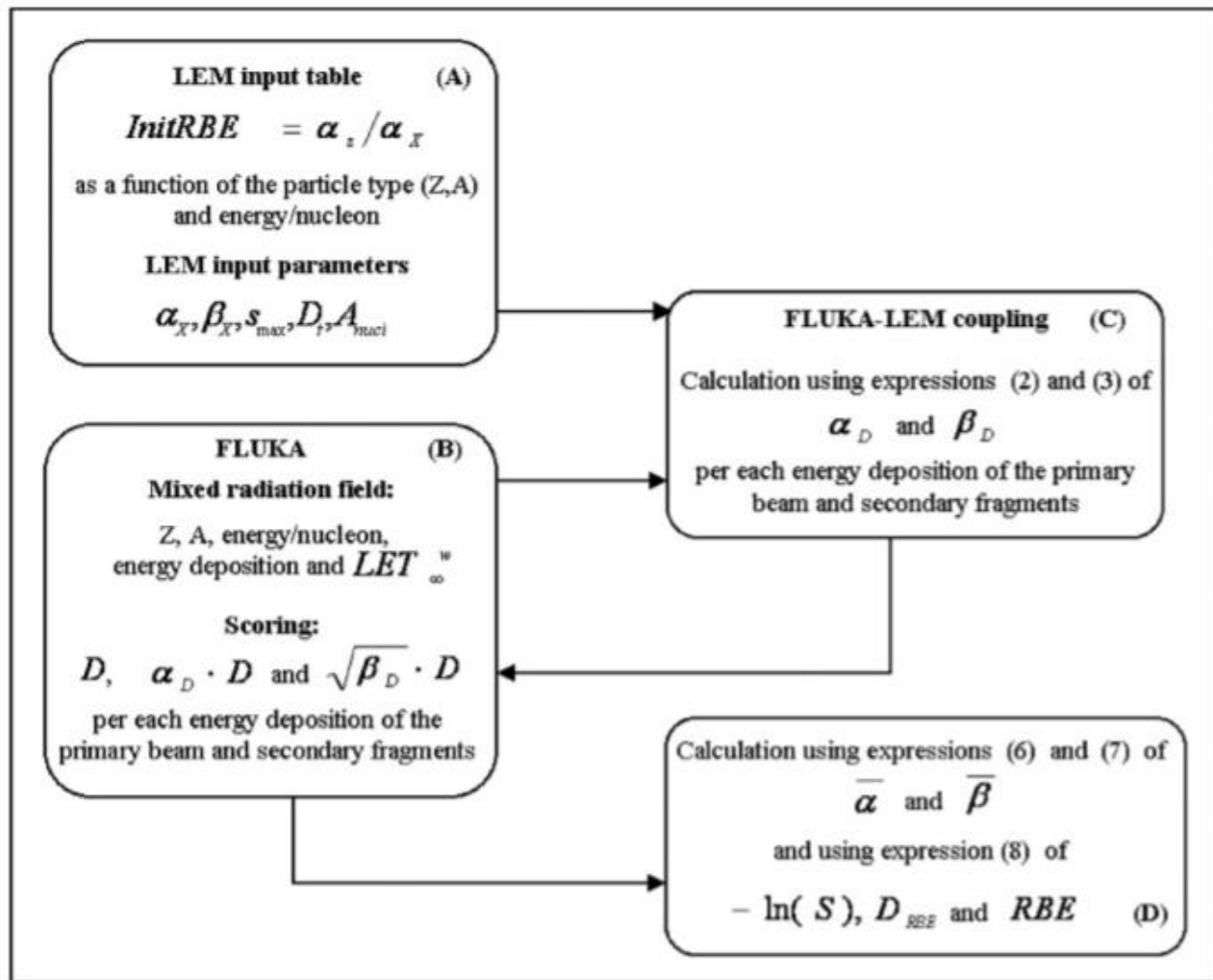


Figure 9 - Schematic representation of the coupling of the FLUKA MC code with the LEM ³³

This methodology isn't model-dependent and has been applied to the LEM and mMKM biophysical models.

In hadrontherapy, many beams of different energies are used during an irradiation and a variety of nuclear fragments and particles with different LET values are produced; this is what is called a mixed field. For every voxel composing the patient, the biological dose is based on the evaluation of the survival parameters for a mixed field.

Therefore, for each voxel, the impact of primary ions and nuclear fragments on the biological quantities is taken into account in the estimation of the biological quantities. In this objective, the mathematical model of Kellerer and Rossi ³⁶ deriving from the TDRA (theory of dual radiation action) has been used.

The authors of the TDRA stated that : “a biological system exposed to more than one radiation type shows synergism, implying that the total number of lesions is larger than the sum of the lesions produced by each particle, due to interactions between sub-lesions produced by different components.”³³.

Like shown in equation XX, we define the biological effect of the mixed field as the logarithm of the survival fraction S in function of the macroscopic dose D.

$$-\ln(S(D)) = \alpha_{mix}D + \beta_{mix}D^2 \quad (26)$$

with α_{mix} and β_{mix} as the sum of the α coefficients and the sum of the square of the β coefficients for each ion of each kinetic energy of type T, weighted by the deposited dose fraction f_i .

$$\alpha_{mix} = \sum f_{Ti} \alpha_{Ti} \quad (27)$$

$$\sqrt{\beta_{mix}} = \sum f_{Ti} \sqrt{\beta_{Ti}} \quad (28)$$

Finally, the survival fraction along with the biological dose and the RBE can be estimated for the field. The methodology has been validated with the one-dimensional estimation of the survival fraction shown in Figure 10. As the experimental cell survival was well reproduced, it confirmed the use of such coupling for the estimation of RBE-weighted dose calculations in ion beam therapy³³. In 2013, a Monte Carlo treatment planning tool has been developed in order to calculate a RBE-weighted dose. This tool successfully performed the dose computation and the estimation of absorbed dose and RBE-weighted dose for several test cases in homogeneous water phantom and patient CT scans, as shown in Figure 11 with the comparison of the RBE-weighted dose estimated with the CNAO TPS, Syngo, (first row) and estimated with the newly developed Monte Carlo treatment tool (last row).

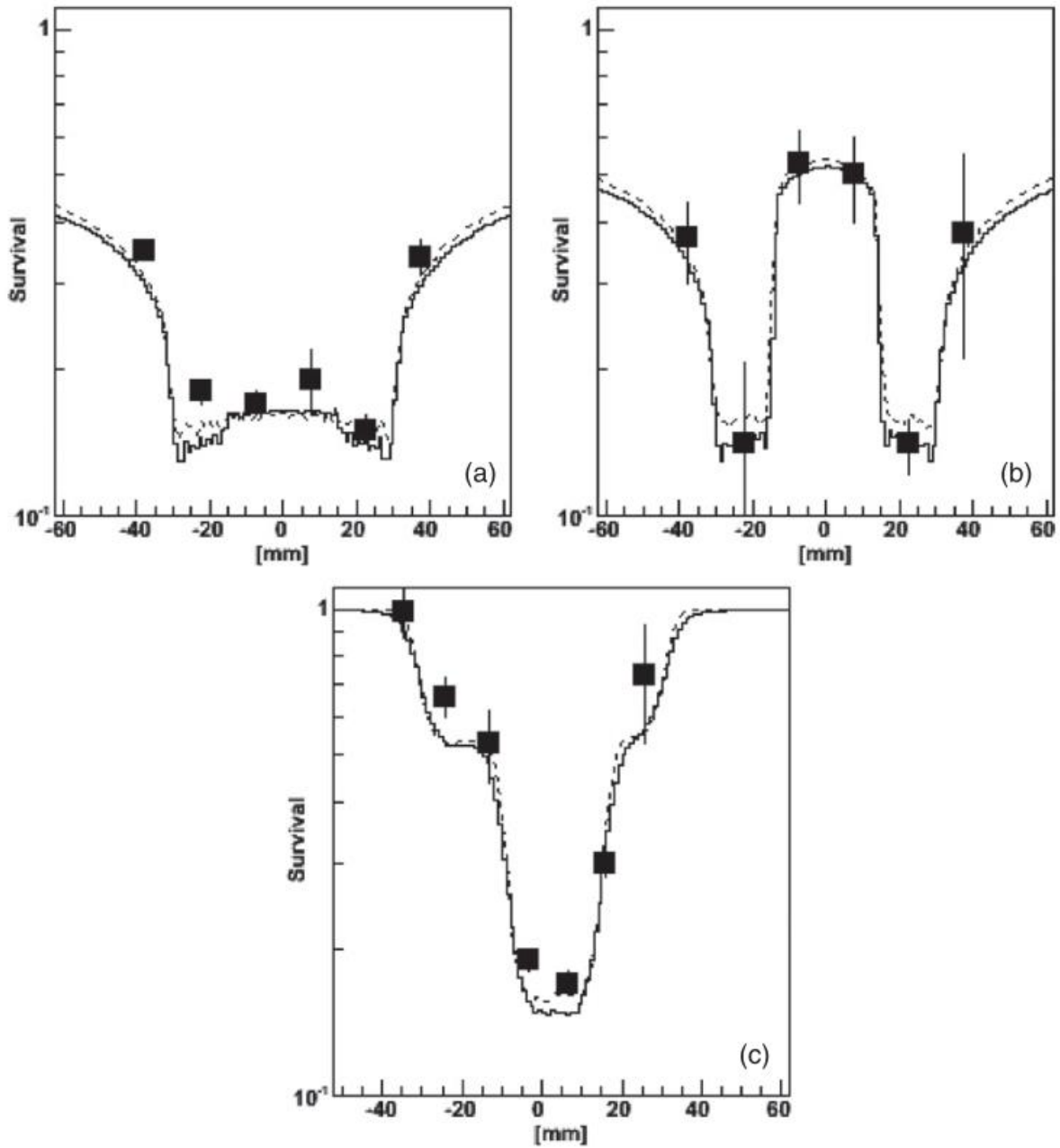


Figure 10 - Cell survival fraction estimated using FLUKA coupled with the LEM (black squares) compared with the HIT TPS TRiP98 calculations (dashed line) and the MC results (solid line).

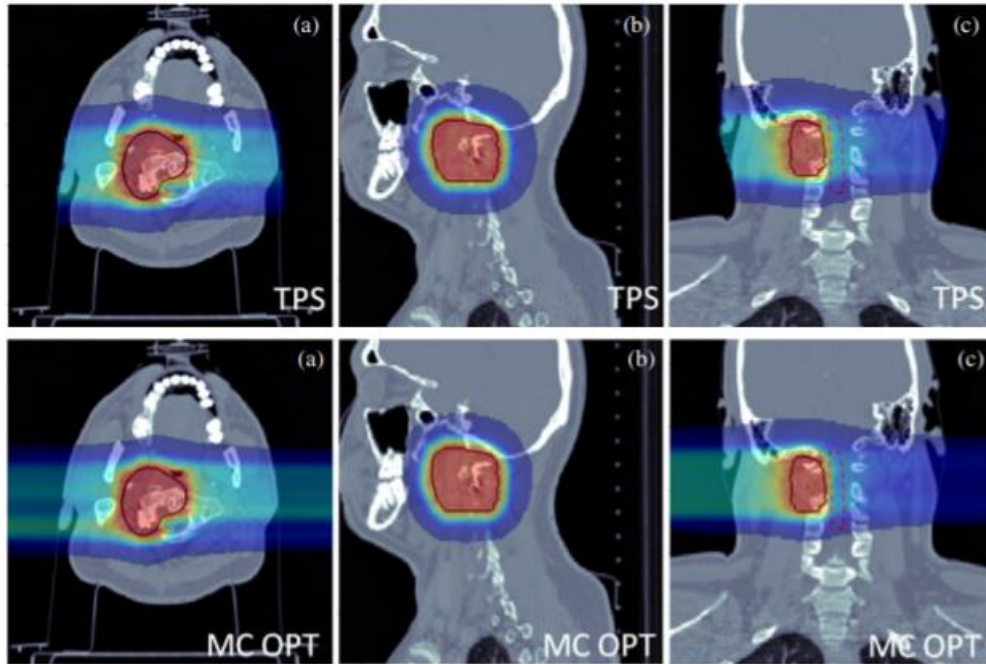


Figure 11 - RBE-weighted dose dose distributions for a patient plan calculation using the Syngo TPS results are depicted in the first row, in the last row MCTP results are shown ³³.

1.4.3. TOPAS

Other codes such as TOPAS, a proton Monte Carlo tool based on the GEANT4 toolkit, proposed extensions to model the RBE and the biological dose. In the case of TOPAS, eight biophysical models for the prediction of the RBE were implemented into the TOPAS framework : the MKM and mMKM, the model by Wedenberg et al. ³⁷, the model by Carabe et al. ³⁸, the model by Chen and Ahmad ³⁹, the model by Wilkens and Oelfke ⁴⁰, the repair-misrepair-fixation (RMF) model ⁴¹ and the track structure model ⁴².

In this case, the estimation of the biological quantities depends on the selected model. Here, we decide to focus on their implementation of the mMKM model. Similarly, to the methodology used by Mairani et al. ³³, a database table containing the survival fraction coefficients estimated with the mMKM are used as input. Then, a dose-weighted sum using the framework by Kellerer and Rossi ³⁶ is used to obtain the survival coefficients α and β values within each voxel.

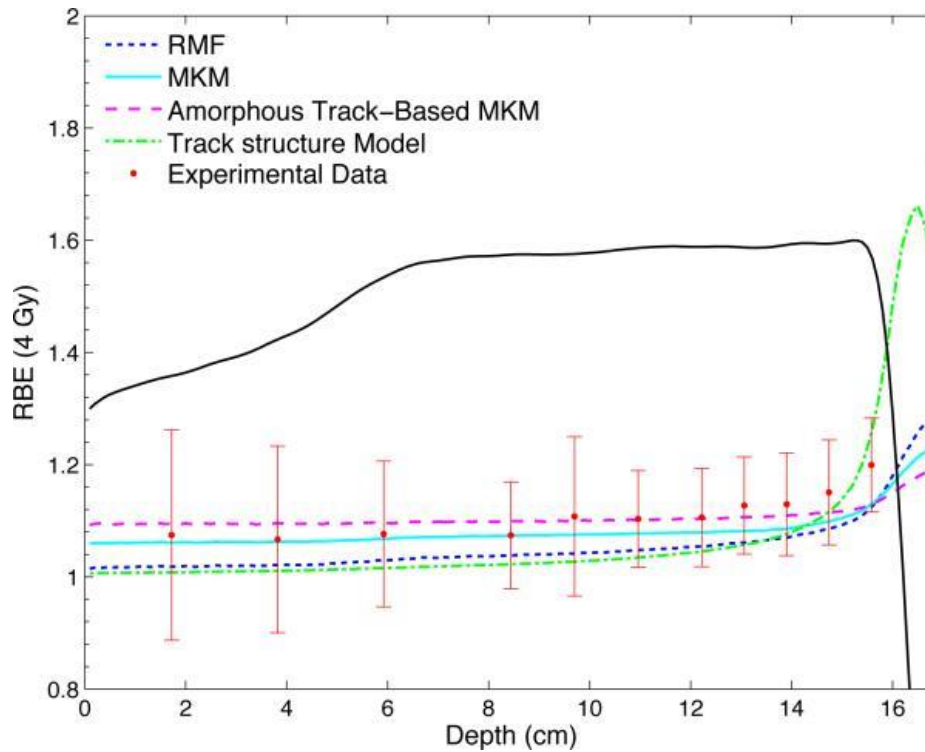


Figure 12 - The predicted RBE values for a dose of 4 Gy according to the RMF model, the MKM, the mMKM (amorphous track based MKM) for 160 MeV protons SOBP.

Their prediction of the RBE has been calculated using several models and compared against experimental data for a 10 cm SOBP of 160 MeV proton beam. Here, the mMKM is labeled as Amorphous Track-Based MKM in the legend. The estimated values for the RBE have been considered well within error bars for all data points.

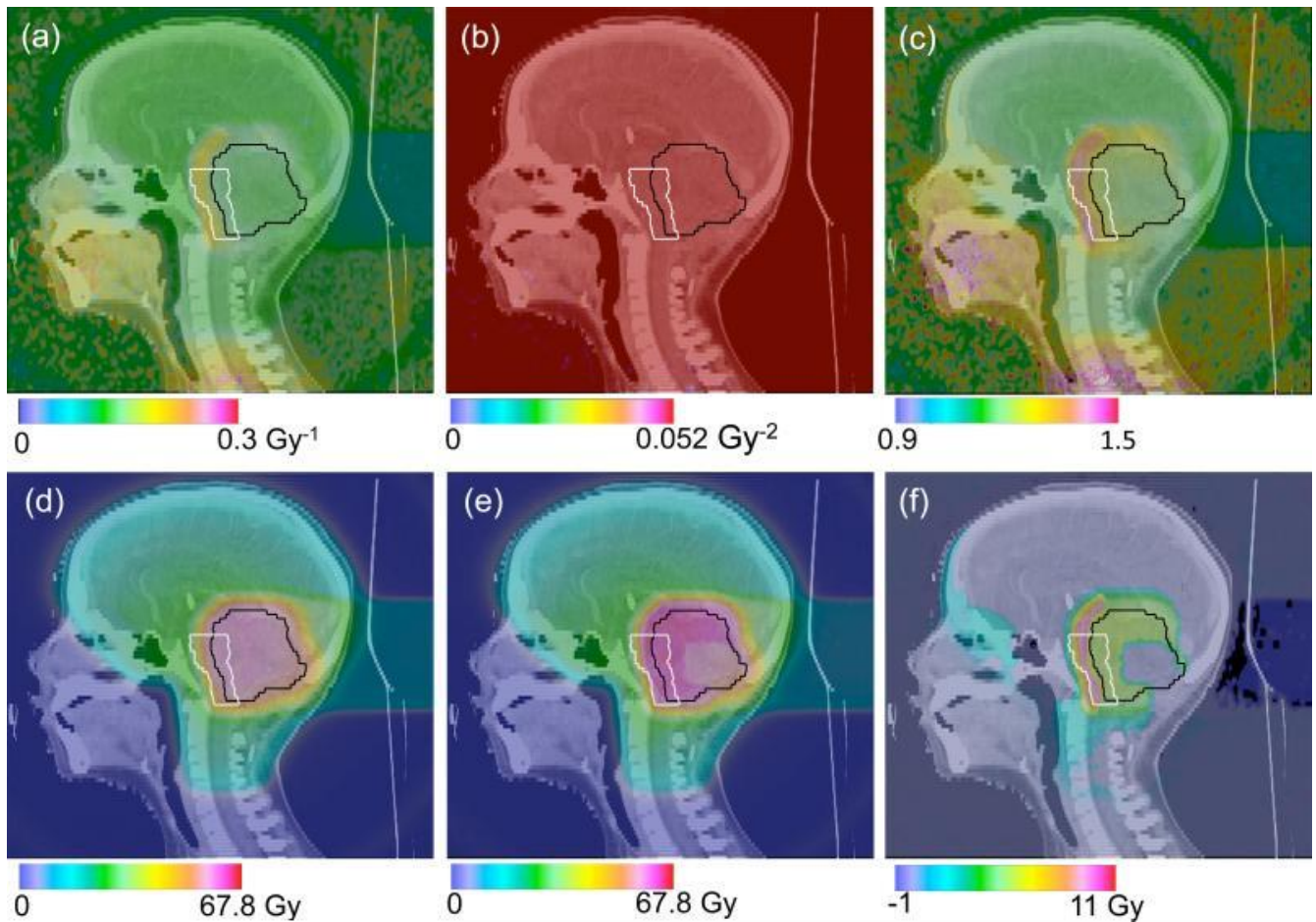


Figure 13 - Patient case simulation study of a pediatric head and neck proton treatment using TOPAS ⁴³

A tool has been developed to link TOPAS to the treatment planning system of the Massachusetts General Hospital. The tool creates TOPAS input parameter files based on the patient CT from the planning system. For this validation, a pediatric head and neck patient has been selected in order for TOPAS to compute the deposited dose along with the RBE and give a complete patient dose distribution. On figure 13 is shown the α values (a), the β values (b), the corresponding RBE value (c), a calculation of the biological dose using a constant RBE of 1.1 (d), the biological dose estimated with the Wedenberg et al. model and finally, on (f), the dose difference between (d) and (e). This study has been used to demonstrate the potential of TOPAS for biological treatment planning, it has to be noticed that the biological input parameters that have been used, are not necessarily representative for the relevant tissues.

It has been admitted that some weaknesses were still present in their framework, notably due to incomplete databases for each model.

1.5. Conclusion

In this chapter, we showed the interest to model the biological dose in hadrontherapy. Many biophysical models have been developed and some of them have been used in Monte Carlo frameworks that are already tested in clinical routine. In the objective of creating an implementation of the biological dose based on the mMKM and the NanOx models within the GATE Monte Carlo simulation platform, we will present in the next chapters our methodology to reach an accurate prediction of the biological dose. For a thorough implementation, Monte Carlo Track structure codes (MCTS) are at the basis of the development of biophysical models. Therefore, in the next chapter, we start by estimating how the implementation of low scale physical interactions could impact physicochemical and chemical reactions in MCTS for proton and electron beams. Geant4-DNA and LPCHEM are the two candidates that we considered to tackle the infinitesimal modeling of direct and indirect radiation effects.

Chapter 2

Monte Carlo simulations of nanodosimetry and radiolytic species production for monoenergetic proton and electron beams. Benchmarking of GEANT4-DNA and LPCHEM codes.

2.1. Introduction

Monte Carlo track structure (MCTS) codes are used for micro and nanodosimetry (molecular level) by estimating the detailed clustering of individual energy depositions (mainly by atomic ionizations and excitations) along the track of ionizing particles and subsequent free chemical species diffusions and interactions in liquid water or with DNA atoms. At such low energies and small dimensions, event-by-event tracking is applied without resorting to condensed history techniques. Codes dedicated to this purpose are numerous but, most of them, are not open to a community of users and stay confidential. Geant4-DNA is the only open-source simulation toolkit aiming at simulating the physical, chemical and biological phases induced after radiation. Most of MCTS codes propose an accurate simulation of the physical phase (e.g. excitations, ionizations and scattering processes in water) together with the chemical phase while the biological phase is not yet as easily accessible. However, only very few papers mention exhaustive comparisons of the MCTS performance. In this paper, we decided to benchmark two MCTS codes, Geant4-DNA and LPCHEM, in order to raise their differences and highlight their potentials into simulating efficiently direct and indirect interactions in a liquid water medium. The mid-term perspective of this study is to make available an open access database of calculated specific energies and radiolytic yields for a large panel of monoenergetic ions in view of using this information for the estimation of the biological dose in hadrontherapy treatments. The GATE Monte Carlo platform aims at becoming the

suitable receptacle for this database in order to provide to a large community of users the ability to compute a biological dose in ion beam therapy.

Geant4-DNA is an open source code released in 2010 by the Geant4-DNA collaboration⁴⁴. The code is an extension of the Geant4 code and therefore has been priority developed by a community of physicists. It has then been adapted to radiation chemistry simulation. LPCHEM, previously called LQD⁴⁵ and MDM⁴⁶, is a code developed since the 1990s by a collaboration between teams from the IP2I (Institute of Physics of the 2 Infinities) in Lyon (France) and the CIMAP (Research center on Ions, Materials and Photonics) in Caen (France), both including researchers specialized in radiobiology, radiochemistry and radio-physics. Both codes are able to perform the simulation of ionizing radiation with their physical and chemical consequences down to a very small scale and are suitable for the simulation of specific energy distributions and radiolytic species yields.

In the work of Cunha et al.⁴⁵, LPCHEM has been tested to calculate dose in micrometer cylindrical targets irradiated with ⁶⁰Co photons. This work proved the ability of the code to model distributions of specific energy probability in very small targets even though⁴⁵ no comparisons are shown with other MCTS codes.

Microdosimetry and nanodosimetry spectra calculated with Geant4-DNA have been compared to several codes (PENELOPE, MCNP6, FLUKA, NASIC and PHITS) by Villagrasa et al.⁴⁷; the authors considered the number of ionization in micrometric and nanometric targets of different sizes in order to study the contribution of cross-section uncertainties. The conclusions of this study raised that, at a nanometric scale, the choice of the Monte Carlo code and the associated physics models had an influence on the mean size of the ionization cluster distribution.

A comparison between the recommended Geant4-DNA options (Option 2, Option 4 and Option 6) for the impact of ionization, excitation and elastic scattering cross section models on electron track structures has been conducted by Kyriakou et al.⁴⁸. The study showed that the inelastic scattering models could modify from 15 to 45 % the penetration ranges of electrons, then impacting physico-chemical and chemical stages. In addition, Shin et al.⁴⁹ demonstrated that elastic scattering impacted electron spatial distribution and therefore the simulation of the water radiolysis at nanometric scales.

Geant4-DNA and LPCHEM codes also provide the possibility to model the production of radiolytic species. At the end of the physical stage, excited and ionized water molecules are present in the medium.

During the physico-chemical stage, chemical bonds of the excited and ionized molecules break which leads to new chemical species. Finally, in the chemical stage, the radiolytic species can either diffuse through the medium or get combined to form new reactive species.

Concerning Geant4-DNA physico-chemical and chemical stages, time dependent yields for OH^- , H_2 , H_2O and H_2O_2 species, generated after interactions with liquid water of protons between 500 keV and 50 MeV, have been compared and validated against Appleby and Schwarz⁵⁰ and Naleway⁵¹ experimental data as shown in the work of Karamitros et al.⁵². Time dependent yields for e_{aq}^- and $\cdot\text{OH}$ species generated after interactions of 1 MeV electrons with liquid water have been compared and validated with respect to PARTRAC⁵³ and Uehara and Nikjoo's⁵⁴ Monte Carlo codes, as shown in the work of Karamitros et al.⁵⁵.

Regarding LPCHEM, time dependent yields for the HO_2 and $\text{HO}_2 + \text{O}_2$ species generated by carbon ions have been compared to LaVerne and Schuler⁵⁶ and Baldacchino et al.⁵⁷ experimental data as shown in the work of Gervais et al.⁵⁸. Simulated results were in good quantitative agreement with the experimental data.

This work is the first comparison between LPCHEM and Geant4-DNA for the simulation of specific energy spectra at nanometric scale and time-dependent G values (the number of chemical species formed per 100 eV of energy deposited in the medium). Contrary to the LPCHEM code, where physical models are provided through a single set of processes, Geant4-DNA grouped the available models as options in dedicated physics lists. Three of them, identified by their option numbers, are recommended by the collaboration and have been used in this study: option 2, 4 and 6. Those options differ by their models of electron and proton interactions and, they are detailed in the work of Incerti et al.⁵⁹.

In this paper, we first describe the LPCHEM and Geant4-DNA codes along with the validation of their total cross sections against experimental data. Then, we outline the approach used to calculate the specific energy distribution in nanometric targets (10 nm) and the production of $\cdot\text{OH}$, e_{aq}^- , H_3O^+ , H_2O_2 , H_2 and OH^- reactive species along time (from 10^{-12} to 10^{-6} s) during water irradiation with 10 MeV protons. The results are then discussed to link elementary processes and probability distributions of specific energy in nanometric targets to radical yields at 10^{-12} s and radical recombination. Finally, the computing times are compared for the physical stage and the physico-chemical and chemical stages in sequential and multithreaded executions.

2.2. Material and methods

2.2.1. Simulation of nanodosimetry spectra

2.2.1.1. Geant4-DNA and LPCHEM Monte Carlo track structure codes

First, we focused our study on the comparison of Geant4-DNA and LPCHEM Monte Carlo codes for the simulation of electromagnetic interactions of electrons and protons in liquid water down to some eV. Geant4-DNA includes models of interactions in liquid water, in DNA related materials ⁵⁹ and in gold nanoparticles ⁶⁰ while LPCHEM can model interactions in liquid water, gaseous water ⁶¹, silica and gold ⁶². In this study, all simulations were performed in liquid water. Both codes propose physical models that have been validated, when possible, with experimental data: Tessaro et al. ⁶³ and Gervais ⁶¹ for LPCHEM and Incerti et al. ⁶⁴ and Bernal et al. ⁶⁵ for Geant4-DNA.

While LPCHEM provides a single set of physical models, several “physics lists” (options) can be used in Geant4-DNA. The present work was based on the “dnaphysics” example of Geant4-DNA that combines Geant4 electromagnetic models (above 1 MeV for electrons) with three recommended options (2, 4 and 6). Option 2 is the default Geant4-DNA physics list. In option 4, alternative models (for elastic scattering, ionization and excitation) are included at low energy (10 eV – 10 keV) but vibration and attachment processes are not taken into account. Option 6 is the implementation of the interaction cross sections of the CPA100 track structure code ^{66,67}. While the interaction processes are listed for the two codes (see appendix 1), we detail hereafter their differences and similarities:

- Ionization and excitation processes are described with two types of models:
 - the binary encounter Bethe model in Geant4-DNA option 6 and LPCHEM with slightly different parameters (e.g. number of excitation levels, level energies...),
 - the Born approximation with slightly different dielectric models in Geant4-DNA options 2 and 4.
- The multi-ionizations process is only simulated in LPCHEM.
- Attachment and vibration processes are modeled in LPCHEM and in Geant4-DNA option 2 with cross sections adjusted to reproduce sets of experimental data.
- Recombination is considered as a physical process in LPCHEM while in Geant4-DNA it is simulated in the physico-chemical stage.

- Solvation is not a physical process but a numerical technique used in Geant4-DNA consisting in thermalizing electrons (thermalization energy is 25 meV) from a given threshold energy of ~10 eV (lowest atomic excitation level)^{59 49} in order to reduce simulation time.
- Elastic scattering is simulated in all Geant4-DNA options as well as in LPCHEM. The energy deposition associated to this process is only registered in Geant4-DNA option 6 though.
- Charge exchange is explicitly modeled in Geant4-DNA but not in LPCHEM.

2.2.1.2. Calculation of nanodosimetry energy spectra of 10 MeV protons

We calculated the probability distributions of specific energy in a liquid water volume following a similar approach described in Beuve et al.²⁷ and Cunha et al.⁴⁵. 10 MeV protons (10^4 particles) were emitted from a point source at the center of a cubic water box along one dimension. The box size (2 μm) was chosen in order to ensure negligible LET variations (1%) along the track in Geant4-DNA. In LPCHEM, ion energy is kept constant along the track and the box size was fixed according to computing time considerations. The 10 MeV proton TEL is 4.82 keV/ μm and 4.44 keV/ μm in LPCHEM and Geant4-DNA respectively.

After simulations, probability distributions of deposited energies in the track core (considered as a parallelepiped with a 200 nm \times 200 nm cross section¹⁹ were calculated through a dedicated C++ program, named TED (Transfer Energy Distribution). Energy deposited were collected in N randomly distributed cylindrical targets. At nanometric scale, 10 nm radius and 10 nm length cylinders were selected to fit approximately the size of 20 base pairs corresponding to a double strand break extension.

The probability distributions of the total specific energy z_i in the target i , $\left(\frac{\delta P}{\delta z_i}(z_i)\right)$ are then calculated with equation 1:

$$\frac{\delta P}{\delta z_i}(z_i) = \frac{1}{N} \frac{N_i}{\Delta z_i} \quad (1)$$

where N corresponds to the total number of targets. N_i corresponds to the targets where are registered a specific energy deposition z_i within a Δz_i bin size.

Specific energies usually result from several energy transfers in a given nano target and therefore from several physical processes. We can however assign a physical process to each specific energy by

considering the dominant process which leads to the largest contribution of energy deposition. This allows us to study the specific energy spectra as a function of dominant processes.

2.2.2. Radiolytic species production

2.2.2.1. Simulation of physico-chemical and chemical stages with Geant4-DNA and LPCHEM

Unlike LPCHEM that provides a single set of chemistry parameters, Geant4-DNA offers different sets of parameters. In this study, we use the “chem6” example with the default constructor “G4EmDNAChemistry” based on a step-by-step method⁵² and the “G4EmDNAChemistry_Option3” constructor based on the IRT method⁶⁸.

To better clarify differences between Geant4-DNA and LPCHEM concerning physico-chemical and chemical stages implementation, we summarized them (see appendix 2).

During the physico-chemical stage, the dissociation of the water molecules in various excited states is taking place. In both codes, two excitation levels are considered: the dissociation channels for the Rydberg and diffusion bands. The dissociation channels associated to the multi-ionization process are taken into account only with LPCHEM (multi-ionization is not modeled in Geant4-DNA). After the dissociation process, the distance separating the products is pre-established for each species in LPCHEM whereas in Geant-4-DNA the distance between the dissociation products is calculated with a density probability.

For the chemical stage, the method used in LPCHEM is inspired by the Independent Reaction Time method (IRT) model while Geant4-DNA can use both the step-by-step (SBS) and the IRT methods.

Concerning the Geant4-DNA SBS method, at the beginning of the chemical stage, the total simulation time is divided in several time steps, and along these time steps all species are diffused and placed at a new position. The reactions are controlled by the diffusion: a reaction occurs as soon as two reactants encounter⁶⁵. For this method, the detailed trajectory of each diffusing chemical species is simulated which provides reliable spatial information to the detriment of an extended computation time.

For the IRT-based method, the detailed trajectory of each species is not simulated. Instead, probability functions are used: at the end of the physico-chemical stage, the probability of reaction for each pair is calculated and associated to a reaction time. A list of pairs ordered by reaction times is then created. The

pair with the shortest reaction time is treated first and replaced by the products of reaction. This method is less time consuming than the SBS method but spatial information on chemical species is lost.

2.2.2.2. Calculation of radiolytic species yields

Time dependent radiolytic species yields for protons have been evaluated. G values which are defined as the number of molecules produced for a total absorbed energy of 100 eV in the irradiated volume have been computed:

$$G(t) = \frac{N(t) \times 100}{E(\text{eV})} \quad (2)$$

where $N(t)$ is the number of molecules of a given radiolytic species as a function of time t and E is the energy deposited in the irradiation volume by the incident particle.

For Geant4-DNA and LPCHEM codes, the simulation medium was a liquid water box as described in section 2.A. The yields were estimated for the $\cdot\text{OH}$, e_{aq}^- , H_3O^+ , H_2O_2 , H_2 and OH^- radiolytic species produced when 1 MeV electrons and 10 MeV protons interact in the liquid water box. 500 primary particles were simulated. The time during which the yields are measured corresponds to the duration of the chemical stage, from 10^{-12} to 10^{-6} seconds.

2.2.3. Computing time

The computing times of LPCHEM and the various options of Geant4-DNA have been compared for water irradiation with 10 MeV incident protons. Computing times of the physical stage and the physico-chemical and chemical stages have been studied. In the latter case, the computing time has been obtained by running the whole simulation chain (from the physical stage to the chemical stage) considering that the computing time associated to the physical stage is negligible (about 1% of the total computing time). For Geant4 simulations, we compared also the sequential and multi-threaded executions. For tests using the multi-threaded mode, we split the simulations over 4 threads. For LPCHEM, the sequential mode is the only execution mode available.

10 MeV proton tracks were simulated in a $20 \mu\text{m}^3$ liquid water box. In the physical stage, we stored the coordinates and the energy for every interaction occurring in the box for 1, 10, 100, 1000 primary protons. For the physico-chemical and chemical stages we calculated G values for $\cdot\text{OH}$, e_{aq}^- , H_3O^+ , H_2O_2 , H_2 and OH^- species between 10^{-12} and 10^{-6} s for 1 and 10 incident protons. The tracks positions were

randomly set on an irradiation surface large enough to ensure that the probability of tracks overlapping is negligible. In order to facilitate the comparisons, we defined the computing time ratio considering the computing time of LPCHEM as the reference. Simulations were executed five times for each configuration using different seeds in order to estimate uncertainties.

All simulation codes have been compiled before the computing tests using the compiler GCC 8.1.0 and the simulations have been run on a two Intel Xeon CPU E5-2623 v4 (4 cores, 10240 KB Cache, 2.60 GHz).

2.3. Results

2.3.1. Nanodosimetry spectra

Figure 14 shows the probability of each dominant process (hatched bars) as well as their contribution to the specific energy deposition in nanometric targets (plain bars) for 10 MeV incident protons.

In order to facilitate the quantitative comparison of the two codes, we can define two main categories of processes: i) ionization, excitation and in the case of LPCHEM multi-ionization and recombination and ii) elastic scattering, solvation, vibration and attachment. The probability of dominant process (PDP) and their contribution to the specific energy deposition (SED) are also listed in Table 1.

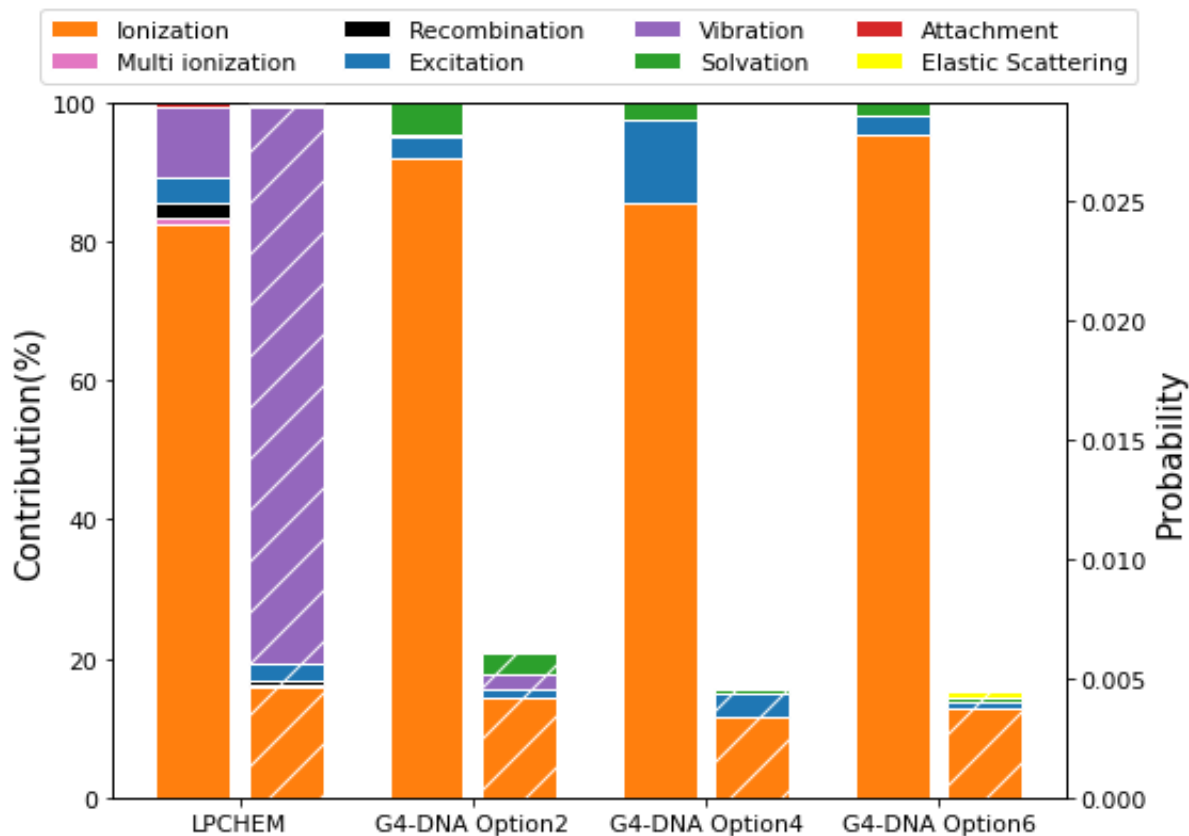


Figure 14 – Plain bars: Dominant process contributions (%) to specific energy deposition for 10 MeV protons; hatched bars: probabilities of dominant processes (PDP).

Table 1 – Probabilities of dominant process (PDP) and their contribution to the specific energy deposition (SED) for the two main categories of processes for 10 MeV protons.

Type of contribution	Ionization, excitation + multi-ionization and recombination (LPCHEM)		Elastic scattering, solvation, vibration and attachment	
	SED	PDP (10^{-3})	SED	PDP (10^{-3})
Geant4-DNA Option 2	94%	4.51	6%	1.60
Geant4-DNA Option 4	96%	4.70	4%	0.215
Geant4-DNA Option 6	98%	4.11	2%	0.55
LPCHEM	90%	5.60	10%	23.5

Figure 15 presents the specific energy probability distributions (SEPD), calculated in liquid water nanometric targets with LPCHEM and the various options of Geant4-DNA for 10 MeV incident protons.

Each figure shows the SEPD associated to a given dominant process (vivid colors) as well as the total SEPD (light colors). The following processes are considered: ionization (figure a), excitation (figure b), vibration (figure c), solvation (figure d), attachment (figure e) and elastic scattering (figure f). Since the incident particles (primaries) are ions, processes refer to both proton and secondary electron processes.

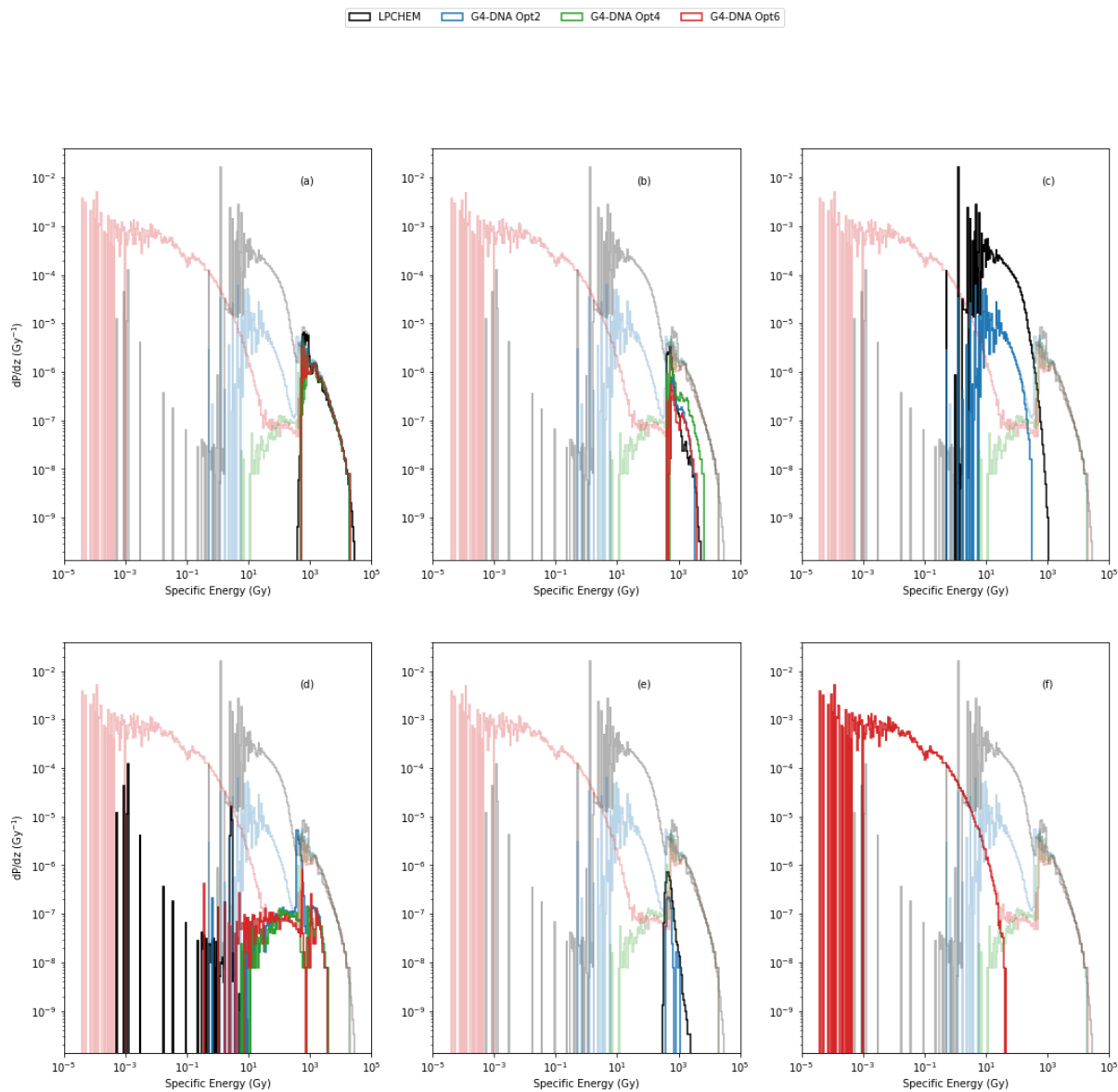


Figure 15 - Specific energy probability distributions (SEPD), calculated in nanometric targets with LPCHEM and the various options of G4-DNA for 10 MeV protons. Each figure shows the SEPD associated to a given dominant process (vivid colors) as well as the total SEPD (light colors). The

following processes were considered: ionization (a), excitation (b), vibration (c), solvation (d), attachment (e) and elastic scattering (f).

2.3.2. Radiolytic species yields

2.3.3. Radical yields comparison against experimental data for 1 MeV electrons

Figure 16 presents the simulated (curves) and experimental (symbols) time dependent yields of some chemical species ($\cdot OH$, e_{aq}^- , H_3O^+ , H_2O_2 , H_2 and OH^-) obtained during liquid water irradiation with 1 MeV incident electrons. These species have been selected because they are the most abundant and are well referenced in literature. The yields obtained with RITRACK and PARTRAC come from Peukert et al.⁶⁹.

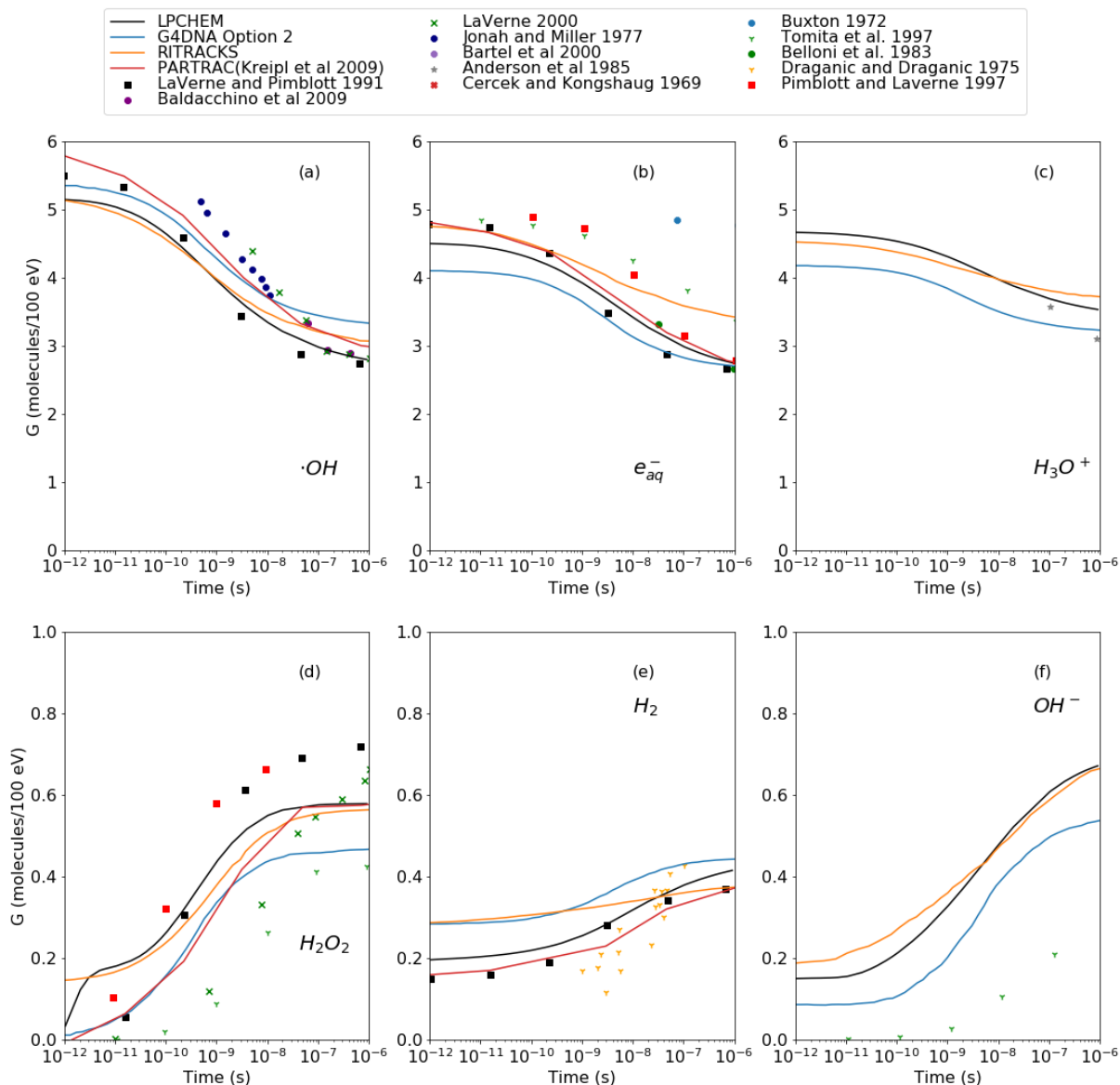


Figure 16 – Simulated (curves) and experimental (symbols) time dependent radical yields (G values) for water irradiations with 1 MeV electrons: (a) $\cdot\text{OH}$, (b) e_{aq}^- , (c) H_3O^+ , (d) H_2O_2 , (e) H_2 , (f) OH^- radiolytic species. Experimental and simulated data obtained with RITRACKS and PARTRAC are from ⁶⁹ and ⁴⁹.

Figures 3a, 3b and 3c show radical species immediately produced after the physical and physico-chemical stages and resulting from the water molecule ionization and dissociation ($\cdot\text{OH}$, e_{aq}^- , H_3O^+). Their recombination leads to the decrease of their yields as a function of time and the production of the other species (H_2O_2 , H_2 and OH^-) presented in Figures 3d, 3e and 3f.

2.3.4. Radical yields simulation for 10 MeV protons

Figure 17 shows the time-dependent yields (G) of $\cdot\text{OH}$, e_{aq}^- , H_3O^+ , H_2O_2 , H_2 and OH^- species predicted with LPCHEM and Geant4-DNA options for water irradiation with 10 MeV protons.

In order to quantify the evolution of the yields along time, we defined the following evolution rate between $t_1 = 10^{-6}$ s and $t_2 = 10^{-12}$ s :

$$\frac{G(t_2) - G(t_1)}{t_2 - t_1} \quad (3)$$

The average values of the evolution rates (in molecule/100 eV/ μs) are the following: $\cdot\text{OH}$ (-3.17), e_{aq}^- (-2.33), H_3O^+ (-1.64), H_2O_2 (0.69), H_2 (0.33) and OH^- (0.66). Figure 18 shows the relative deviations (C_{EV}) in respect to the average of the evolution rates (between 10^{-12} and 10^{-6} s) for each chemical species. The average values of the relative deviations are the following: LPCHEM (10%), Geant4-DNA option 2 (-8%), option 4 (4%) and option 6 (-6%).

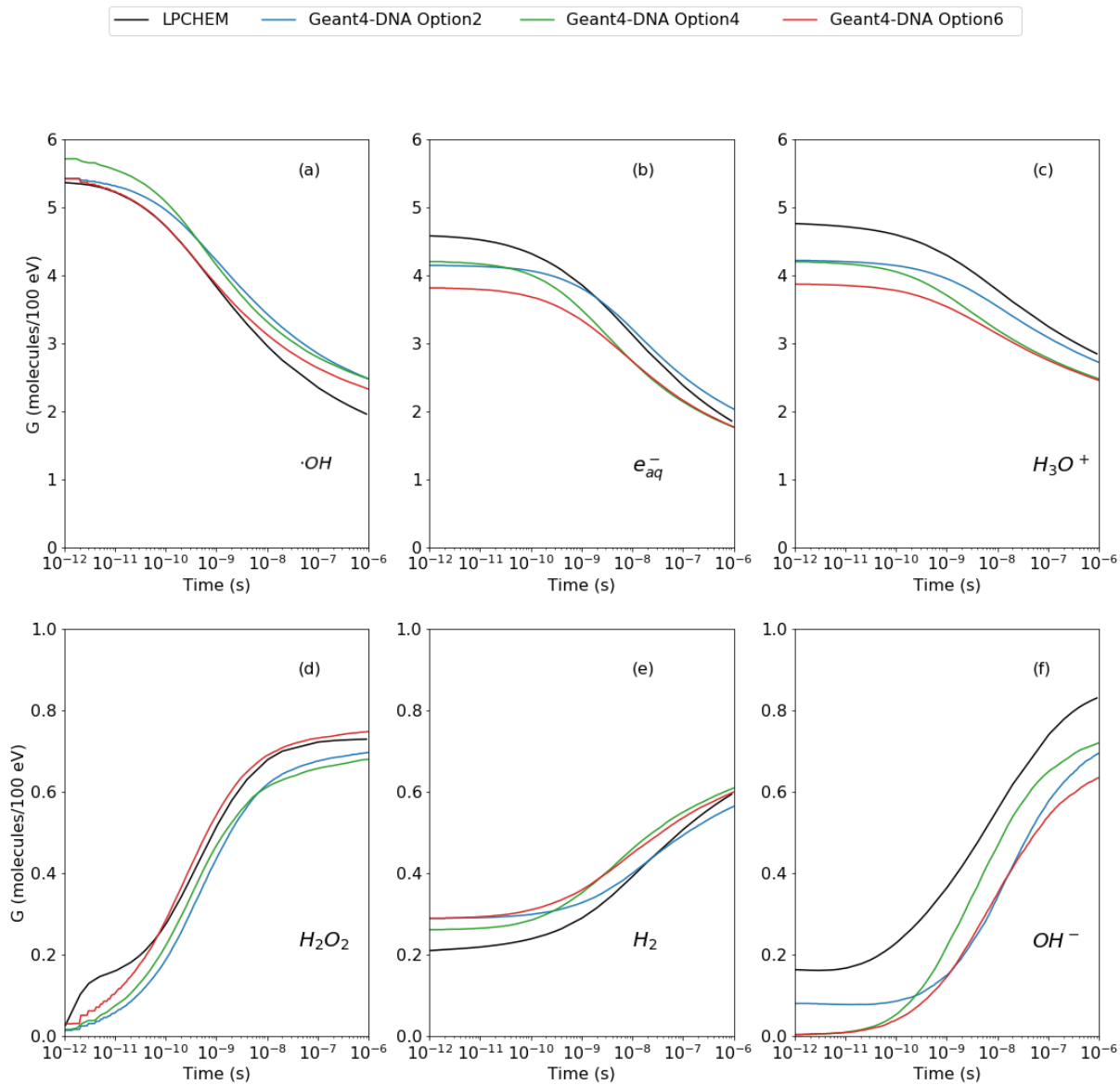


Figure 17 – Time dependent G values for 10 MeV protons for (a) $\cdot OH$ (b) e_{aq}^- (c) H_3O^+ (d) H_2O_2 (e) H_2 (f) OH^- radiolytic species

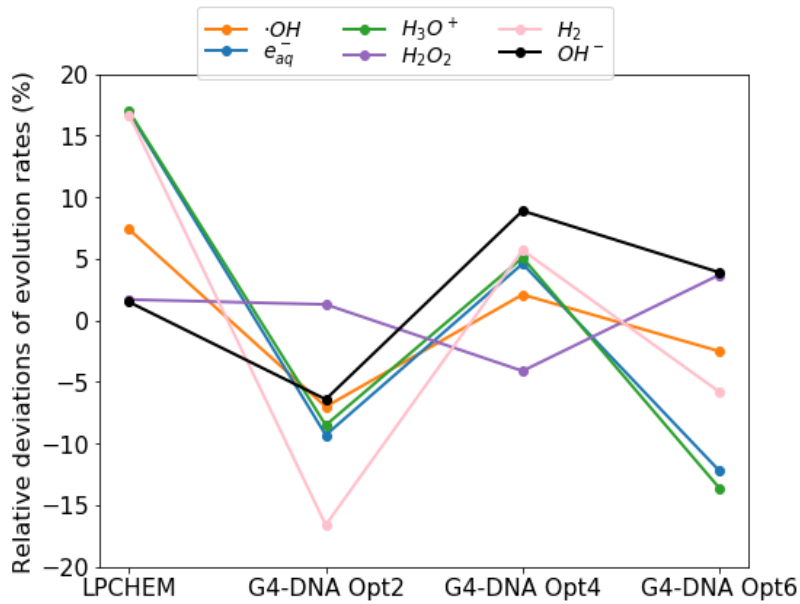


Figure 18– Relative deviations (C_{EV}) in respect to the average of evolution rates of the radical yields between 10^{-12} and 10^{-6} s.

2.3.5. Computing time

Computing times per primary particle (CTPP) and computing time ratios of the physical stage and the physico-chemical and chemical stages expressed in terms of the number of primary particles for water irradiation with 10 MeV protons are presented in Figure 6 and Figure 7, respectively.

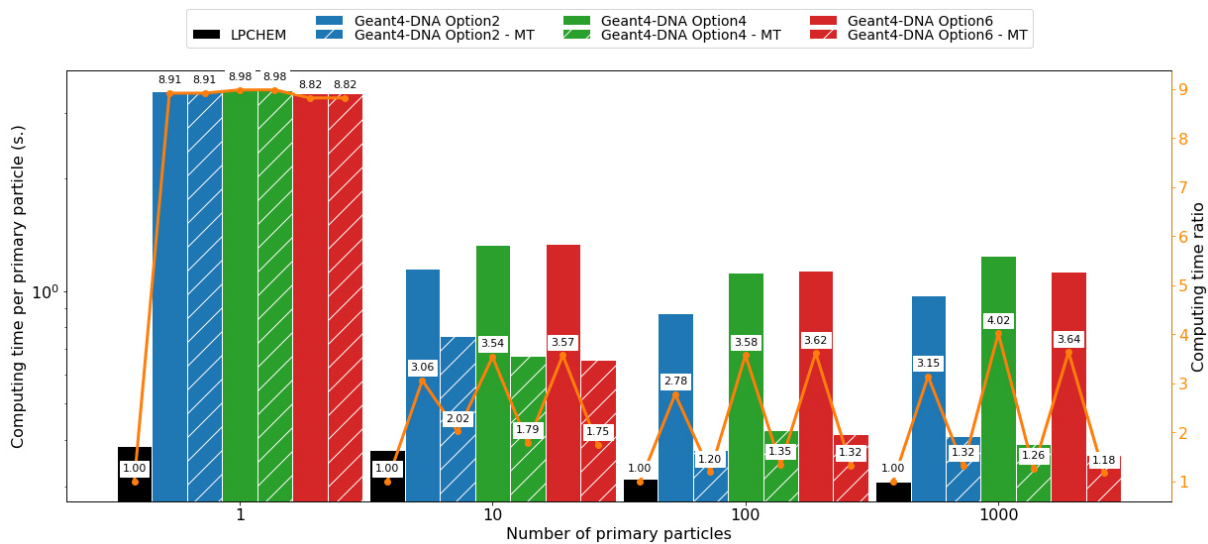


Figure 19- Computing times per primary particle and computing time ratios for the simulation of the *physical stage* with LPCHEM and Geant4-DNA codes for water irradiations with 10 MeV primary protons as a function of the number of primary particles. LPCHEM is considered as the reference code for computing time ratios. MT stands for multi-thread calculations over 4 threads.

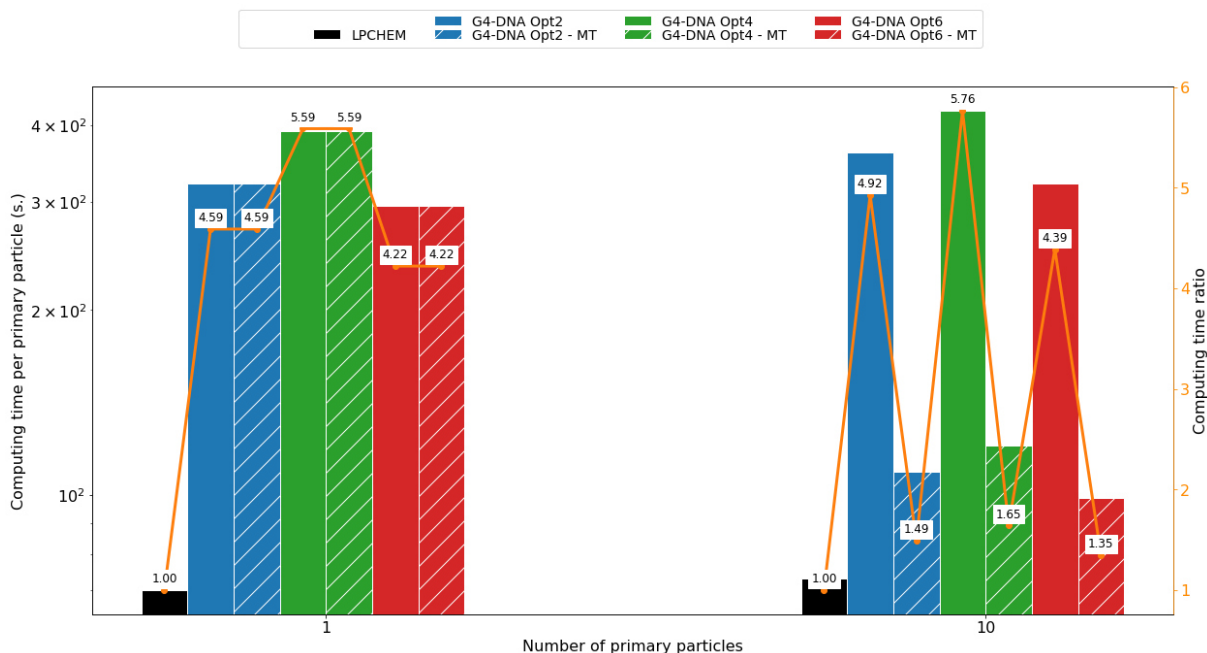


Figure 20- Computing times per primary particle and computing time ratios for the simulation of the physico-chemical and chemical stages with LPCHEM and Geant4-DNA codes for water irradiations with 10 MeV primary protons as a function of the number of primary particles. LPCHEM is considered as the reference code for computing time ratios.

2.4. Discussion

In this work, we compared the predictions of LPCHEM and several options of Geant4-DNA for water irradiations with 10 MeV protons (the predictions of the chemical stages have been also compared to experimental data only available for 1 MeV electrons). In the following sub-sections, our analysis follows the three main stages of irradiation modeling: the physical stage illustrated with nanodosimetry spectra, the physico-chemical stage with the chemical yields at 10^{-12} s and the chemical stage with the evolution of chemical yields until 10^{-6} s.

2.4.1. Nanodosimetry spectra (physical stage)

The relative weights of the various dominant processes in terms of probabilities (PDP) and energy deposition (SED) are similar in options 4 and 6 of Geant4-DNA (Figure 14) because the processes modeled in these options lead to similar (and relatively large) energy deposition (except elastic scattering). Much larger differences between process frequencies and specific energy contributions are observed with LPCHEM and Geant4-DNA option 2. Indeed, these codes account for vibration (and solvation in option 2) that are frequent processes leading to low energy depositions. The probability of the vibration process is much larger in LPCHEM because the electrons are tracked until their kinetic energy matches the temperature of the medium. Overall, although the probability of dominant processes in nano targets can significantly vary from one code to another, the specific energy contributions assigned to the various dominant processes are in relatively good agreement. As expected, the first category of processes (ionization, excitation...) is predominant with a specific energy contribution larger than 90 %. The contributions obtained from the various options of Geant4-DNA are in agreement with a mean value of 96 % and relative differences of 2 %. We can notice that the contribution of excitation in Geant4-DNA option 4 is about three to four times larger than in options 2, 6 and in LPCHEM.

In term of specific energy probability distributions (SEPD), ionization and excitation are responsible for the component at high specific energies between 10^2 and 10^5 Gy (Figure 2), as expected. The SEPD obtained with the different codes are very similar; we can nevertheless identify in Figure 2b that excitation process for option 4 is responsible for higher specific energies. Regarding the attachment and vibration processes the shapes of the SEPD are also similar in the codes accounting for such processes (LPCHEM and Geant4-DNA option 2), but even so, there is a factor of about 10 between SEPD values. Attachment SEPD presents a narrow peak at $\sim 10^3$ Gy while vibration SEPD ranges from ~ 10 to 10^3 Gy. For solvation, SEPD are very close except for LPCHEM that is following electrons until thermalization. Finally, Geant4-DNA option 6 is the only code considering energy deposition through elastic scattering that leads to a broad SEPD ranging from 10^{-4} to tens of Gy.

2.4.2. Radiolytic yields at 10^{-12} s (physico-chemical stage)

The yields at 10^{-12} s result from the physical and physico-chemical stages. For 1 MeV electrons, the yield predictions for the two types of codes are rather similar and in accordance with experimental data for water irradiations (see Figure 3).

With respect to 10 MeV protons, regarding $\cdot\text{OH}$ species, its production comes from ionization, excitation, recombination and attachment processes (see appendix 2). For ionization, attachment as well as recombination processes, Geant4-DNA and LPCHEM have similar physico-chemical stages for the production of $\cdot\text{OH}$. On the contrary, Geant4-DNA favors $\cdot\text{OH}$ production in respect to LPCHEM due to the excitation process with different dissociation channels and dissociation probabilities. Therefore, Geant4-DNA is more likely to produce $\cdot\text{OH}$ species than LPCHEM per excitation process. Moreover, the probability of excitation as dominant process in Geant4-DNA option 4 is about twice as large as for other codes which explains to obtain a higher G value for $\cdot\text{OH}$ at 10^{-12} s.

The production of H_3O^+ and e_{aq}^- mainly comes from the ionization process. In this case, deviations can only be due to differences in the physical stage since the physico-chemical stages are identically simulated in the two codes. Indeed, the probability of ionization as dominant process in LPCHEM is slightly larger than the one in Geant4-DNA options which explains larger G values for this code for H_3O^+ , e_{aq}^- and OH^- at 10^{-12} s. In an opposite way, the relatively low probability of ionization as dominant process in Geant4-DNA option 6 is responsible for the lowest G values for these radicals at 10^{-12} s. It is worth noticing that H_3O^+ and e_{aq}^- yields are very close since they are produced through the same dissociative channels.

The production of OH^- essentially comes from the attachment process that is taken into account by LPCHEM and Geant4-DNA Option 2 (in the physical stage). These OH^- yields in options 4 and 6 are therefore equal to zero and the yield predicted by LPCHEM is larger than for Geant4-DNA option 2 due to a larger probability of the attachment process (see Figure 14 and Figure 15).

In general, we note that the trends of H_3O^+ , e_{aq}^- and OH^- time dependent G values are closely correlated. Indeed, H_3O^+ time dependent G value corresponds to the sum of e_{aq}^- and OH^- values.

Regarding the H_2 molecule, the two main production channels are excitation and dissociative attachment. Geant4-DNA (all options) is producing more H_2 molecules (roughly 3 times more) through excitation process than LPCHEM.

Finally, whatever the code, there is no H_2O_2 production at 10^{-12} s since no dissociative channel is encoded for this species in the physico-chemical stage.

2.4.3. Evolution of the radiolytic yields up to 10^{-6} s (chemical stage)

Overall, the evolution of the calculated yields follows the same trends for 1 MeV electrons (section 3.B.1) and 10 MeV protons (section 3.B.2). Moreover, these yields are in a rather close agreement with respect to experimental data available for 1 MeV electrons.

In comparison with the RITRACKS code for 1 MeV electrons, for all the chemical species ($\cdot\text{OH}$, e_{aq}^- , H_3O^+ , H_2O_2 , H_2 and OH^-) there is a good agreement between RITRACKS and LPCHEM. Both codes present close initial and final yields at 10^{-6} and 10^{-12} s and only differ in the yield's evolution through the chemical stage. Indeed, the yields seem to evolve more monotonically for the code RITRACKS which indicates a slower recombination process than LPCHEM. In comparison with the PARTRAC code, for the $\cdot\text{OH}$, e_{aq}^- , H_2O_2 , and H_2 species, LPCHEM and PARTRAC present similar evolution through the chemical stage which indicates a close recombination speed. In comparison with the experimental data, for the $\cdot\text{OH}$, e_{aq}^- , H_2O_2 , and H_2 species we observe a good agreement between LPCHEM and the experimental values from the work of Laverne and Pimblott ⁷⁰. For the $\cdot\text{OH}$ chemical species, we observe some deviations between LPCHEM and the experimental values from the work of LaVerne from 2000 as the yield's values at 10^{-6} and 10^{-12} s are larger for the experimental values. The evolution also appears faster for these experimental values than for LPCHEM.

For the 10 MeV protons, the C_{EV} values (relative deviations in respect to the average over the whole set of simulation codes of the evolution rates for each radical species) remained below 10% (LPCHEM). From Figure 18, we can notice similar trends in the evolution of C_{EV} . Whatever the code, C_{EV} values for H_2O_2 species remain below 5%. Geant4-DNA option 4 shows more recombination between the species due to smaller distances between energy transfer points but this is not observed in specific energy spectra in Figure 2. This could be explained by the fact that the difference in recombination happens before 10^{-8} s (Figure 17) which corresponds to short scale diffusion of chemical species (< 10 nm) remaining lower than nanometric target dimension (10 nm).

Overall, evolution rates of LPCHEM have larger values than Geant4-DNA which can be related to higher concentrations of chemical species. The specific energy spectra of LPCHEM seem to confirm this hypothesis with slightly larger spectra associated to ionization and excitation dominant processes. The relatively large H_2O_2 production at early stage in LPCHEM (before 10^{-10} s) can also be due to clusters of $\cdot\text{OH}$.

2.4.4. Computing time

The various options of Geant4-DNA lead to similar computing times for the simulation of the physical stage (see Figure 19) using sequential and multi-threaded modes. LPCHEM is always faster than Geant4-DNA, even using the multi-threaded mode. In sequential mode, the computing time ratio of Geant4-DNA ranges from 9 for one primary particle down to 4 for 1000 primary particles. This shows that the initialization time for Geant4-DNA is relatively long (close to 3 s) compared to LPCHEM. For multi-thread calculations, the gain in computing time varies from 1.5 with 10 primary particles up to 2.4 with 1000 primary particles which remains well below the ideal gain factor of 4 corresponding to the number of threads. Sub-optimal management of multi-threading may therefore be suspected due to the fact that the code is more likely not CPU-bound, but memory-bound. Finally, one can observe a slight increase of Geant4-DNA computing time per primary with 1000 primaries. This effect might be due to an increase of memory access time with a relatively large number of primaries.

The computing time of the physico-chemical and chemical stages (see Figure 20) is longer than for the physical stage by two orders of magnitude. The computing times of the various options of Geant4-DNA are very similar. In sequential mode, the computing time ratio is around 5. For 10 primary protons, one could expect an increase of computing time related to more reactions between radiolytic species of different tracks. The fact that it is not the case demonstrates the efficiency of the optimization methods implemented in the two types of codes (see section 2.A). Finally, for multi-threaded mode, Geant4-DNA is close to an ideal gain factor of 4 which might be explained by the fact that these stages are now more CPU intensive.

2.5. Conclusion

This study is the first comparison between the LPCHEM and Geant4-DNA codes for the simulation of nanodosimetry spectra in the track core as well as the production of chemical species yields for water irradiations with charged particles (10 MeV protons). The goal and the originality of this benchmark is to study the link between elementary processes, probability distributions of specific energy in nanometric targets of 10 nm (physical stage) in the track core, radical yields ($\cdot\text{OH}$, e_{aq}^- , H_3O^+ , H_2O_2 , H_2 and OH^-) at 10^{-12} s (physico-chemical stage) and radical recombination between 10^{-12} and 10^{-6} s (chemical stage). The computing times associated to the physical stage and the physico-chemical and chemical stages have also been evaluated for sequential and multi-threads execution modes.

Overall, the total specific energy spectra in nanometric targets predicted by the two codes are in very good agreement despite the significant differences observed in the probabilities of (dominant) processes. The radical yields are also in good agreement with the available data considering the relatively large experimental uncertainties. Additional measurements are definitely needed especially at early times. Nevertheless, the differences observed in the various stages of the simulations were systematically discussed in the light of the lists of physical processes, dissociative channels (physico-chemical stage) and chemical reactions of the two types of codes. In further investigations, higher LET ion beams could be considered in order to estimate the impact of large concentrations of chemical species at 10^{-12} s.

Regarding the computing time, LPCHEM is always faster than Geant4-DNA in sequential execution mode but the difference between the codes is decreasing with the number of primary particles (since the initialization stage becomes less significant) and the use of multi-threads.

This study is preliminary to the implementation of the mMKM and NanOx biophysical models into the GATE platform. These models are partially or fully based on the quantification of specific energy spectra and radiolytic species production at nanometric or micrometric scales through MCTS codes. The validation of MCTS codes is therefore of utmost importance in order to ensure that input data of the biophysical models are reliable.

Chapter 3

Cell survival predictions using mMKM and NanOx models

3.1. Introduction

In hadrontherapy treatment planning, the calculation of the relative biological effectiveness (RBE) is associated to the dose distribution. Historically, in the 1990s, the first trials for carbon ion treatments at the National Institute of Radiological Sciences (NIRS) (Chiba, Japan) used RBE calculations based on in-vitro cell responses. Since then, biophysics models have been developed in order to overcome the limitations of such empirical approaches. One the main input of these models are the specific energy distributions calculated at nano and/or micro scales by Monte Carlo track structure codes (MCTS).

The models estimate cell survival coefficients α and β for different types of ions of different kinetic energies that are used as input in Monte Carlo codes for biological dose calculations and sometimes integrated in TPS. It has been the case at the NIRS, with the development and the integration of a mMKM-based RBE dose calculation using the track structure of the Kiefer–Chatterjee model ²⁵, at the HIT (German Heavy Ion Research Center, Germany) in Germany with the integration of a LEM-based RBE dose calculation system using the FLUKA code ³³ and at CNAO (Italian National Center for Oncological Hadrontherapy) in Italy with the integration of both a LEM and mMKM-based RBE dose calculations using the FLUKA code as well. ³⁵

The Microdosimetric Kinetic Model developed by Hawkins ^{23 15}, was based on the theory of dual radiation action (TDRA) and was then refined into the Modified Microdosimetric Kinetic Model (mMKM) by the NIRS Japanese researchers ^{2 16}. In the mMKM, the surviving fraction of cells can be predicted from the specific energy deposited into a micrometric scaled volume called domain.

The NanOx model ⁴ was developed to overcome the potential shortcomings of the existing models by taking into account the impact of the energy deposition at both micrometric and nanometric scales. For that purpose, the NanOx model defines two types of damage that can impact the survival of the cells. First, the local lethal events consisting in biological events taking place at nanometric scale and can lead to cell death through severe DNA damage. Secondly, the non-local events consisting for instance in the accumulation of sub-lethal DNA damage at micrometric scale and represented by the production of chemical reactive species that induce cell oxidative stress. Each model requires MCTS calculations to define specific energy or chemical species produced in a cell nucleus.

In this PhD thesis, we consider two MCTS codes: LPCHEM ^{61 71} and Geant4-DNA ⁷². Both codes are able to perform the simulation of ionizing radiation consequences (physical, physico-chemical and chemical stages) to water. We have shown that the two codes provide good results for the simulation of specific energy spectra at micrometric and nanometric scale and time-dependent G values necessary for the NanOx and mMKM models.

In this work, we estimated the α values as function of the LET for human salivary glands (HSG) cell line with the mMKM and the NanOx model and with input data provided by LPCHEM and Geant4-DNA track structure codes. Our results have been compared to data retrieved from literature, i.e. experimental data as well as data obtained with other combinations of biophysical models and Monte Carlo codes and retrieved from literature.

3.2. Materials and Methods

We focus our study on the human tumor cells from salivary glands (HSG) cell line and its response to hydrogen, helium, carbon and oxygen ion mono-energetic beams (from 0.1 MeV/n to 400 MeV/n). The experimental α values come from the database made available by the PIDE (Particle Irradiation Data Ensemble) project ¹⁸ for helium and carbon mono-energetic beams. Errors associated to the experimental measurements have not been reported.

We first recall the parameters used in Nanox and mMKM models. For mMKM, as a prerequisite to the benchmark, we will also validate the input parameters for HSG cell line computed by LPCHEM and Geant4-DNA codes with respect to those obtained by Inaniwa et al ¹⁶. The figure of merit used for the benchmark is finally detailed.

3.2.1. NanOx parameters for HSG cell line

A detailed description of the NanOx model has been provided by Cunha et al. ⁴. Therefore, in this work, we do not detail the model framework and only focus on the descriptions of the parameters required to simulate the cell survival coefficients.

The NanOx model input parameters can be classified into two categories.

- First, parameters to calculate the effective local lethal function F are used to estimate the local lethal events contribution to the survival of the cells (equation 1). F was built assuming a monotonical increase with specific energy z deposited in local targets. The outcome of the construction procedure was close to an error-like function as describe in the work of Monini et al. ¹⁹. It consisted in deriving coefficients related to local lethal events from the representative data (experimental α values) in order to constrain F and optimize its parameters. A threshold value z_0 , a factor σ controlling the width and a function maximum h are used.

$$F(z) = \frac{h}{2} \left[1 + \operatorname{erf} \left(\frac{z - z_0}{\sigma} \right) \right] \quad (1)$$

- Secondly, the input parameters related to the estimation of the contribution of global events β_G (Gy^{-2}) is determined from the cell survival coefficient β for a reference radiation and R_{SV} (μm) is the radius of the cell nucleus. We report in Table 2 the different NanOx input parameters that have been estimated for the cell lines HSG and the LPCHEM MCTS ¹⁹.

Table 2 – NanOx input parameters for the HSG cell line and the LPCHEM MCTS.

z_0 (Gy)	σ (Gy)	h	β_G (Gy^{-2})	R_{SV} (μm)
15654	549	179439	0.096	7

3.2.2. mMKM parameters for HSG cell line

A detailed description of the mMKM has been provided by Kase et al. ² and Inaniwa et al.¹⁶, therefore in this work we will not detail the model framework and only focus on the description of the parameters required to simulate the cell survival coefficients.

For α values predicted by the mMKM model, we retrieved predictions from several works by Chen et al. ⁷³ and Russo et al. ⁷⁴ that used different MCTS and input parameters sets. We decided to use LPCHEM and Geant4-DNA track structure codes and followed the methodology of Magro et al. ³⁵ using the set of input parameters defined by Inaniwa et al ¹⁶.

The mMKM parameters are the domain radius R_d (μm), the nucleus radius R_n (μm), the constant α_0 (Gy^{-1}) that represents the initial slope of the survival fraction curve at the limit value of LET = 0 and the reference survival coefficient β that is a constant term. The reference set of parameters have been reported in Table 3 for the HSG cell lines by Inaniwa et al.¹⁶.

Table 3 – mMKM input parameters for the HSG cell line from various works.

References	R_d (μm)	R_n (μm)	α_0 (Gy^{-1})	β (Gy^{-2})
This work Inaniwa 2010 ¹⁶ and Chen et al. 2017 . ⁷³	0.32	3.9	0.172	0.0615
Russo 2011 ⁷⁴ and Furusawa et al. 2000 ⁷⁵	0.20	4.6	0.313	0.0615

As these input parameters have been determined using the track structure of the Kiefer–Chatterjee model, it is important to verify these parameters for the LPCHEM and Geant4-DNA codes. The methodology we followed was the one used for the implementation of the mMKM model in the FLUKA MC code by Magro et al. ³⁵.

The first step was to calculate the saturation corrected dose mean specific energy z_{1D}^* (Gy) (equation 2) using LPCHEM and Geant4-DNA and compare these distributions to the ones obtained by Inaniwa et al. ¹⁶

$$z_{1D}^* = \frac{l z_0^2 \int_0^\infty \left(1 - e^{-\left(\frac{y}{z_0}\right)^2}\right) f_1(y) dy}{m \int_0^\infty y f_1(y) dy} \quad (2)$$

with l the mean cord length of the domain, m the mass of the domain, $f_1(z)$, the probability density of the specific energy z deposited by a single energy-deposition event in the domain and z_0 the saturation-corrected specific energy (equation 3).

$$z_0 = \frac{\rho\pi R_n R_d^2}{\sqrt{\beta(R_d + R_n^2)}} \quad (3)$$

Then, using the z_{1D} values calculated with LPCHEM and Geant4-DNA, we could estimate the dose at 10% of survival for HSG cells (D_{10} (Gy)) as a function of the LET (see equation 4). We finally compared our results to the work of Inaniwa et al. who validated these D_{10} values using the experimental data from Furusawa et al. ¹⁶

$$D_{10} = \frac{1}{2\beta} (- (\alpha_0 + \beta z_{1D}^*) + \sqrt{(\alpha_0 + \beta z_{1D}^* - 4\beta \ln 0.1)}) \quad (4)$$

Figure 1 shows the comparison of z_{1D}^* values as a function of energy for hydrogen, helium and carbon ions. Hydrogen, helium, carbon and oxygen ions for kinetic energies up to 400 MeV/n have been simulated with LPCHEM, but only hydrogen and helium ions up to 100 MeV/n with Geant4-DNA. Figure 2 **Erreur ! Source du renvoi introuvable.** shows the comparison of the dose at 10% of survival (D_{10} (Gy)) calculated with LPCHEM and Geant4-DNA for hydrogen and helium ions as a function of the LET for HSG cell line as well as the values obtained by Inaniwa et al. ¹⁶ (using the track structure of the Kiefer–Chatterjee model) and Furusawa et al. ⁷⁵(experimental data).

Overall the z_{1D}^* values obtained with the MCTS codes (LPCHEM, Geant4-DNA) the track structure of the Kiefer–Chatterjee model are in good agreement except in the case of carbon ions. The values obtained with LPCHEM for low energy helium ions (< 1MeV/n) are slightly lower than the ones obtained with the other codes.

Regarding the D_{10} values, for the helium ion, there is a good agreement between LPCHEM and Inaniwa et al. while a slight over estimation by LPCHEM is observed for intermediate and low LET values (< 50 MeV/n). For the carbon ion D_{10} values, we observe a good agreement for relatively low LET values (< 100 keV/μm) between LPCHEM and Inaniwa et al. and Furusawa et al. while deviations appear for higher LET values (> 100 keV/μm) with an under estimation of these values by LPCHEM.

Regarding Geant4-DNA (helium ions), there is an under estimation compared to Inaniwa et al. results, though a better agreement is observed with the experimental data.

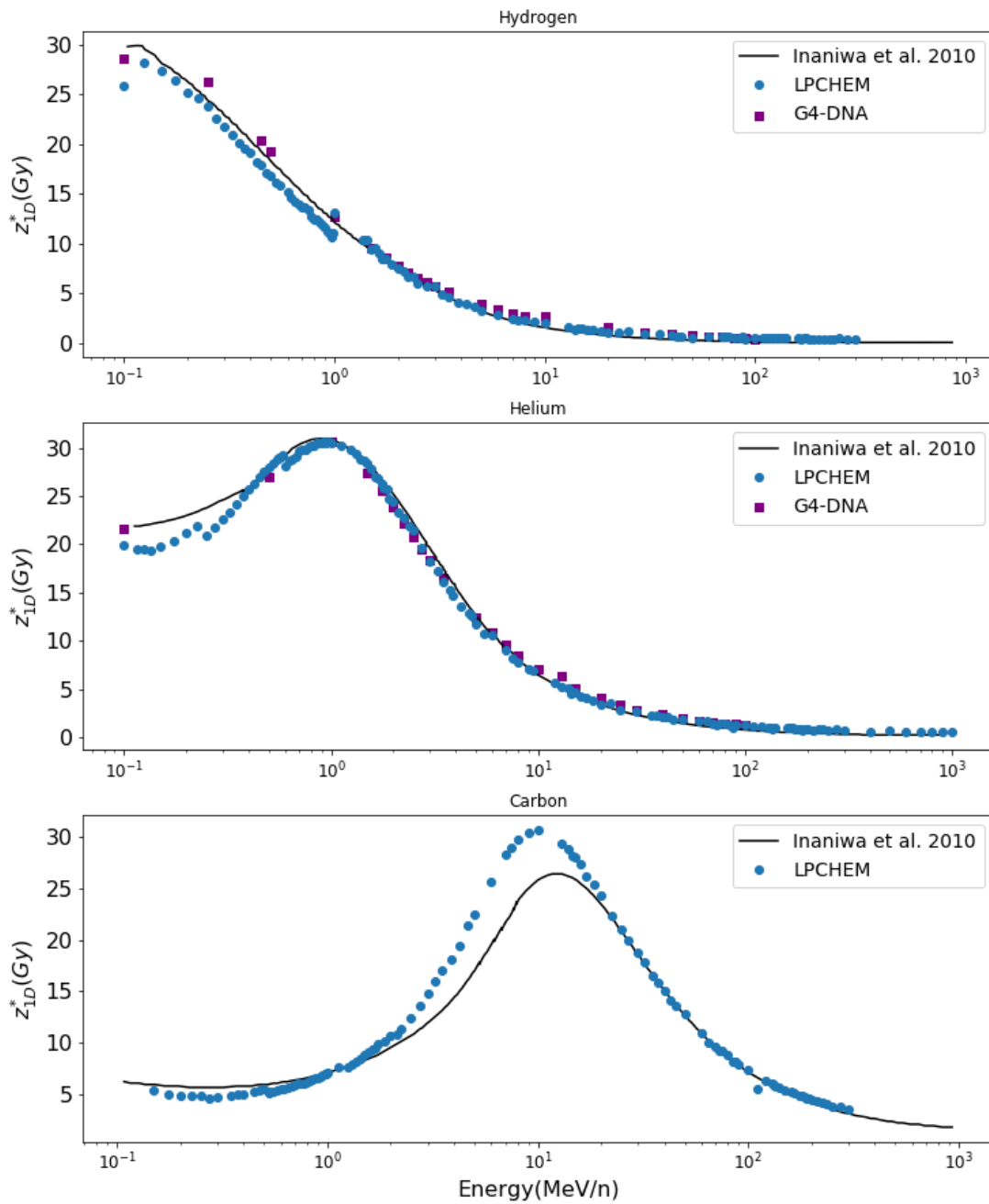


Figure 22 - z_{1D}^* values as a function of the kinetic energy of hydrogen, helium and carbon ions for HSG cells. Values from Inaniwa et al. were obtained with the track structure of the Kiefer–Chatterjee model ¹⁶.

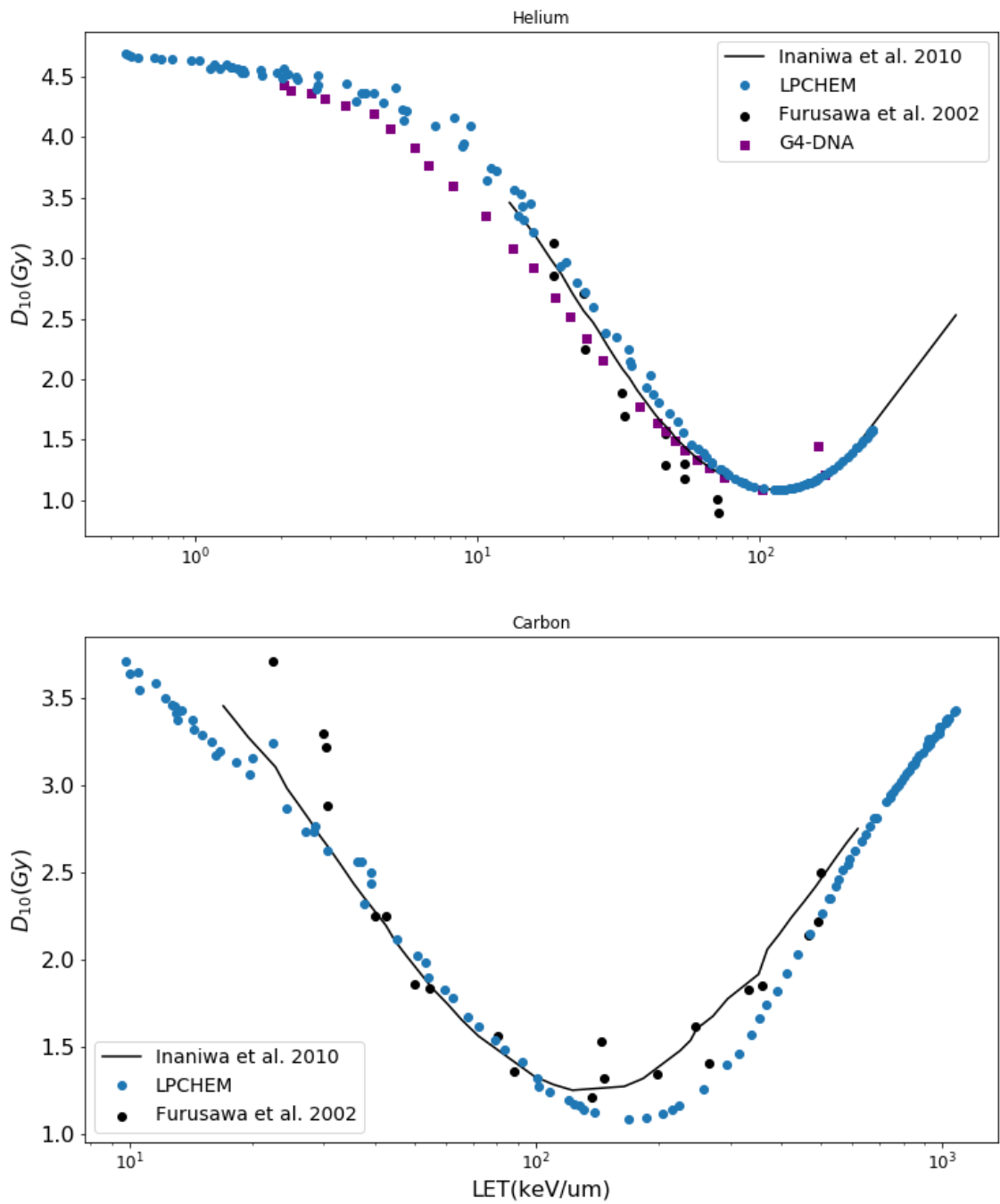


Figure 23 - D_{10} values under aerobic conditions as a function of the LET for helium and carbon beams for HSG cells: values obtained by Inaniwa et al. come from ¹⁶ (using the track

structure of the Kiefer–Chatterjee model) and the experimental data of Furusawa et al come from ⁷⁵.

3.3.3. Figure of merit

In order to benchmark the α values from our work with predictions from the literature and experimental data, we used a χ^2 estimator (see equation 5).

$$\chi^2 = \frac{1}{M} \sum_{i=1}^M \left(\frac{\alpha_{exp}^i - \alpha_{pred}^i}{\alpha_{exp}^i} \right)^2 \quad (5)$$

where M is the total number of experimental points from the PIDE database, α_{exp}^i is the i^{th} experimental α value and α_{pred}^i is the i^{th} predicted α value.

3.3. Results

Figure 24 **Erreur ! Source du renvoi introuvable.** shows predictions of α values as a function of LET for the HSG cell line in response to irradiations with hydrogen, helium, carbon and oxygen ions. The predicted α and β values are reported in the appendix for the NanOx (see appendix 3) and mMKM (see appendix 4) models.

- Concerning carbon ions, α values reproduce the PIDE experimental data trend for all authors.
- Concerning helium ions, α values calculated with the NanOx model are in close agreement with the PIDE experimental data. mMKM predictions from Russo et al. ⁷⁴ and Chen et al. ⁷³ give close predictions except between 50 and 70 keV/ μm . Geant4-DNA leads to the highest discrepancies to the PIDE experimental data.
- Concerning hydrogen ions, there is no experimental data nor predictions available in literature to compare our work with. mMKM predictions, calculated with either LPCHEM or Geant4-DNA, and the NanOx model predictions lead to close results up to 25 keV/ μm . For higher LET values, NanOx model gives higher values than mMKM.

- Concerning oxygen ions, there is no experimental data nor predictions available in literature to compare our work with. NanOx and mMKM models using LPCHEM give close α values.

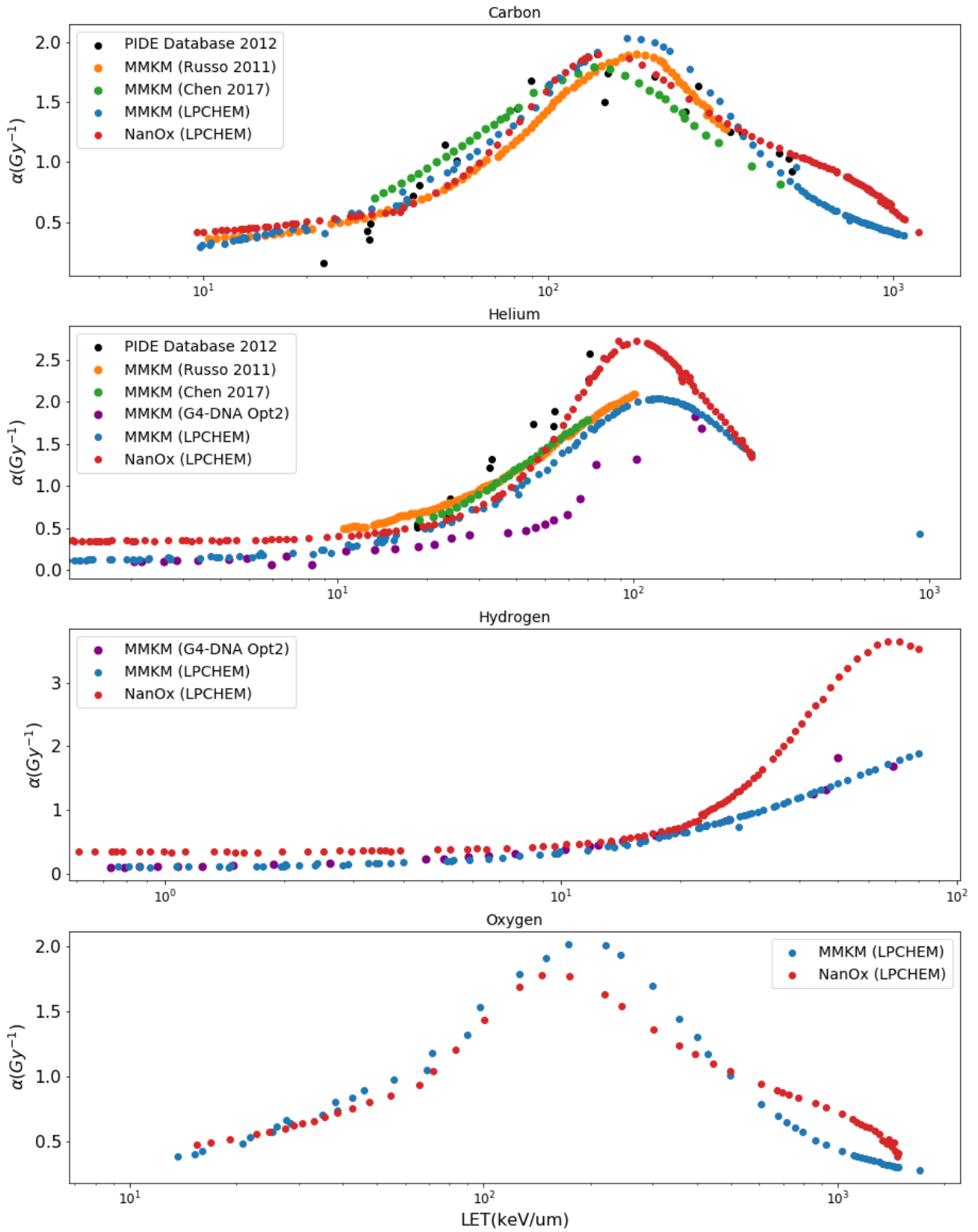


Figure 25 - predictions of α values as a function of LET for the HSG cell line in response to irradiations with carbon, helium, hydrogen, oxygen ions. α values predictions for NanOx and mMKM models.

3.4. Discussion

3.4.1. Validation of the mMKM input parameters for HSG cell line

For the validation of the mMKM parameters we chose to follow the methodology from the work of Magro et al.³⁵ by comparing our results for the z_{1D}^* values as a function of energy and for the dose at 10% of survival to the work of Inaniwa et al.¹⁶

The z_{1D}^* values estimated with LPCHEM display discontinuities, at 1 MeV/n for hydrogen ions, 0.2 and 0.6 MeV/n for helium ions and 0.4 MeV/n and 1 MeV/n for carbon ions. These discontinuities are expected as the LPCHEM code does not model the charge increase nor decrease processes⁵⁸ unlike Geant4-DNA and therefore an effective charge is chosen for each kinetic energy. These effective charge values are chosen in order to have less than 10% of relative variation between LPCHEM and reference (SRIM) LET.

We observe a good agreement between the LPCHEM and the Geant-4-DNA code. It is expected as in the Chapter 2 of this PhD work, we benchmarked the two codes for the simulation of the specific energy distributions in micrometric and nanometric targets and we concluded that for the total specific energy spectra in sensitive volumes at such scale, the two types of codes are in very good agreement despite a few disparities due to different cross sections in their physics models. Concerning the results of Inaniwa et al.¹⁶, they were obtained with a radial dose approach, the track structure of the Kiefer–Chatterjee model. The radial dose is defined as the averaged local dose deposited by a single ion in an infinitely thin hollow cylinder whose axis corresponds to the ion trajectory. The radial dose being an averaged quantity, it leads to neglecting the stochastic nature of the radiations. Despite such an approximation and a few disparities, the values obtained with the two MCTS and the Kiefer–Chatterjee model present similar trends. To our knowledge, the present work is the first study of the impact of track calculations on microdosimetric quantities and on prediction of the mMKM model. Elsässer et al. proposed a similar study with LEM⁷⁶ but their methodology was significantly different since

the LEM estimates cell damage through dose deposition at nanometric scale, which is estimated by means of the radial dose approach.

The general good agreement between the z_{1D}^* and D_{10} values obtained with LPCHEM and Geant4-DNA and the ones of Inaniwa et al. validates the use of LPCHEM and Geant4-DNA for the production of input data for mMKM with the reference set of parameters of Inaniwa et al. for estimating the input parameters in mMKM.

3.4.2. Comparison of α values estimated with NanOx and mMKM using LPCHEM and Geant4-DNA

We observe a good agreement at low and intermediate LET values (<200 keV/um for carbon ions, <40keV/um for helium ions, <20keV/um for hydrogen ions and <400 keV/um for oxygen ions), while at higher LET values for the same ions, the NanOx predictions are larger than the mMKM predictions. These similarities at low and intermediate LET and differences at high LET values depend not only on their difference in mathematical formalisms but also on the experimental data that were used to constraint the models.

Firstly, concerning the mathematical formalisms, the mMKM and NanOx models have a similar approach based on the analysis of the combined effect of lethal and sublethal lesions created within nanometric and/or micrometric sensitive volumes and the fact that the stochastic nature of the radiation is taken into account. In the case of the comparison of the α values, we focus on the models ability to predict the lethal lesions for which the main observable is the specific energy deposition in these sensitive volumes. In both models, the sensitive volumes are modeled as cylinders, which however are of different dimensions. In the mMKM model, the diameter of the targets is chosen as the distance a sub-lethal lesion can travel through the nucleus before being repaired. The domains represent the compartments of a typical mammalian cell which is estimated to have around several hundred domains, each with a diameter of 0.5 to 1.0 μm .²³ In the NanOx model, the targets are defined as volumes of 10 nm of radius and length, dimensions chosen to represent direct DNA damage (such a DSB) and consider the diffusion of chemical reactive species.

Such differences in the target size can explain the fact that mMKM leads to lower α values than the NanOx model for high LET values. Indeed the smaller the target region, the larger the maximum specific energy in the ion track core (with high density of energy depositions).

Secondly, the experimental data used to constraint the models predictions are different. Some α values from the PIDE database have been used as constraints for the lethal function in NanOx, while for the mMKM model the α values extracted from the survival fractions measured in the work of Furusawa et al.⁷⁵ have been used for the input parameters. At equivalent LET values, the experimental data used for NanOx and mMKM are close at low and intermediate LET values, while at high LET values the experimental values are larger than the ones used for the mMKM model, which is the potential second explanation of mMKM model giving lower α values than the NanOx model for high LET values.

For the mMKM α predictions resulting from the Geant4-DNA code, as said in the Chapter 2 of this PhD work, we benchmarked the two codes for the simulation of this observable and we concluded that for the total specific energy spectra in sensitive volumes at such scale, the two types of codes are in very good agreement. It explains why for the mMKM predictions for the α values with the LPCHEM and Geant4-DNA codes are superimposed for the hydrogen ions.

3.4.3. Comparison of α values with the literature

In the case of the mMKM values retrieved from the literature, these predictions have been calculated either with different MCTS or track structure model or different input parameters. For the predictions from the work of Chen et al.⁷³ in 2017, the mMKM predictions have been calculated with the Kiefer–Chatterjee MCTS model, similarly as for the work of Inaniwa et al.¹⁶ in 2010 that we are also using for our work, as reported in Table 3.

For the predictions from the work of Russo et al., Geant4 has been used for the simulation of the deposited energy but with a set of parameters from the work of Furusawa et al.⁷⁵ in 2000 which differs from our choice of parameters. Yet even with a different set of parameters, we also observe a good agreement between their results and the rest of the predictions by the mMKM model.

In order to provide a better comparison between the models predictions and to estimate the agreement of the predictions with the experimental data, a χ^2 calculation was performed for the carbon and helium ions. It is reported in **Erreur ! Source du renvoi introuvable..**

Table 4 - χ^2 calculation for carbon, helium and neon ions comparing the NanOx and mMKM models predictions to the PIDE experimental data. MCTS: Monte Carlo Track Structure code.

TS model: Track Structure model.

Labels in Figuresq				Ion types
--------------------	--	--	--	-----------

	Biophysical models	MCTS or TS model	Sets of parameters	Carbon	Helium	Neon
NanOx (LPCHEM)	Nanox	LPCHEM	Monini 2020	0.022	0.045	0.034
mMKM (LPCHEM)	mMKM	LPCHEM	Chen 2017	0.031	0.032	0.032
mMKM (G4-DNA)		G4-DNA			0.056	
mMKM (Chen 2017)		Kiefer-Chatterjee model		0.019	0.027	0.014
mMKM (Russo 2011)		G4-DNA	Russo 2011 (Furusawa 2000)	0.024	0.040	0.010

There are only little experimental values and for a limited number of ions: 12 values for carbon ion predictions, 10 for helium ion and 15 for neon ions, which makes it difficult to properly determine which model and which set of parameters among all the mMKM results could be considered closer to experiments only based on these χ^2 values. The need for additional experimental measurements for such a comparison are definitely needed. However, despite the disparities the models present rather small χ^2 values and close to one another, which quantifies the good agreement between the models.

Therefore, our study shows that our predictions using NanOx or the mMKM models with the LPCHEM and Geant4-DNA codes gave satisfactory results in agreement with the literature, considering the wide dispersion of the experimental data.

3.5. Conclusion

In conclusion, the NanOx and mMKM predictions for the HSG cells with input data provided by LPCHEM and G4-DNA for the carbon and helium ions give results that are considered in good agreement with the experimental data. As for the hydrogen and oxygen ions, even though there is no available experimental data, we observe a coherence between the results of both the NanOx and mMKM models, with LPCHEM and Geant4-DNA codes. These survival coefficient predictions are therefore stored in databases that will be used as input for the Biodose Actor in Gate.

Chapter 4

Estimate of the biological dose in hadrontherapy with GATE: development and validation of the BioDose actor

4.1. Introduction

Treatment Planning Systems (TPS) are software with fast calculation performances. They have been developed to maintain their performances while improving the accuracy of their analytical algorithms for dosimetry planning. However, there are still limits, especially using ions, to take into account heterogeneities. Monte Carlo codes can overcome such limits. Despite being more time consuming than analytical algorithms, they are more accurate for planning doses in radiation therapy. Such codes consider tumor heterogeneity by modeling specific material properties, electron density, mass density, ionization potential, etc. ⁷⁷ Consequently, Monte Carlo toolkits have been used for medical applications. In hadrontherapy, some of these toolkits are used to provide an RBE-weighted dose using databases of survival fraction coefficients predicted through biophysical models. For example the Monte Carlo code FLUKA ³² has been coupled with the LEM biophysical model ³³ and is now adopted in the Heidelberg Ion-Beam (HIT) center in Germany and in the National Center for Oncological Hadrontherapy (CNAO) center in Italy to support validation/improvement of both dose and RBE-weighted dose calculations performed by the analytical TPS ³⁴. FLUKA has then been also coupled with the mMKM model ³⁵. Among the existing Monte Carlo toolkits for medical applications, GATE is an open-source toolkit based on the GEANT4 Monte Carlo code. The platform has been validated for clinical use in the field of light ion beam therapy and it is currently used in different clinical centers as the independent tool for dose calculation in the proton therapy center at the Christie NHS Foundation Trust (Manchester, UK) and in the MedAustron Ion Therapy center (Wiener Neustadt, Austria) ⁷⁸. Recently, GATE has been validated for proton pencil beam scanning therapy ⁷⁹. The next step in the development of the platform for hadrontherapy applications is to estimate the biological quantities (cell survival fractions, biological dose and RBE) for hadrontherapy treatments. Therefore, we considered the implementation of the

BioDose actor based on the biophysical models mMKM and NanOx to predict, at a voxel scale, biological outcomes when treating a patient with ion beams, typically protons and carbon ions.

First, in this study, we describe the mathematical formalism of the BioDose actor. Secondly, we present some tests of validity. Finally, we estimate cell survival fractions, biological doses and RBE for the 67.4 MeV/n helium pre-clinical beam line from ARRONAX (Nantes, France) and the 320 and 290 MeV/n carbon-ion clinical beam line from HIMAC/ HIBMC (Japan).

4.2. Material and methods

4.2.1. Implementation of the BioDose actor

4.2.1.1. Prediction of cell survivals for Spread Out Bragg Peaks (SOBP)

The BioDose actor aims at calculating biological quantities at the voxel scale in CT-scan based geometry (typically a patient CT-scan) imported into a GATE application. Therefore, the actor has to be attached to the voxelized volume of interest taking into account the matrix resolution and position within the coordinate system. Each voxel of the matrix is indexed and recovers energy deposited by incoming ions and nuclear fragments. Cell survival fractions $S_{mix}(D)$ are then predicted as a function of the dose D , using the parametrization of the Linear Quadratic (LQ) model:

$$S_{mix}(D) = e^{-(\alpha_{mix}D + \beta_{mix}D^2)} \quad (1)$$

$$\alpha_{mix} = \sum_t \sum_i f_{t,i} \alpha_{t,i} \quad (2)$$

$$\sqrt{\beta_{mix}} = \sum_t \sum_i f_{t,i} \sqrt{\beta_{t,i}} \quad (3)$$

with α_{mix} and $\sqrt{\beta_{mix}}$ are respectively the mean values of $\alpha_{t,i}$ and $\sqrt{\beta_{t,i}}$ weighted by the deposited dose fraction $f_{t,i}$, where $\alpha_{t,i}$ and $\beta_{t,i}$ are the coefficients associated to the ion type t and kinetic energy i (approximation proposed by Kanai *et al.*⁸⁰)

Fractions $f_{t,i}$ (see equation 4) are defined as the ratio between the total deposited energy in the voxel ($Edep$) and the deposited energy by ions of type t and kinetic energy i . ($Edep_{t,i}$):

$$f_{t,i} = \frac{Edep_{t,i}}{Edep} \quad (4)$$

When α and β coefficients are not available in the data base for a given kinetic energy a linear interpolation is performed.

This “Kanai approximation” has been tested and adopted by the Japanese researchers at the NIRS (National Institute of Radiobiological Sciences, Chiba, Japan) who obtained satisfactory results in 1999⁸¹. The approach has then been adopted by the GSI (German Heavy Ion Research Center, Germany) in Germany starting in 2000¹ and the HIT (Heidelberg Ion-Beam center) in Germany as well.

4.2.1.2. Biological dose and RBE

Biological dose and RBE are then deduced from the calculated survival fractions. In order to do so, we first express the survival fraction using the α_{ref} and β_{ref} coefficients estimated with a reference X ray beam , an expression that includes the biological dose D_{bio} .

$$S_{mix}(D_{bio}) = e^{-(\alpha_{ref} D_{bio} + \beta_{ref} D_{bio}^2)} = S_{mix}(D) = e^{-(\alpha_{mix} D + \beta_{mix} D^2)} \quad (5)$$

By solving this second-degree equation, we calculate the D_{bio}

$$D_{bio} = \frac{-\alpha_{ref} + \sqrt{\alpha_{ref}^2 + 4\beta_{ref}(\alpha_{mix} D + \beta_{mix} D^2)}}{2\beta_{ref}} \quad (6)$$

With the estimation of the biological dose, we estimate the RBE (equation 13), the ratio between the biological dose D_{bio} and the physical dose D .

$$RBE = \frac{D_{bio}}{D} \quad (13)$$

4.2.1.3. BioDose actor algorithm

Figure 26 shows a diagram describing the algorithm of the BioDose actor. The input files (ASCII files) are the databases of survival fraction coefficients α and β calculated with the chosen biophysical models. These databases currently are built with pre-calculated coefficients associated to HSG, SQ20B, V79, CHO-K1 cell lines. As output, we obtain an ASCII file that reports for each voxel of the irradiated volume: the index, the (x, y, z) coordinates, the α_{mix} value (Gy^{-1}), the β_{mix} value (Gy^{-2}), the physical dose (Gy), the biological dose (Gy), the RBE value.

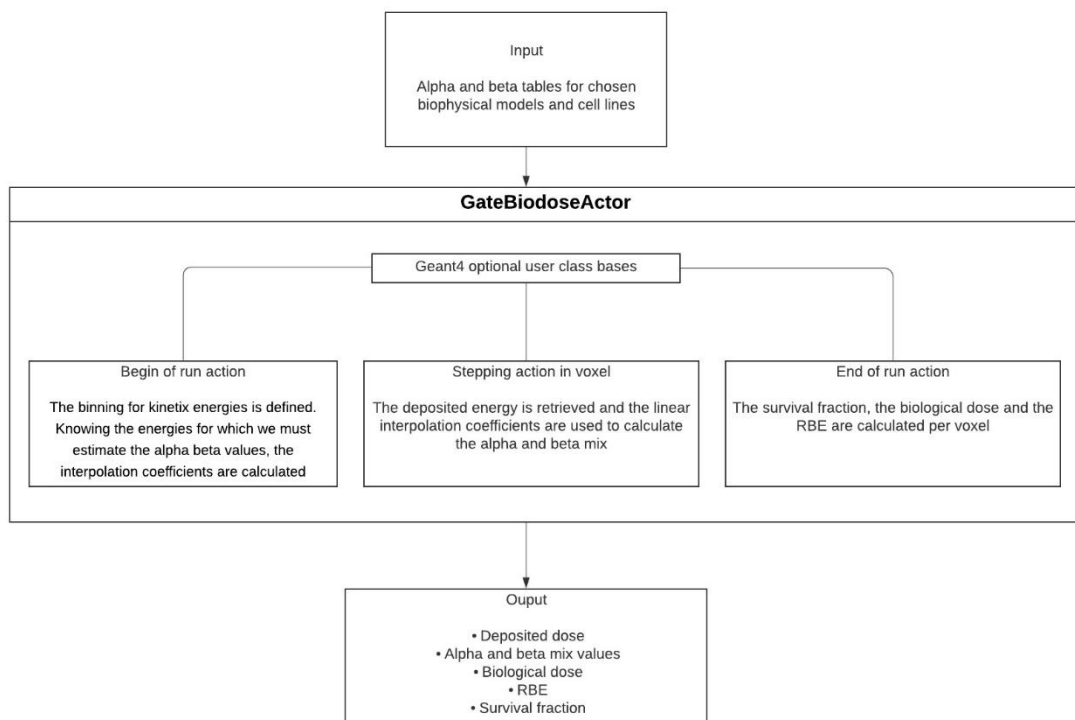


Figure 26 – BioDose actor algorithm

However, as the voxel size can be millimetric or sub millimetric, the BioDose actor uses C++ maps to store and exploit data. Maps are associative containers that store elements formed by a combination of a key value and a mapped value. Maps provide several advantages over objects such as lists, arrays and vectors as they are internally represented as binary search tree. Therefore, data insertion, deletion and access are fast and proportional to $\log(n)$ where n is the

number of elements in the map. The three maps involved in the BioDose actor are reported in Table 4 **Erreur ! Source du renvoi introuvable.**

Map name	Key value	Mapped value
InterpolationCoefficientsMap	A pair with the atomic number Z of the ion and its kinetic energy i	Pairs of coefficients a_i, b_i (for α coefficients), c_i, d_i (for β coefficients) for each kinetic energy interval $[E_{kin_i}, E_{kin_{i+1}}]$
DepositedEnergyMap	Index of the voxel	Deposited dose in voxel
AlphaBetaMixValuesMap	Index of the voxel	The calculated α_{mix} and $\sqrt{\beta_{mix}}$ values for each voxel

Table 4 - Key and mapped values of the three maps in the BioDose actor.

4.2.2. Validation tests

4.2.2.1. Dose computing

The accuracy of the calculations performed by the BiodoseActor depends on both an accurate computation of the dose and an accurate application of the mathematical formalism. Therefore, for the technical validation of the BiodoseActor, we performed tests in order to evaluate both of them.

The dose calculation in the BiodoseActor has been implemented using the same methodology as for the DoseActor. The first test is aiming to verify that the BiodoseActor provides the same dose output as the DoseActor. We compare the energy deposition estimated by the two actors for each voxel of a 320 MeV/n carbon ion mono energetic beam and a SOBP in a water phantom of 250 mm of depth. Figure 27 shows the comparison between the dose deposition for a mono energetic (on the left) beam and SOBP (on the right) calculated by the BioDoseActor (red curves) and the DoseActor (black curves) as a function of the depth. We obtained exactly the same outputs for both configurations within the statistical error bars.

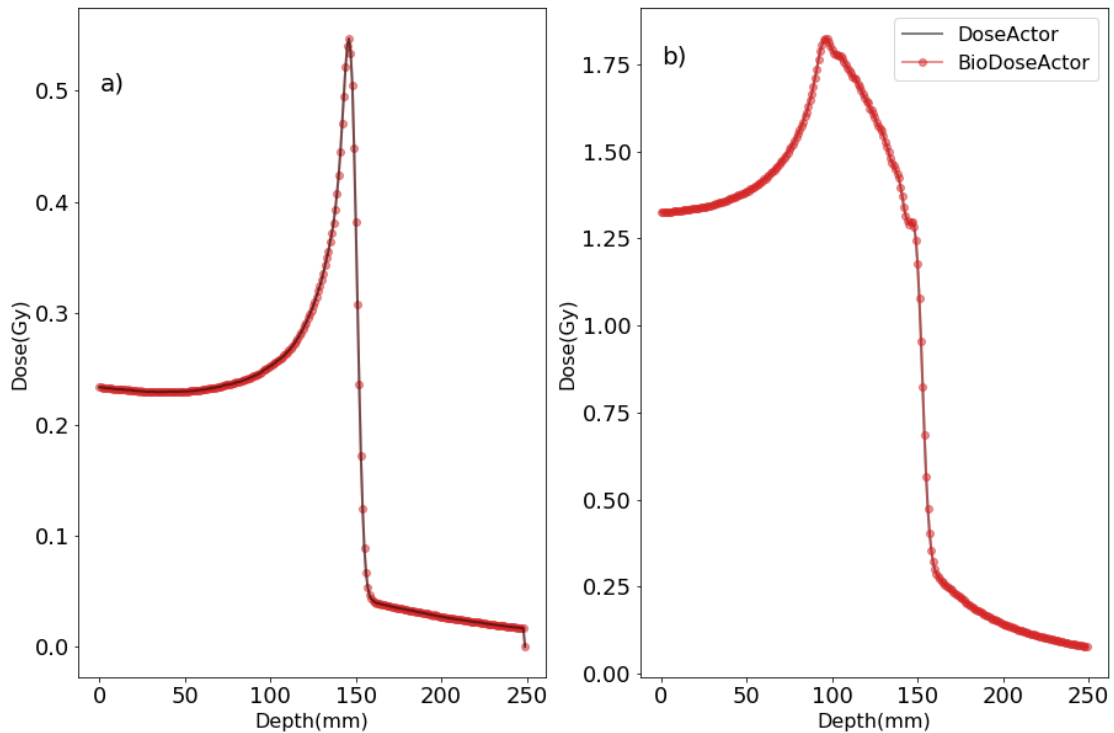


Figure 27 - Deposited dose calculation with the DoseActor (black curve) and the BioDoseActor (red dots) for a mono-energetic beam (a) and a SOBP (b)

4.2.2.2. Geant4 simulation settings

The accuracy of the BioDose actor depends on the appropriate setting of the Geant4 parameters in the simulations. We considered the cuts, production thresholds for secondary particles (gammas, electrons and positrons) and the step size.

Concerning particle cuts, we chose high values (1m for gamma, electron and positron) in order not to generate any secondary electrons in the simulation of the irradiation (the whole energy loss must be associated to ions to apply biophysical models such as mMKM or NanOx).

The step size limitations are related to the approximation of constant ion energy (hence constant LET) along every step that allows the assignment of a given pair of α and β coefficients to each step. In Geant4, there are different ways to artificially limit the step size. We decided to explore two different step limitation options. The first one is the StepLimiter option that imposes a fixed step size that is applied to all steps. The second option is the StepFunction, which does not

allow the stopping range of the particle to decrease more than a ratio α_R along the step to the lowest possible value called the final range ρ_R .

Small cut values and small step sizes lead to an increase of the computing time. Therefore, we looked for a compromise between accuracy and computing time. In this study, we tested different step limiters: 100 μm , 10 μm and 1 μm , as well as one parametrization of the StepFunction with ratio $\alpha_R = 0.01$ and final range $\rho_R = 1 \mu\text{m}$.

Since the biological effect is closely related to LET, we applied the following criterion to determine the step size limitation: a mean relative variation of LET (DEDX variation) below 1% per step. Figure 28 shows DEDX as a function of kinetic energy (a) and target depth (b).

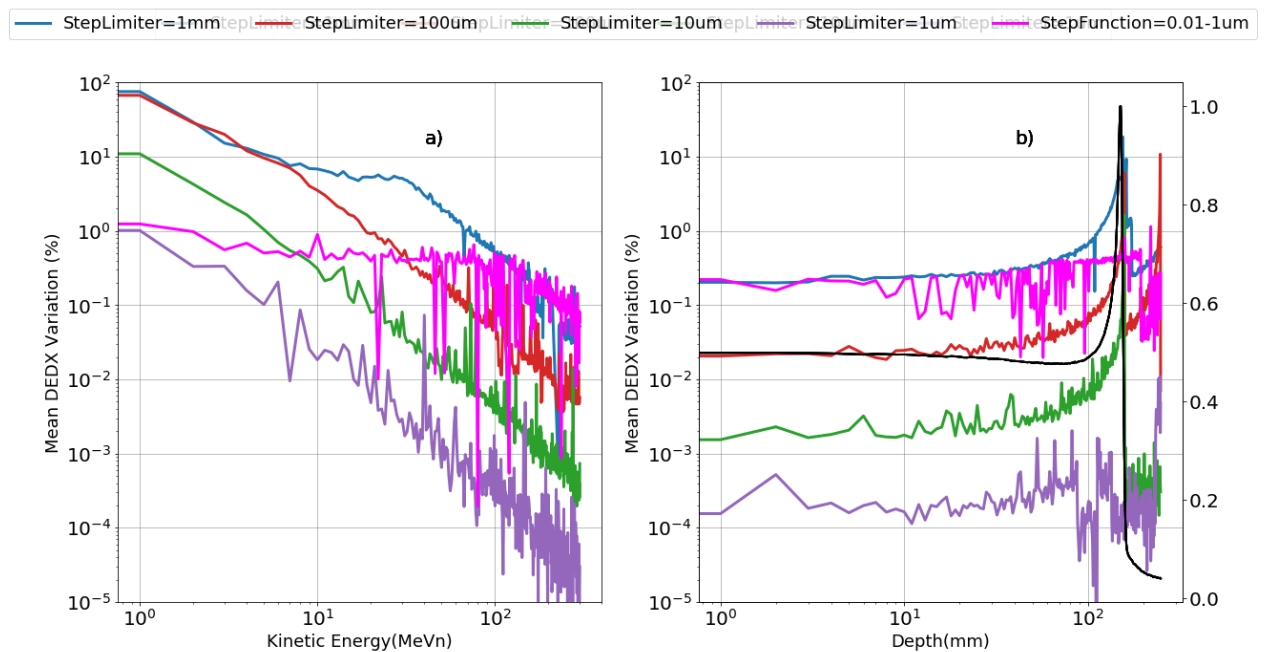


Figure 28 – Mean relative variation of LET (%) for different step parametrization as a function of kinetic energy and depth.

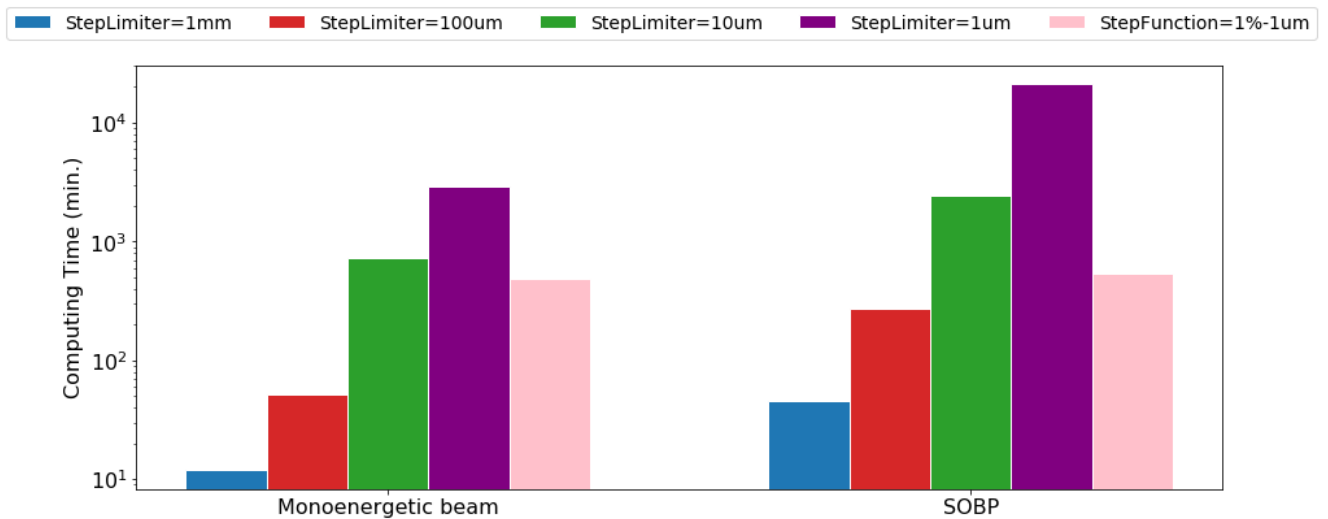


Figure 29 - Computing times in minutes for a monoenergetic beam and a SOBP with different step limitations.

In Figure 29, we compared the computing times for a monoenergetic beam and a SOBP with different step limitations. The simulations have been performed on a two Intel Xeon CPU E5-2623 v4 (4 cores, 10240 KB Cache, 2.60 GHz). As expected, the computing time increases when the step limiter size decreases. However, it is interesting to note that using the step function with the set of parameters $\alpha_R = 0.01$ et $\rho_R = 1 \mu\text{m}$, we obtain a considerably lower computing time than with the $1\mu\text{m}$ step limiter even though these two parametrizations fulfil the specifications.

4.2.2.3. Statistical fluctuations

Another source of uncertainty for the BioDoseActor predictions comes from statistical fluctuations. In order to quantify these fluctuations, we simulate 30 SOBP of 10^6 carbon ions for each step parametrization. The standard deviations of the mean values (physical dose, biological dose, coefficient α_{mix} and RBE) is calculated for each target depth as shown in Figure 30.

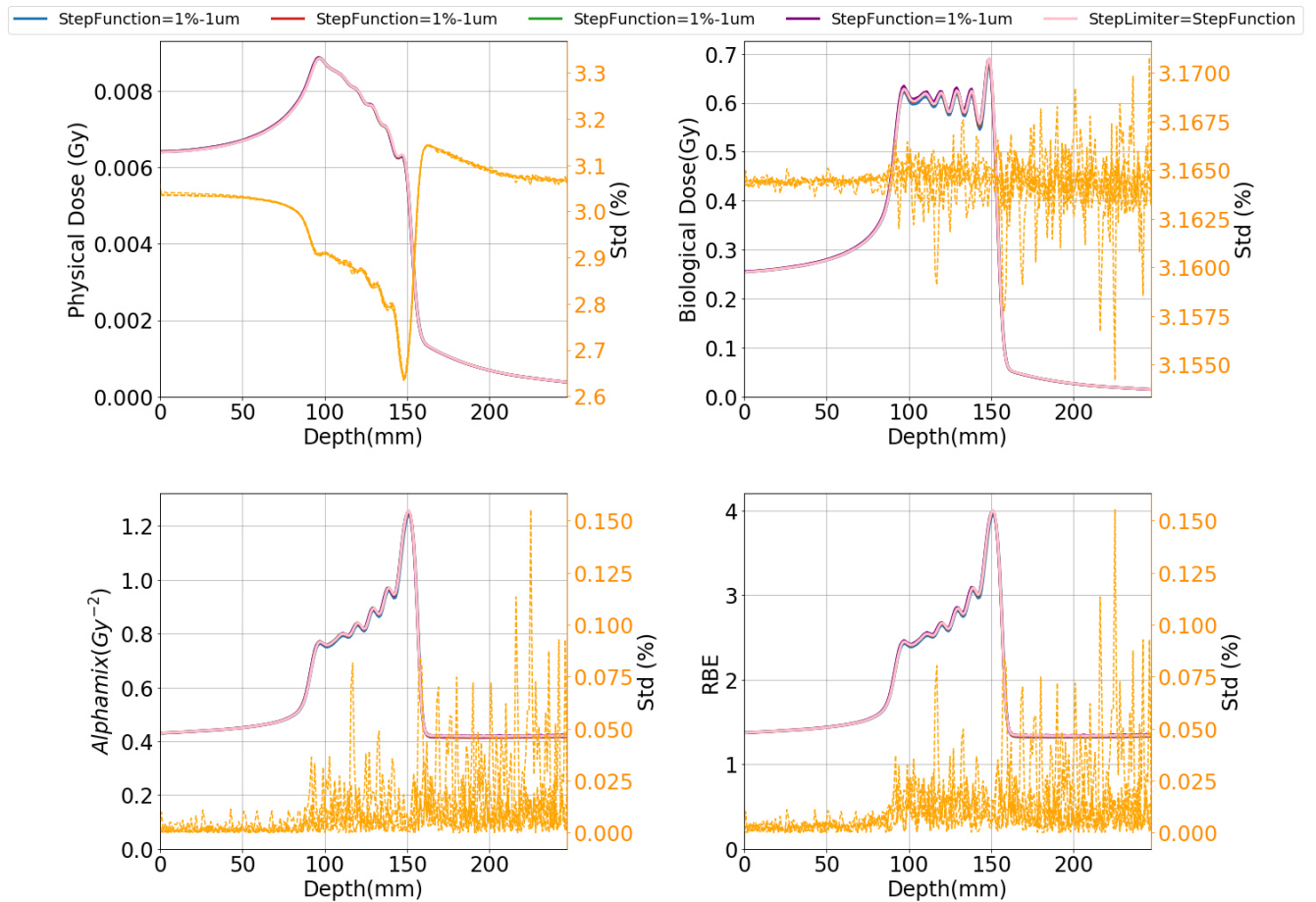


Figure 30 - Standard deviation of means values (physical dose, biological dose, coefficient α_{mix} and RBE) for 30 SOBPs of 10^6 particles using different step parametrizations.

For 30 SOBPs of 10^7 particles, standard deviations of the mean values are of the order of 3% for physical and biological doses and below 1% for the coefficient α_{mix} and the RBE.

4.2.3. Estimate of cell survival fractions, biological doses and RBE for carbon and helium beam lines using GATE

4.2.3.1. HIMAC AND HIBMC clinical beams

The Heavy Ion Medical Accelerators in Chiba (HIMAC) and in Hyogo (HIBMC) have been used to irradiate different cell lines in order to estimate the biological parameters (alpha and beta values). We decided to model a simplified version of these beam lines as shown in Figure 31. The geometrical set up has been reproduced according to the literature^{81 82 83}. The geometry has been validated by comparing the dose deposition with the dose reported in the literature. In

the work of Kagawa et al. ⁹, the survival fraction and the biological dose have been measured for HSG cell line irradiated with a 320 MeV/n SOBP in HIBMC. We reproduced the experience by irradiating a phantom of water with a dose of 2.4 Gy at the isocenter of the SOBP.

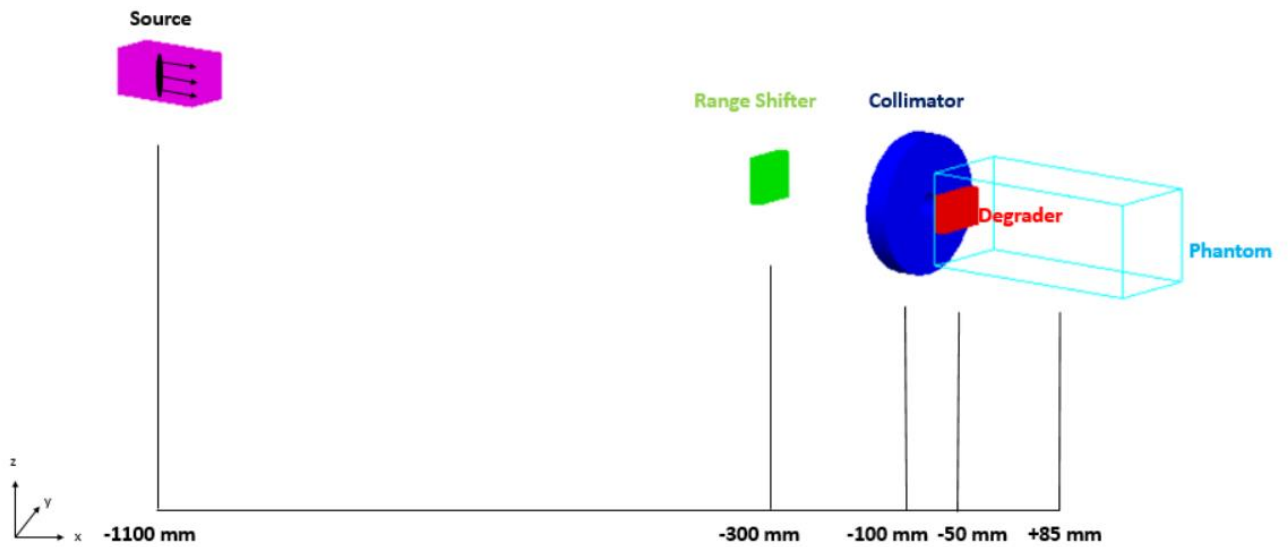


Figure 31 –HIMAC/HIBMC clinical beam line modeled with GATE.

4.2.3.1.1. Source and phantom

As we combined the HIMAC and HIBMC lines into a simplified version of both, the ions and energies simulated for this study are the ones used in the database of experimental values from the literature: 190 MeV/n protons, 320 MeV/n and 290 MeV/n carbon ions. In

Table 5 **Erreur ! Source du renvoi introuvable.** are listed the characteristics of the sources for each energy and each ion used in this study.

In order to reproduce the experimental measurements settings, we model the 290 MeV/n carbon ion and 190 MeV/n protons beam source with a radius of 7.5 cm as in the work of Kagawa et al. ⁹, the field irradiation size is 15 cm x 15 cm. The irradiated HSG cells were irradiated attached to a flask wall and encompassed in a 7 cm x 15 cm irradiation field. We then model

the 290 MeV/n carbon ion beam source with a radius of 5.5 cm as in the work of Inaniwa et al.³. The irradiation field has a size of 10 x 10 cm². The irradiated HSG cells were then placed in a target volume of 10 cm x 6 cm. In order to cover both experiments, we chose to model the phantom as a box with a section of 15 x 15 cm. The deepest pristine peak's position in the phantom is 250 mm and 220 cm for 320MeV/n carbon ions and 190 MeV protons, respectively. The phantom is then split along the z-axis in 1 mm slices. The phantom is therefore constituted of 250 bins.

	320 MeV/n Carbon	290 MeV/n Carbon	190 MeV/n Proton
Particle	Carbon	Carbon	Proton
Energy	3840 MeV	3480 MeV	190 MeV
Energy distribution type	Gauss		
Sigma Energy	40 MeV	40 MeV	1 MeV
Radius of the source	7.5 cm	5.5 cm	7.5 cm
Phantom shape	Box		
Phantom dimensions	150 x 150 x 250 cm ³		
Resolution and voxel size	250 slices of 1 mm in depth		

Table 5– Source and phantom parameters for the HIMAC/HIBMC simulation in GATE.

4.2.3.1.2. Physics list and cut values

4.2.3.1.3. Simulation of the SOBP

We chose the QGSP_BIC_HP physicslist as recommended in the field of hadrontherapy. Regarding secondaries production, we applied relatively high cut values to prevent any secondary electron generation (as mentioned in section 4.2.0).

Gamma	1m
Electron	1m
Positron	1m

Table 6 – Cut values for gamma, electron and positron

The SOBP is made by inserting in the beam a ridge filter made of aluminum (light material in order to reduce ion scattering). Its design intends to provide a uniform biological dose over the SOBP, i.e. a constant survival fraction of HSG cells in our case ⁸⁴. Unfortunately, no information on the number and the weight of the monoenergetic beams and the different thickness values of the ridge filter is available in literature. Therefore, we performed a non-negative least square regressing using python in order to determine the closest parameters to be able to reproduce the SOBP. As input, we used the depth-dose deposition for each ion beam ²⁵ ^{9 16} and obtain the weight values reported in Table 7 for each beam.

320 MeV/n Carbon		290 MeV/n Carbon	
Shifter thickness	Weight	Shifter thickness	Weight
6mm	1	0 mm	0.35
10mm	0.30	6 mm	1
12mm	0.23	7 mm	0.2
15mm	0.31	8 mm	0.15
18mm	0.24	11 mm	0.74
20mm	0.12	14 mm	0.079
22mm	0.042	15 mm	0.28
23mm	0.24	17 mm	0.22
26mm	0.065	19 mm	0.24
27mm	0.16	21 mm	0.053
29mm	0.061	23 mm	0.29
31mm	0.094	26 mm	0.14
32mm	0.16	30 mm	0.2
33mm	0.0053	32 mm	0.023
		34 mm	0.12
		36 mm	0.38

Table 7 - Range shifter thicknesses and pristine peaks weight values for the simulation of the HIMAC/HIBMC SOBP using GATE.

4.2.3.2. ARRONAX beam line

The Accelerator for Research in Radiochemistry and Oncology at Nantes Atlantique (ARRONAX), is a pre-clinical beam line used for radionuclide production in nuclear medicine

and for radiolysis and radiobiology studies. In Figure 8 is represented the schematic layout of the beam modeled with the GATE platform.

The IP2I laboratory has conducted experimental irradiations of SQ20B cells with 67.4 MeV helium beam in September and December 2019 at several position in the SOBP. We reproduced the experimental set up by irradiating a liquid water phantom with a 1 Gy dose at the isocenter of the SOBP. Then, we calculated the survival fractions at 600, 800 and 1000 μm in depth in the central axis of the SOBP. We also calculated the biological dose and RBE for the whole SOBP.

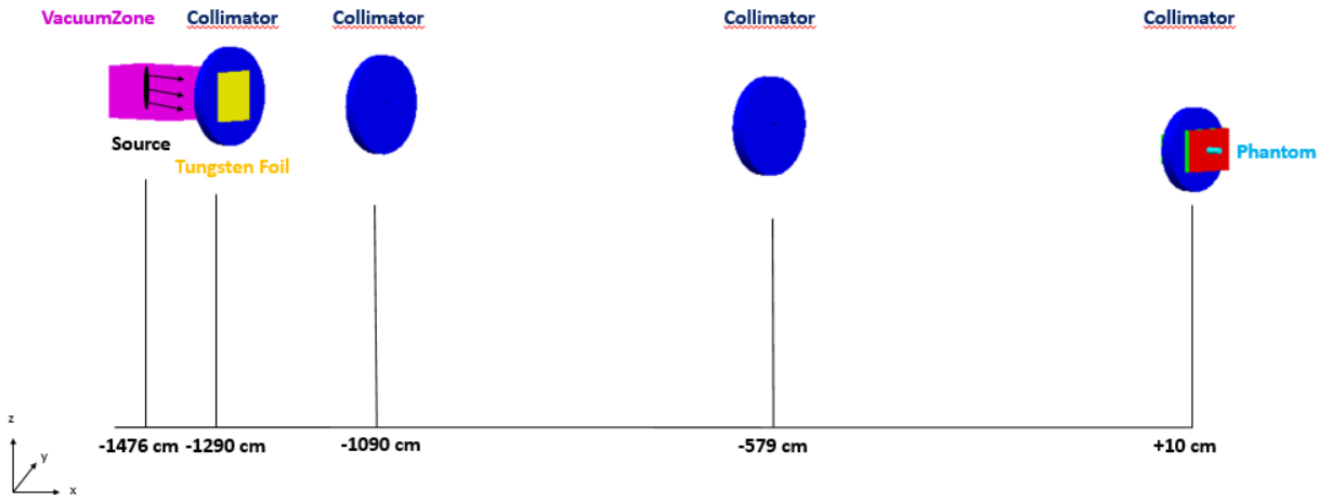


Figure 5 –ARRONAX pre-clinical beam line modeled with GATE

4.2.3.2.1. Source and detector

The SQ20B cell irradiation was performed using a 67.4 MeV Helium ion beam. In the experimental setting, box containing 24 cell wells have been irradiated. In the simulation, we decided to model the irradiation of one cell well only. It is represented by a phantom of water with the shape of a cylinder of 3.3 mm in diameter and 15 mm in depth, split along the x-axis in 5 μm slices. The phantom is therefore constituted of 3000 bins. We report the source and phantom characteristics in Table 8.

Particle	Helium
----------	--------

Energy	67.4 MeV
Energy distribution type	Gauss
Sigma Energy	1 MeV
Shape of the source	Circle
Radius of the source	7.5 mm
Phantom shape	Cylinder
Phantom dimensions	3.3 mm x 15 mm
Resolution and voxel size	3000 slices of 5 μm in depth

Table 8 - Source and phantom parameters for ARRONAX modeling in GATE

4.2.3.2.2. Simulation of the SOBP

The SOBP is made by passive modulation, by inserting an aluminum range shifter in the beam course. We used the same thickness of range shifters as well as well the weights that were used during the experiments performed in September and December 2019 as reported in table 3.

Range shifter thickness	Weight
0 μm	0.85
50 μm	0.21
100 μm	0.22
150 μm	0.18
200 μm	0.14
250 μm	0.16
300 μm	0.095
350 μm	0.17

Table 9 - Range shifter thicknesses and pristine peaks weight values for the simulation of the ARRONAX SOBP using GATE.

4.3. Results

4.3.1. Cell survival fractions, biological doses and RBE of carbon and helium beam lines in HIMAC AND HIMBC

4.3.1.1. Survival fractions as a function of the dose

Figure 6 shows the comparison between the survival fraction as a function of the dose predictions of the BioDose actor with the NanOx and mMKM models and experimental data from Kagawa et al.⁹ for five positions in the SOBP: 5 mm, 101 mm, 123 mm, 145 mm, 149 mm.

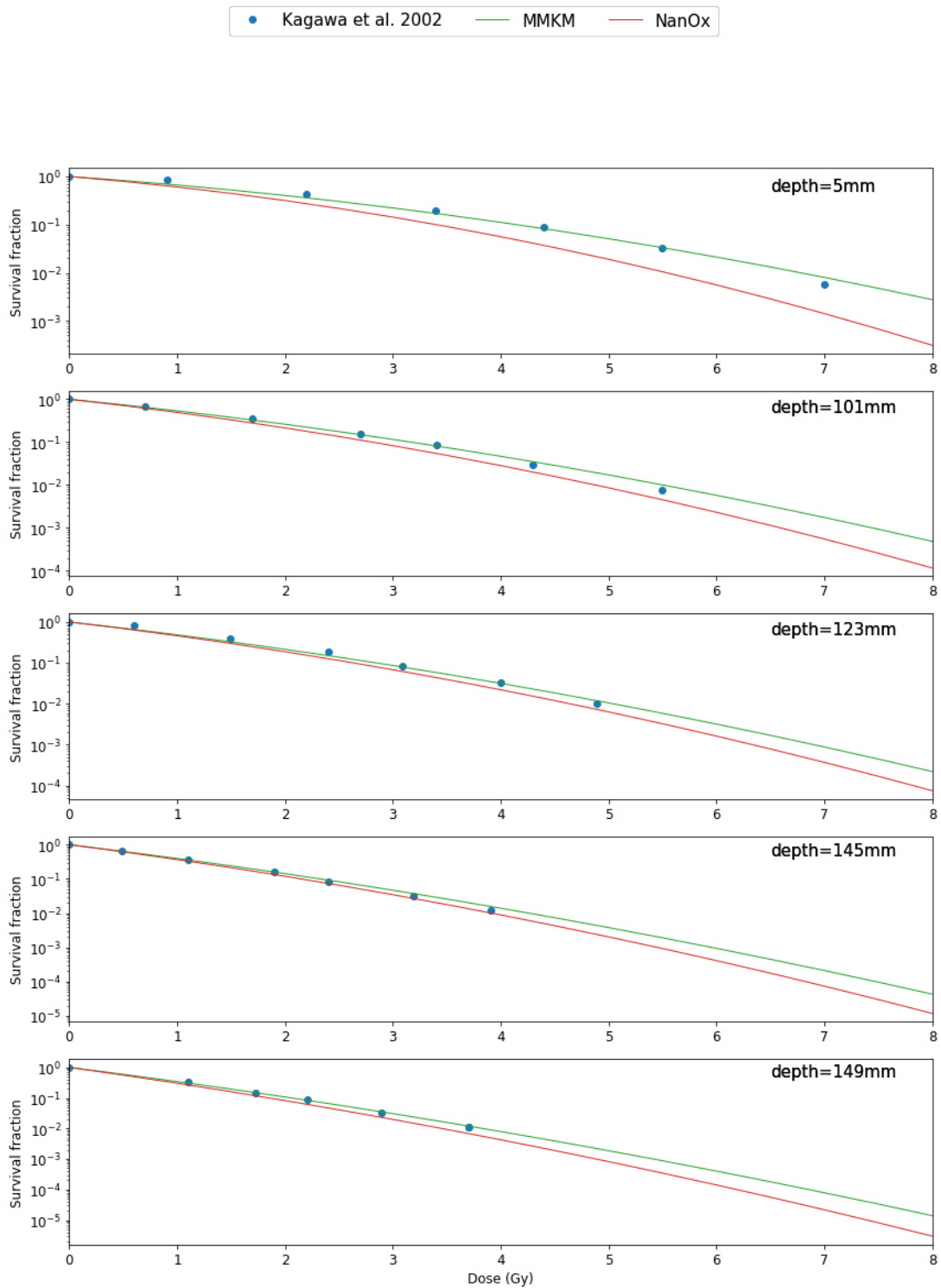


Figure 6 - Survival fractions of HSG cells as a function of the dose using the BioDose actor with the NanOx model (red curve) and the mMKM model (green curve) and experimental data from Kagawa et al.⁹ for five positions in the SOBP: 5 mm, 101 mm, 123 mm, 145 mm, 149 mm.

We observe that the survival fractions predicted by the NanOx and the mMKM models present the same trends and are in good agreement with the experimental data

4.3.1.2. Physical dose, biological dose, RBE and survival fraction using the NanOx and mMKM models

Figure 7 shows the comparison between the survival fraction as a function of the dose predictions of the BioDose actor with the NanOx and mMKM models and experimental data from Kagawa et al. ⁹ for five positions in the SOBP: 5 mm, 101 mm, 123 mm, 145 mm, 149 mm.

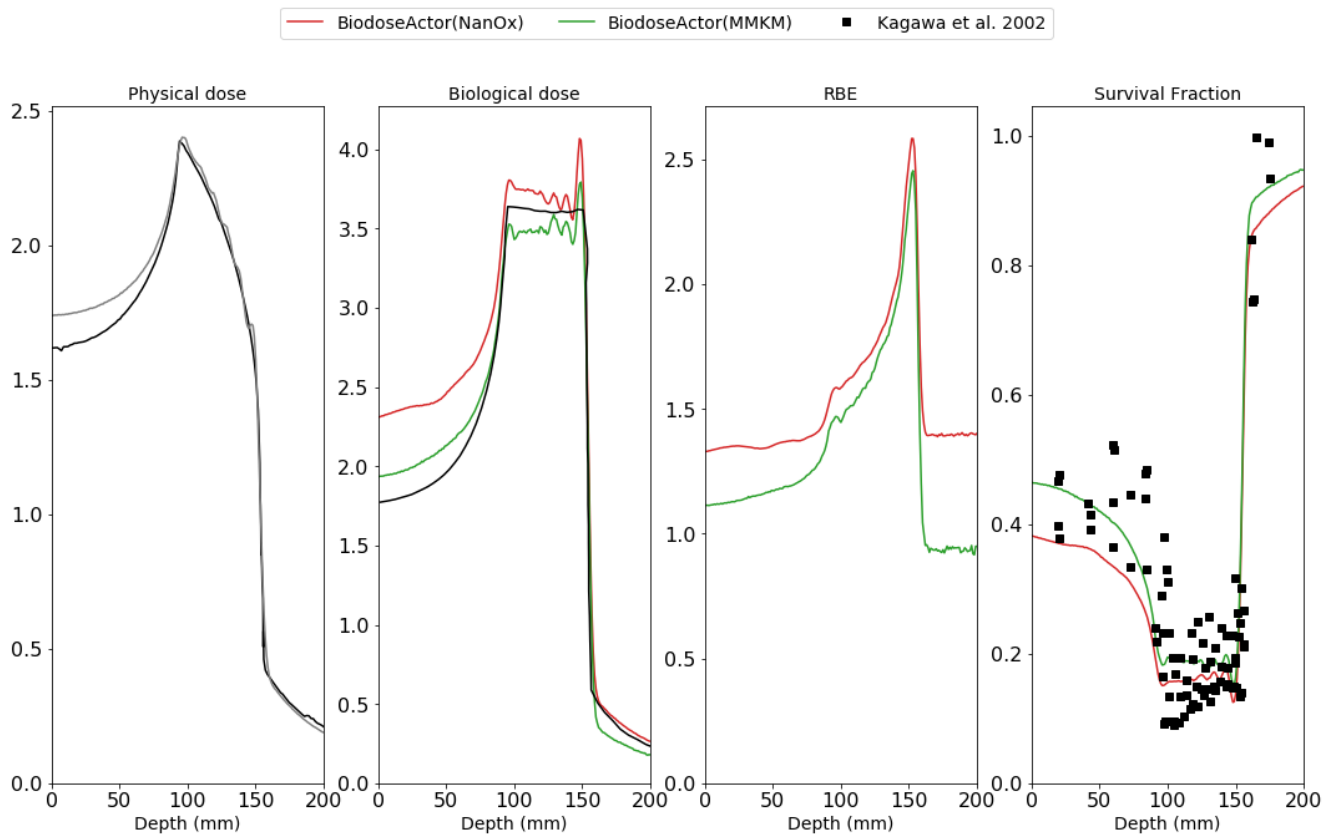


Figure 7 – Physical dose (light grey), biological dose, RBE and survival fractions provided by the BioDose actor as a function of target depth : NanOx model (red curve), mMKM model (green curve) and experimental data from Kagawa et al. ⁹ (black curves and dots).

4.3.2. ARRONAX preclinical line

4.3.2.1. Survival fractions at different positions of the SOBP with the NanOx model

Figure 8 presents survival fractions of SQ20B cells as a function of the dose using the BioDose actor with the NanOx model and experimental data for 3 positions in the SOBP.

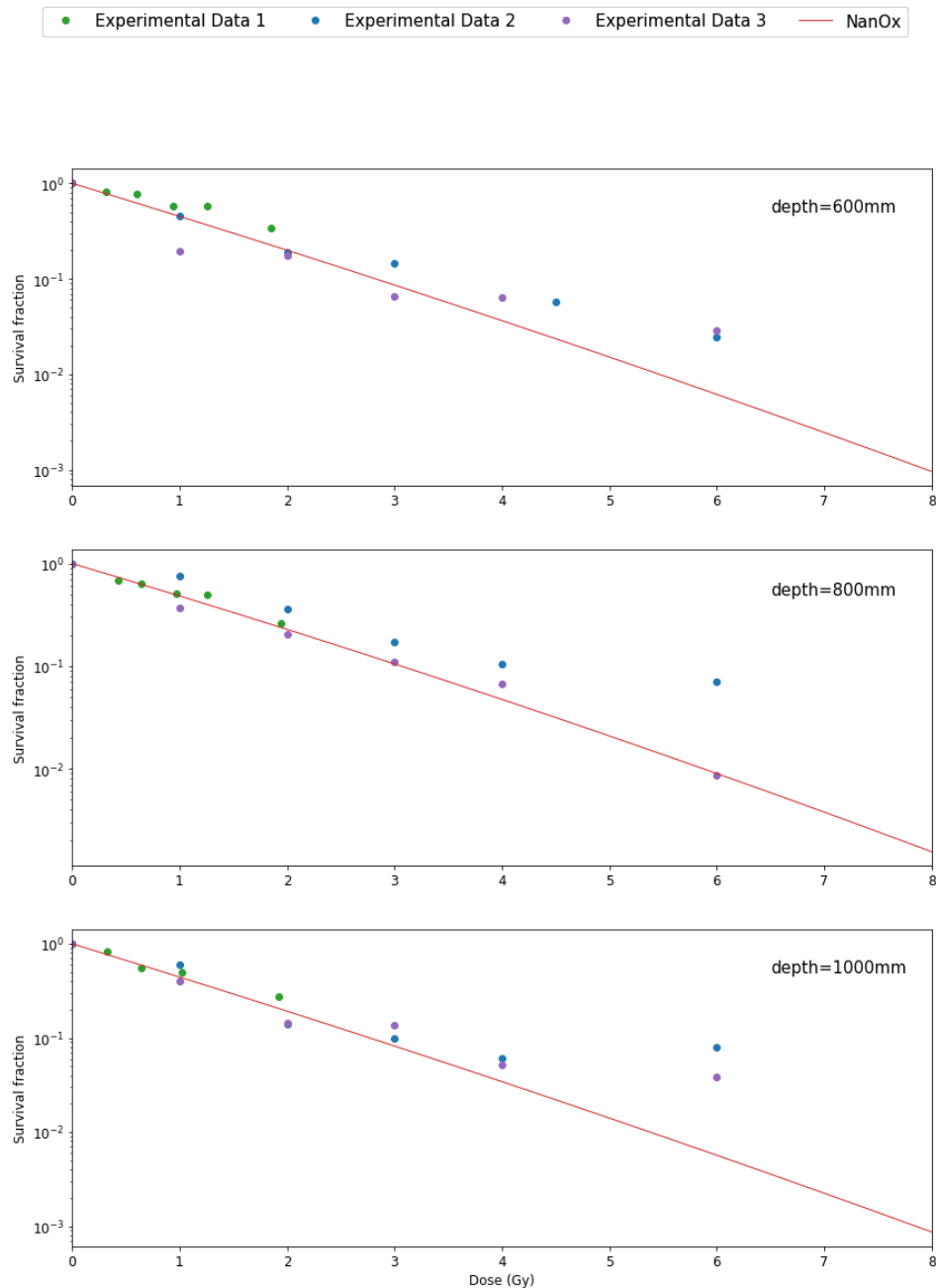


Figure 8 - Survival fractions of SQ20B cells as a function of the dose using the BioDose actor with the NanOx model (red curve) and experimental data (not published) for 3 positions in the SOBP.

4.3.2.2. Physical dose, biological dose, RBE and survival fraction with the NanOx and mMKM model

Physical dose, biological dose, RBE and survival fraction provided by the BioDose actor with the NanOx model as a function of target depth (red curve)

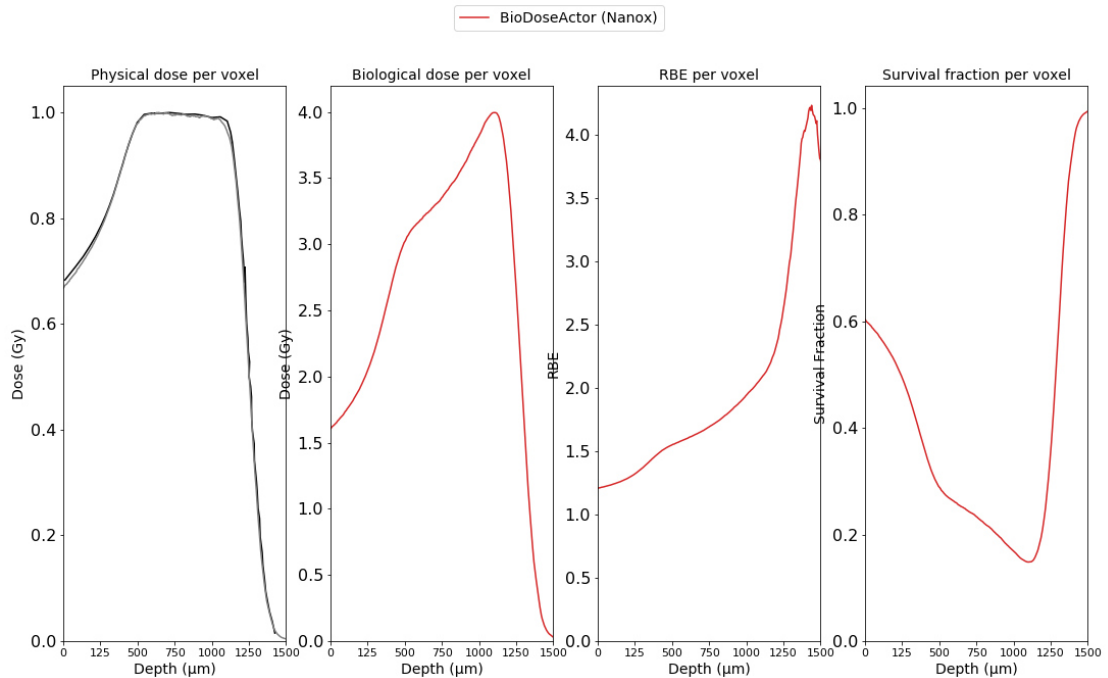


Figure 9 – Physical dose (light grey) with experimental data (black curve), biological dose, RBE and survival fraction provided by the BioDose actor with the NanOx model as a function of target depth (red curve).

4.4. Discussion

4.4.1. Validation tests

In order to validate the BioDoseActor we performed tests to ensure of the reliability of the performed calculations as well as providing recommendations for carbon ions irradiations.

The superimposition between the deposited dose calculated by the DoseActor and BioDoseActor for a mono-energetic beam (Figure 27a) and a SOBP (Figure 27b) confirmed the reliability of the dose computation by the BioDoseActor.

In order to provide recommendations on the step size limitations in Geant4, we explored the use of both the StepLimiter and the StepFunction options. For both options, the mean relative variation of LET (DEDX variations) as a function of kinetic energy appears higher for low kinetic energies (Figure 28a) which is expected since LET variations are larger at lower kinetic energies. That is why, among the calculations performed with the StepLimiter option, only a step limiter value of 1 μm leads to a mean DEDX variation compatible with our criterion of variations below 1% for all kinetic energies. Though, as shown in Figure 29, the smaller the size of the step is, the higher the computing time which leads to prohibitive computing time for step limiter values of the order of 1 μm . The step function allows to adapt step size limitation according to the residual range which is closely related to LET variations. Using the step function with the ratio $\alpha_R = 0.01$ and the final range $\rho_R = 1 \mu\text{m}$ enables to keep the mean DEDX variation below 1 % for all kinetic energies while reducing the computing by one or two orders of magnitude.

We then evaluated the standard deviations of the mean values (physical dose, biological dose, coefficient α_{mix} and RBE) per voxel in the SOBP for all step parametrizations. With a typical SOBP of 10^7 carbon ions we obtained standard deviations on mean values respecting our criterion of 3% for all quantities for all step parametrizations. We therefore used the same number of primaries in the modeling of the HIMAC/HBMC and ARRONAX beam lines.

4.4.2. Estimate of cell survival fractions, biological doses and RBE for carbon and helium beam lines

As we are using a simplified version of the HIMAC/HIMBC line, we observe disparities between the physical dose calculated with GATE and the physical dose retrieved from the literature (Figure 7a), notably, a shift at the entrance of the SOBP with a maximum of relative error of 8%. The shift is also observable in the biological dose predicted by the NanOx and mMKM models at the entrance of the SOBP, the models both overestimate the biological dose due to the overestimation of the physical dose in this area with a maximum of relative error of 20% for NanOx and 10% for mMKM (Figure 7b).

Though, there is a good agreement between the physical dose calculated with GATE and the reference dose in the plateau of the SOBP where the maximum relative error is of 2% (Figure 7a). And as the plateau is the region of interest in the irradiation setting, we focus our analysis on this region.

In the plateau of the SOBP the NanOx model overestimates the biological dose with a relative error of 6% (Figure 7b). This overestimation of the biological dose therefore leads to an underestimation of survival fraction compared to the experimental data values for different positions in the plateau of the SOBP (Figure 7d). The mMKM model underestimates the biological dose with a relative error of 5% and leads as expected to higher predicted values of survival fraction.

Regarding the irradiations of SQ20B cell in a helium ion SOBP in ARRONAX, the cell survival predicted by the NanOx model are in very good agreement with experimental data. The SOBP was defined in order to lead to a constant physical dose in the plateau region. This results in a biological depth-dose profile with a peak in the distal region is about 25% larger than the dose in the proximal region which illustrates the biological effectiveness of helium ions.

4.5. Conclusion

The aim of this work was to develop and implement the BioDoseActor in Gate. This tool uses as input databases of α and β coefficients currently provided by the mMKM and NanOx models for the HSG, CHO-K1, V79, SQ20B cell lines. It allows the calculation of the biological dose, the RBE and the survival fraction for each voxel of a voxelized volume.

The technical validation was successful in showing a reliable dose computation. In order to reduce uncertainties related to the step size in the estimation of biological quantities while optimizing the computing time, we recommend to the users an application of the step function with the ratio $\alpha_R = 0.01$ and the final range $\rho_R = 1 \mu\text{m}$.

General conclusion

The evaluation of the biological dose in hadrontherapy treatments, using the GATE Monte Carlo simulation platform, has been conducted through three principal steps. The first step has concerned the benchmarking of two Monte Carlo Track Structure codes (MCTS), Geant4-DNA and LPCHEM, in charge of simulating energy depositions at nanometric scales as well as the production of chemical reactive species during water radiolysis induced by ion radiation. This step was fundamental to specify any diverging calculations between the codes in order to use them afterward in biophysical models; in this PhD work we focused on mMKM and NanOx models. In a second phase, Geant4-DNA and NanOx have been used to calculate cell survival parameters for different energies and types of ion beams. Those parameters have been stacked in databases called by the GATE platform through the implementation of a specific actor: the BioDoseActor. Finally, as third step, the BioDoseActor has been implemented and validated in liquid water for the prediction of the biological dose of carbon- and helium-ion clinical beams available at the HIMBC (Chiba, Japan) and ARRONAX (Nantes, France) beam facilities respectively.

LPCHEM and Geant4-DNA are two MCTS codes that had never been compared yet. It was therefore a challenging opportunity to benchmark them on their ability to simulate specific energy spectra and radiolytic species ($\cdot\text{OH}$, e_{aq}^- , H_3O^+ , H_2O_2 , H_2 and OH^-) at nanometric scale. We focused on a 10 MeV proton beam interacting in a liquid water volume and collected specific energies in 10 nm cylindrical targets. For options 2, 4 and 6 of Geant4-DNA physics lists as for LPCHEM, we compared every process involved and linked their predominance to probability distributions of specific energy and also to radical yields at 10^{-12} s and radical recombination. No significant discrepancies were noticed between the codes concerning the specific energy probability distributions, nevertheless, more excitation process in Geant4-DNA option 4 combined to different excitation states and fractions of the water molecule involves a higher G value for $\cdot\text{OH}$ species at 10^{-12} s for Geant4-DNA. In a same way, the H_2 yield at 10^{-12} s is more elevated for Geant4-DNA options compared to LPCHEM. On the contrary, for e_{aq}^- , H_3O^+ and OH^- species, LPCHEM provides higher G values, this is mainly due to the higher probability of the attachment (linked to OH^- production) and ionization (linked to H_3O^+ , e_{aq}^- and OH^- production) processes. These differences remains however of the order of experimental uncertainties. The computing time tests included in the benchmarking of the codes have shown

a lower computing time for LPCHEM but using the G4 multi-threaded mode the difference in computing time is less significant.

Concerning the second step for this work, we first investigated the comparison of saturation corrected dose mean specific energy z_{1D}^* (Gy) using Geant4-DNA and LPCHEM for hydrogen and helium ions concerning HSG cells. We obtained very coherent results between the codes and the literature. Then, we benchmarked the α values predicted by mMKM and NanOx using input data from LPCHEM and/or Geant4-DNA with experimental data from the PIDE database as well as mMKM predictions from the literature. For helium and hydrogen, we showed higher discrepancies for LET higher than 10 keV/ μ m, for carbon and oxygen ions all the models were in close agreement. Because (i) in Geant4-DNA the maximum simulated kinetic energy is 100 MeV/n for hydrogen and helium ions and (ii) the code does not manage yet carbon ions, we produced databases of survival fraction coefficients using only the LPCHEM code. The databases have been simulated for energies that are suitable for hadrontherapy, covering a range from hundreds of eV to 400 MeV/n for proton, helium, carbon and oxygen ions.

As final step, we implemented the BioDoseActor within the GATE platform. The methodology we followed was inspired from the work of Mairani et al.³³ for the FLUKA Monte Carlo code. We validated the implementation predicting cell survival fraction, RBE and biological dose for the HIMBC 290 MeV/u carbon-ion beamline and the ARRONAX 67.4 MeV helium-ion beam line. We obtained satisfying results for the simulation of HSG cell survival fraction for respectively five and three specific positions in the SOBPs with experimental measurements. However, for the prediction of the biological dose in every voxel of the irradiated volume, especially for the HIMBC line, our predictions showed a similar trend to the literature with 10% relative difference between mMKM and NanOx.

This PhD work has raised perspectives in order to improve the models and their application in the BioDoseActor:

- The benchmarking between Geant4-DNA and LPCHEM should be extended to different ions with a large range of energies and using different target sizes to be close to realistic biological targets.

- It would be interesting to extend the databases to lower energy ranges to be more adapted to other applications such as therapies using alphas (like BNCT).
- It would be suitable to generate databases of input survival fraction coefficients with other models, such as the LEM for example, in order to get more comparisons.
- Additional studies should be performed in order to validate the BioDoseActor. Especially for the improvement of the modeling of the HIMBC beam line at the beam entrance for a 320 MeV/n carbon ion SOBP. We are also aiming to perform the same study for the 290 MeV/n carbon-ion beam line from HIMAC as more recent experimental data are available for comparison, especially with the work of Inaniwa et al. in 2015 ³.
- The BioDoseActor has been used for the predictions of biological quantities in liquid water only, the next step would be to validate it for patient CT scans.
- Finally, comparisons with treatment planning system (TPS) predictions would enrich the understanding of the behavior of each model. Efficiency tests in terms of computing time and storage capacities could allow to improve the implementation of the BioDoseActor.

Curriculum vitae of this thesis

Submitted publications :

- Monte Carlo simulations of nanodosimetry and radiolytic species production for monoenergetic proton beams. Benchmarking of GEANT4-DNA and LPCHEM codes. Medical Physics, September 2021.

Conférences:

2018

- Evaluation of biological effectiveness of 65MeV therapeutic proton beams using the GATE platform , Geant4, Third Geant4 International User Conference , Bordeaux, October 2018
- Evaluation of biological effectiveness of 65MeV therapeutic proton beams using the GATE platform, OpenGATE collaboration Technical meeting , Paris, December 2018

2019

- Benchmarking micro and nanodosimetry spectra and free radicals simulated with GEANT4DNA and LPCHEM for ion beams , PTCOG58, Manchester, June 2019
- Benchmarking micro and nanodosimetry spectra and free radicals simulated with GEANT4DNA and LPCHEM for ion beams , MCMA, Montreal , June 2019
- Implementation and benchmarking of radiobiological models for the prediction of biological dose in hadrontherapy , OpenGATE collaboration Technical meeting, Lyon, July 2019
- Simulation of micro nanodosimetry spectra and free radicals with Geant4 DNA and LPCHEM for ion beams, General Assembly Labex , Lyon, October 2019
- Simulation of micro nanodosimetry spectra and free radicals with Geant4 DNA and LPCHEM for ion beams, Fourth Geant4 International User Conference , Athens , October 2019
- Simulation of micro nanodosimetry spectra and free radicals with Geant4 DNA and LPCHEM for ion beams, JRJC SFPM/Mi2B/GDR, November 2019

2020

- Biodose actor implementation in GATE, OpenGATE collaboration Technical meeting, Via conference call September 2020

- Biodose actor implementation in GATE, General Assembly Labex, Lyon, September 2020

2021

- Biodose actor implementation in GATE, Technical Meeting de la collaboration OpenGATE, Via conference call, May 2021

References

1. Kramer M, Scholz M. Treatment planning for heavy-ion radiotherapy: Calculation and optimization of biologically effective dose. *Phys Med Biol.* 2000;45(11). doi:10.1088/0031-9155/45/11/314
2. Kase Y, Kanai T, Matsumoto Y, et al. Microdosimetric measurements and estimation of human cell survival for heavy-ion beams. *Radiat Res.* 2006;166(4):629-638. doi:10.1667/RR0536.1
3. Inaniwa T, Kanematsu N, Matsufuji N, et al. Reformulation of a clinical-dose system for carbon-ion radiotherapy treatment planning at the National Institute of Radiological Sciences, Japan. *Phys Med Biol.* 2015;60(8):3271-3286. doi:10.1088/0031-9155/60/8/3271
4. Cunha M, Monini C, Testa E, Beuve M. NanOx, a new model to predict cell survival in the context of particle therapy. *Phys Med Biol.* 2017;62(4):1248-1268. doi:10.1088/1361-6560/aa54c9
5. Leenhouts HP, Chadwick KH. An analytical approach to the induction of translocations in the spermatogonia of the mouse. *Mutat Res Regul Pap.* 1981;82(2). doi:10.1016/0027-5107(81)90160-3
6. Kellerer AM, Rossi HH. A generalized formulation of dual radiation action. *Radiat Res.* 1978;75(3). doi:10.2307/3574835
7. Baskar R, Lee KA, Yeo R, Yeoh KW. Cancer and radiation therapy: Current advances and future directions. *Int J Med Sci.* 2012;9(3). doi:10.7150/ijms.3635
8. Karger CP, Peschke P. RBE and related modeling in carbon-ion therapy. *Phys Med Biol.* 2018;63(1). doi:10.1088/1361-6560/aa9102
9. Kagawa K, Murakami M, Hishikawa Y, et al. PRECLINICAL BIOLOGICAL ASSESSMENT OF PROTON AND CARBON ION BEAMS AT HYOGO ION BEAM MEDICAL CENTER. 2002;54(3):928-938.
10. Weyrather WK, Ritter S, Scholz M, Kraft G. RBE for carbon track-segment irradiation in cell lines of differing repair capacity. *Int J Radiat Biol.* 1999;75(11):1357-1364.

doi:10.1080/095530099139232

11. Kraft G. Radiobiological effects of very heavy ions: inactivation, induction of chromosome aberrations and strand breaks. *Nucl Sci Appl*. Published online 1987.
12. Tobias CA, Blakely EA, Chang PY, Lommel L, Roots R. Response of sensitive human ataxia and resistant T-1 cell lines to accelerated heavy ions. *Br J Cancer*. 1984;49(SUPPL. 6). doi:10.2172/7005318
13. Endo M, Koyama-Ito H, Minohara SI, et al. Hiplan- a heavy ion treatment planning system at himac. *J JASTRO*. 1996;8(3). doi:10.11182/jastro1989.8.231
14. Scholz M, Elsässer T. Biophysical models in ion beam radiotherapy. *Adv Sp Res*. 2007;40(9). doi:10.1016/j.asr.2007.02.066
15. Hawkins RB. A microdosimetric-kinetic model for the effect of non-poisson distribution of lethal lesions on the variation of RBE with LET. *Radiat Res*. 2003;160(1):61-69. doi:10.1667/RR3010
16. Inaniwa T, Furukawa T, Kase Y, et al. Treatment planning for a scanned carbon beam with a modified microdosimetric kinetic model. *Phys Med Biol*. 2010;55(22):6721-6737. doi:10.1088/0031-9155/55/22/008
17. Elsässer T, Krämer M, Scholz M. Accuracy of the Local Effect Model for the Prediction of Biologic Effects of Carbon Ion Beams In Vitro and In Vivo. *Int J Radiat Oncol Biol Phys*. 2008;71(3). doi:10.1016/j.ijrobp.2008.02.037
18. Friedrich T, Scholz U, Elsässer T, Durante M, Scholz M. Systematic analysis of RBE and related quantities using a database of cell survival experiments with ion beam irradiation. *J Radiat Res*. 2013;54(3). doi:10.1093/jrr/rrs114
19. Monini C, Cunha M, Chollier L, Testa E, Beuve M. Determination of the Effective Local Lethal Function for the NanOx Model. *Radiat Res*. 2020;193(4):331-340. doi:10.1667/RR15463.1
20. Scholz M, Kraft G. Track structure and the calculation of biological effects of heavy charged particles. *Adv Sp Res*. 1996;18(1-2). doi:10.1016/0273-1177(95)00784-C
21. Elsässer T, Weyrather WK, Friedrich T, et al. Quantification of the relative biological effectiveness for ion beam radiotherapy: Direct experimental comparison of proton and

- carbon ion beams and a novel approach for treatment planning. *Int J Radiat Oncol Biol Phys.* 2010;78(4):1177-1183. doi:10.1016/j.ijrobp.2010.05.014
22. Grün R, Friedrich T, Elsässer T, et al. Impact of enhancements in the local effect model (LEM) on the predicted RBE-weighted target dose distribution in carbon ion therapy. *Phys Med Biol.* 2012;57(22). doi:10.1088/0031-9155/57/22/7261
 23. Hawkins RB. A microdosimetric-kinetic model of cell death from exposure to ionizing radiation of any LET, with experimental and clinical applications. *Int J Radiat Biol.* 1996;69(6):739-755.
 24. Hawkins RB. A microdosimetric-kinetic theory of the dependence of the RBE for cell death on LET. *Med Phys.* 1998;25:1157-1170.
 25. Kase Y, Kanai T, Matsufuji N, Furusawa Y, Elsässer T, Scholz M. Biophysical calculation of cell survival probabilities using amorphous track structure models for heavy-ion irradiation. *Phys Med Biol.* 2008;53(1):37-59. doi:10.1088/0031-9155/53/1/003
 26. Moniniy C, Testa É, Beuve M. NanOx predictions of cell survival probabilities for three cell lines. In: *Acta Physica Polonica B.* Vol 48. Jagellonian University; 2017:1653-1659. doi:10.5506/APhysPolB.48.1653
 27. Beuve M, Colliaux A, Dabli D, et al. Statistical effects of dose deposition in track-structure modelling of radiobiology efficiency. *Nucl Instruments Methods Phys Res Sect B Beam Interact with Mater Atoms.* 2009;267(6):983-988. doi:10.1016/j.nimb.2009.02.016
 28. Ravanat JL, Douki T, Cadet J. Direct and indirect effects of UV radiation on DNA and its components. *J Photochem Photobiol B Biol.* 2001;63(1-3):88-102. doi:10.1016/S1011-1344(01)00206-8
 29. Anagnostopoulos G, Baltas D, Pantelis E, Papagiannis P, Sakelliou L. The effect of patient inhomogeneities in oesophageal ¹⁹²Ir HDR brachytherapy: A Monte Carlo and analytical dosimetry study. *Phys Med Biol.* 2004;49(12). doi:10.1088/0031-9155/49/12/014
 30. Dubey S, Roulin A. Evolutionary and biomedical consequences of internal melanins. *Pigment Cell Melanoma Res.* 2014;27(3):327-338. doi:10.1111/pcmr.12231

31. Cirrone GAP, Cuttone G, Di Rosa F, et al. Validation of Geant4 physics models for the simulation of the proton bragg peak. *IEEE Nucl Sci Symp Conf Rec.* 2006;2:788-792. doi:10.1109/NSSMIC.2006.355969
32. Ferrari, A. Sala, P.R. Fasso, A. Ranft J. FLUKA: A multi-particle transport code (Program version 2005). *Cern-2005-010.* 2005;(October).
33. Mairani A, Brons S, Cerutti F, et al. The FLUKA Monte Carlo code coupled with the local effect model for biological calculations in carbon ion therapy. *Phys Med Biol.* 2010;55(15):4273-4289. doi:10.1088/0031-9155/55/15/006
34. Rossi S. The National Centre for Oncological Hadrontherapy (CNAO): Status and perspectives. *Phys Medica.* 2015;31(4). doi:10.1016/j.ejmp.2015.03.001
35. Magro G. The FLUKA Monte Carlo code coupled with the NIRS approach for clinical dose calculations in carbon ion therapy. *Certain distance degree based Topol indices Zeolite LTA Fram.* 2017;(December 2016):11-14.
36. Zaider, M., & Rossi HH. Radiation Research Society. *Radiat Res.* 1980;83(3):732-739. <https://www.jstor.org/stable/3575352?seq=1>
37. Wedenberg M, Lind BK, Hårdemark B. A model for the relative biological effectiveness of protons: The tissue specific parameter α/β of photons is a predictor for the sensitivity to LET changes. *Acta Oncol (Madr).* 2013;52(3). doi:10.3109/0284186X.2012.705892
38. Carabe-Fernandez A, Dale RG, Jones B. The incorporation of the concept of minimum RBE (RBE_{min}) into the linear-quadratic model and the potential for improved radiobiological analysis of high-LET treatments. *Int J Radiat Biol.* 2007;83(1). doi:10.1080/09553000601087176
39. Chen Y, Ahmad S. Empirical model estimation of relative biological effectiveness for proton beam therapy. *Radiat Prot Dosimetry.* 2012;149(2). doi:10.1093/rpd/ncr218
40. Wilkens JJ, Oelfke U. A phenomenological model for the relative biological effectiveness in therapeutic proton beams. *Phys Med Biol.* 2004;49(13). doi:10.1088/0031-9155/49/13/004
41. Carlson DJ, Stewart RD, Semenenko VA, Sandison GA. Combined use of Monte Carlo DNA damage simulations and deterministic repair models to examine putative

- mechanisms of cell killing. *Radiat Res.* 2008;169(4). doi:10.1667/RR1046.1
42. Katz R. The Parameter-Free Track Structure Model of Scholz and Kraft for Heavy-Ion Cross Sections. *Radiat Res.* 2003;160(6). doi:10.1667/RR3088
 43. Polster L, Schuemann J, Rinaldi I, et al. Extension of TOPAS for the simulation of proton radiation effects considering molecular and cellular endpoints. *Phys Med Biol.* 2015;60(13):5053-5070. doi:10.1088/0031-9155/60/13/5053
 44. Incerti S, Baldacchino G, Bernal M, et al. THE Geant4-DNA project. *Int J Model Simulation, Sci Comput.* 2010;1(2). doi:10.1142/S1793962310000122
 45. Cunha M, Testa E, Beuve M, Balosso J, Chaikh A. Considerations on the miniaturization of detectors for in vivo dosimetry in radiotherapy: A Monte Carlo study. *Nucl Instruments Methods Phys Res Sect B Beam Interact with Mater Atoms.* 2017;399:20-27. doi:10.1016/j.nimb.2017.03.078
 46. Poignant F, Ipatov A, Chakchir O, et al. Theoretical derivation and benchmarking of cross sections for low-energy electron transport in gold. *Eur Phys J Plus.* 2020;135(4). doi:10.1140/epjp/s13360-020-00354-3
 47. Villagrasa C, Bordage MC, Bueno M, et al. ASSESSING the CONTRIBUTION of CROSS-SECTIONS to the UNCERTAINTY of MONTE CARLO CALCULATIONS in MICRO- And NANODOSIMETRY. *Radiat Prot Dosimetry.* 2019;183(1-2). doi:10.1093/rpd/ncy240
 48. I. Kyriakou, M. Sefl, V. Nourry SI. The impact of new Geant4-DNA cross section models on electron track structure simulations in liquid water. *J Appl Phys.* 2016;119(19). doi:10.1063/1.4950808
 49. Shin WG, Ramos-Mendez J, Faddegon B, et al. Evaluation of the influence of physical and chemical parameters on water radiolysis simulations under MeV electron irradiation using Geant4-DNA. *J Appl Phys.* 2019;126(11). doi:10.1063/1.5107511
 50. Schwarz A. Radical and Molecular Yields in Water Irradiated by. 1965;79(6):6-10.
 51. Naleway CA, Sauer MC, Jonah CD, Schmidt KH. Theoretical analysis of the LET dependence of transient yields observed in pulse radiolysis with ion beams. *Radiat Res.* 1979;77(1):47-61. doi:10.2307/3575076

52. Karamitros M, Luan S, Bernal MA, et al. Diffusion-controlled reactions modeling in Geant4-DNA. *J Comput Phys*. 2014;274:841-882. doi:10.1016/j.jcp.2014.06.011
53. Ballarini F, Biaggi M, Merzagora M, et al. Stochastic aspects and uncertainties in the prechemical and chemical stages of electron tracks in liquid water: A quantitative analysis based on Monte Carlo simulations. *Radiat Environ Biophys*. 2000;39(3):179-188. doi:10.1007/s004110000060
54. Uehara S, Nikjoo H. Monte Carlo simulation of water radiolysis for low-energy charged particles. *J Radiat Res*. 2006;47(1):69-81. doi:10.1269/jrr.47.69
55. Karamitros M, MANTERO A, INCERTI S, et al. Modeling Radiation Chemistry in the Geant4 Toolkit. *Prog Nucl Sci Technol*. 2011;2(0). doi:10.15669/pnst.2.503
56. LaVerne JA, Baidak A. Track effects in the radiolysis of aromatic liquids. *Radiat Phys Chem*. 2012;81(9):1287-1290. doi:10.1016/j.radphyschem.2011.11.014
57. Baldacchino G, Bouffard S, Balanzat E, et al. Direct time-resolved measurement of radical species formed in water by heavy ions irradiation. *Nucl Instruments Methods Phys Res Sect B Beam Interact with Mater Atoms*. 1998;146(1-4):528-532. doi:10.1016/S0168-583X(98)00463-7
58. Gervais B, Beuve M, Olivera GH, Galassi ME. Numerical simulation of multiple ionization and high LET effects in liquid water radiolysis. *Radiat Phys Chem*. 2006;75(4):493-513. doi:10.1016/j.radphyschem.2005.09.015
59. Incerti S, Kyriakou I, Bernal MA, et al. Geant4-DNA example applications for track structure simulations in liquid water: A report from the Geant4-DNA Project. *Med Phys*. 2018;45(8). doi:10.1002/mp.13048
60. Sakata D, Kyriakou I, Tran HN, et al. Electron track structure simulations in a gold nanoparticle using Geant4-DNA. *Phys Medica*. 2019;63(May):98-104. doi:10.1016/j.ejmp.2019.05.023
61. Gervais B, Beuve M, Olivera GH, Galassi ME, Rivarola RD. Production of HO₂ and O₂ by multiple ionization in water radiolysis by swift carbon ions. *Chem Phys Lett*. 2005;410(4-6):330-334. doi:10.1016/j.cplett.2005.05.057
62. Poignant F, Charfi H, Chan CH, et al. Monte Carlo simulation of free radical production

- under keV photon irradiation of gold nanoparticle aqueous solution. Part I: Global primary chemical boost. *Radiat Phys Chem.* 2020;172. doi:10.1016/j.radphyschem.2020.108790
63. Tessaro VB, Poignant F, Gervais B, Beuve M, Galassi ME. Theoretical study of W-values for particle impact on water. *Nucl Instruments Methods Phys Res Sect B Beam Interact with Mater Atoms.* 2019;460:259-265. doi:10.1016/j.nimb.2018.11.031
 64. Incerti S, Ivanchenko A, Karamitros M, et al. Comparison of GEANT4 very low energy cross section models with experimental data in water. *Med Phys.* 2010;37(9):4692-4708. doi:10.1118/1.3476457
 65. Bernal MA, Bordage MC, Brown JMC, et al. Track structure modeling in liquid water: A review of the Geant4-DNA very low energy extension of the Geant4 Monte Carlo simulation toolkit. *Phys Medica.* 2015;31(8):861-874. doi:10.1016/j.ejmp.2015.10.087
 66. MC B, J B, S E, et al. Implementation of new physics models for low energy electrons in liquid water in Geant4-DNA. *Phys Med.* 2016;32(12):1833-1840. doi:10.1016/J.EJMP.2016.10.006
 67. Terrissol M, Beaudré A. Simulation of Space and Time Evolution of Radiolytic Species Induced by Electrons in Water. *Radiat Prot Dosimetry.* 1990;31(1-4):175-177. doi:10.1093/oxfordjournals.rpd.a080660
 68. Ramos-Méndez J, Shin WG, Karamitros M, et al. Independent reaction times method in Geant4-DNA: Implementation and performance. *Med Phys.* Published online 2020. doi:10.1002/mp.14490
 69. Peukert D, Incerti S, Kempson I, et al. Validation and investigation of reactive species yields of Geant4-DNA chemistry models. *Med Phys.* 2019;46(2):983-998. doi:10.1002/mp.13332
 70. Pastina B, Laverne JA, Pimblott SM. Dependence of Molecular Hydrogen Formation in Water on Scavengers of the Precursor to the Hydrated Electron. *J Phys Chem A.* 1999;103(29):5841-5846. doi:10.1021/jp991222q
 71. Gervais B, Beuve M, Olivera GH, Galassi ME. Numerical simulation of multiple ionization and high LET effects in liquid water radiolysis. *Radiat Phys Chem.* 2006;75(4):493-513. doi:10.1016/j.radphyschem.2005.09.015

72. Incerti S, Baldacchino G, Bernal M, et al. THE Geant4-DNA project. *Int J Model Simulation, Sci Comput.* 2010;1(2):157-178. doi:10.1142/S1793962310000122
73. Chen Y, Li J, Li C, Qiu R, Wu Z. A modified microdosimetric kinetic model for relative biological effectiveness calculation. *Phys Med Biol.* 2017;63(1):015008. doi:10.1088/1361-6560/aa9a68
74. Monini C, Alphonse G, Rodriguez-Lafrasse C, Testa É, Beuve M. Comparison of biophysical models with experimental data for three cell lines in response to irradiation with monoenergetic ions. *Phys Imaging Radiat Oncol.* 2019;12(May):17-21. doi:10.1016/j.phro.2019.10.004
75. He- A, Beams N, Furusawa AY, et al. Inactivation of Aerobic and Hypoxic Cells from Three Different Cell Lines by Inactivation of Aerobic and Hypoxic Cells from Three Different Cell. 2000;154(5):485-496.
76. Elsässer T, Cunrath R, Krämer M, Scholz M. Impact of track structure calculations on biological treatment planning in ion radiotherapy. *New J Phys.* 2008;10. doi:10.1088/1367-2630/10/7/075005
77. Paganetti H, Jiang H, Parodi K, Slopsma R, Engelsman M. Clinical implementation of full Monte Carlo dose calculation in proton beam therapy. *Phys Med Biol.* 2008;53(17):4825-4853. doi:10.1088/0031-9155/53/17/023
78. Grevillot L, Boersma DJ, Fuchs H, et al. Technical Note: GATE-RTion: a GATE/Geant4 release for clinical applications in scanned ion beam therapy. *Med Phys.* 2020;47(8). doi:10.1002/mp.14242
79. Winterhalter C, Taylor M, Boersma D, et al. Evaluation of GATE-RTion (GATE/Geant4) Monte Carlo simulation settings for proton pencil beam scanning quality assurance. *Med Phys.* 2020;47(11). doi:10.1002/mp.14481
80. Kanai T, Furusawa Y, Fukutsu K, Itsukaichi H, Eguchi-Kasai K, Ohara H. Irradiation of mixed beam and design of spread-out Bragg peak for heavy- ion radiotherapy. *Radiat Res.* 1997;147(1). doi:10.2307/3579446
81. Kanai TA, Eedo MA, Minohara SH, et al. BIOPHYSICAL CHARACTERISTICS OF HIMAC CLINICAL IRRADIATION SYSTEM FOR HEAVY-ION RADIATION THERAPY. 1999;44(1):201-210.

82. Yamada S. Commissioning and performance of the HIMAC medical accelerator. In: *Proceedings of the IEEE Particle Accelerator Conference*. Vol 1. ; 1995. doi:10.1109/pac.1995.504557
83. Akagi T, Kanematsu N. Ridge filter design for proton therapy at Hyogo Ion Beam Medical Center Ridge filter design for proton therapy at Hyogo Ion. Published online 2003.
84. Lam GKY. of Mixed Beam and Design of Spread-Out Irradiation Bragg Peak for Radiotherapy. 1997;147(1):78-85. doi:10.2307/3576901
85. Colliaux A, Gervais B, Rodriguez-Lafrasse C, Beuve M. Simulation of ion-induced water radiolysis in different conditions of oxygenation. *Nucl Instruments Methods Phys Res Sect B Beam Interact with Mater Atoms*. 2015;365:596-605. doi:10.1016/j.nimb.2015.08.057
86. Frongillo Y, Goulet T, Fraser MJ, Cobut V, Patau JP, Jay-Gerin JP. Monte carlo simulation of fast electron and proton tracks in liquid water - II. Nonhomogeneous chemistry. *Radiat Phys Chem*. 1998;51(3):245-254. doi:10.1016/S0969-806X(97)00097-2
87. Green NJB, Pilling MJ, Pimblott SM, Clifford P. Stochastic modeling of fast kinetics in a radiation track. *J Phys Chem*. 1990;94(1):251-258. doi:10.1021/j100364a041

Appendix

Appendix 1 - Geant4-DNA and LPCHEM physics processes. The present work uses the “dnaphysics” examples that combines Geant4 electromagnetic models (above 1 MeV for electrons) with various sets (options) of Geant4-DNA models. Option 2 is the default Geant4-DNA physics list. In option 4, alternative models (for elastic scattering, ionization and excitation) are included at low energy (10 eV – 10 keV) but vibration and attachment processes are not taken into account. Option 6 is the implementation of the interaction cross section of the CPA100 track structure code.

	Geant4-DNA Option 2	Geant4-DNA Option 4	Geant4-DNA Option 6	LPCHEM
Electronic Interactions				
Elastic Scattering				
Model	Champion Elastic Model (7.4 eV – 1 MeV)	Screened Rutherford Model (9 eV – 10 keV)	Independent Atom Model (11 eV – 256 keV)	Michaud and Sanche (1987)
excitation				
Model	First Born approximation - Emfietzoglou Dielectric Model (11 eV – 1 MeV)	First Born approximation - Emfietzoglou-Kyriakou dielectric model (10 eV – 10 keV)	Binary Encounter Bethe model CPA100 (11 eV – 256 keV)	Binary Encounter Bethe Model (Rudd Kim, 1994)
Excitation levels	5	5	5	2
Excitation level energies	A1B1 (8.22 eV) B1A1 (10.0 eV) Ryd A+B (11.3 eV) Ryd C+D (12.6 eV) Bande diffuse (13.8 eV)	A1B1 (8.22 eV) B1A1 (10.0 eV) Ryd A+B (11.3 eV) Ryd C+D (12.6 eV) Bande diffuse (13.77 eV)	A1B1 (8.17 eV) B1A1 (13.4 eV) Ryd A+B (16.1 eV) Ryd C+D (12.3 eV) Bande diffuse (13.77 eV)	A1B1 (7.34 eV) B1A1 (8.62 eV)
ionization				

Model	First Born approximation - Emfietzoglou Dielectric Model (11 eV – 1 MeV)	First Born approximation - Emfietzoglou-Kyriakou dielectric model (10 eV – 10 keV)	Binary Encounter Bethe model CPA100 (11 eV – 256 keV)	Binary Encounter Bethe Model (Kim, 2001)
ionization levels	5	5	5	5
Ionization level energies	1b1: 10.79 eV 3a1: 13.39 eV 1b : 16.05 eV 2a : 32.30 eV 1a : 539.0 eV	1b1: 10.00 eV 3a1: 13.00 eV 1b2: 17.00 eV 2a1: 32.20 eV 1a1: 539.7 eV	1b1: 10.00 eV 3a1: 13.39 eV 1b2: 16.05 eV 2a1: 32.30 eV 1a1: 539.0 eV	1b1: 11.97 eV 3a1: 14.69 eV 1b2: 16.59 eV 2a1: 32.37 eV 1a1: 539.6 eV
Multi ionization	No			Yes
vibration				
Data	Michaud and Sanche (2003) (2 eV – 100 eV)			Michaud and Sanche (1987)
Vibrational excitation level	Lattice phonon (vT): 10 meV Lattice phonon (vT): 24 meV Librational phonon (vL): 61 meV Librational phonon (vL): 92 meV Bending mode (v2): 204meV Stretching mode (v1, 3): 417 meV Stretching mode (v3): 460meV Stretching mode (v1,3+vL): 500 meV Stretching mode 2 (1,3): 835 meV			Lattice phonon (vT): 10 meV Lattice phonon (vT): 25 meV Librational phonon (vL): 62 meV Librational phonon (vL): 95 meV Bending mode (v2): 205 meV Stretching mode (v1, 3): 422 meV Stretching mode (v3): 460 meV Stretching mode (v1,3+vL): 500 meV Stretching mode 2 (1,3): 840 meV
Vibrational interactions types	All vibrational interactions treated the same way			The intermolecular and intramolecular interactions are treated separately
Attachment				
Data	Melton (4 eV – 13 eV)			Pastina et al. (6.25 eV – 12.40 eV)
Proton interactions				
Elastic Scattering				
Model	Classic approach Coulombic potential energy (0 – 1 MeV)			

	Ionization	
Model	Rudd Ionization Model (0 – 500 keV) Born Ionization Model (500 keV – 100 MeV)	CDW-EIS approximation
	Excitation	
Model	Miller Green Excitation Model (0 – 500 keV) Born Excitation Model (500 keV – 100 MeV)	Cobut et al. Approximation
	Capture	
Model	Dingfelder Charge Decrease Model (100 eV – 100 MeV)	

Appendix 2 - Geant4-DNA and LPCHEM physico-chemical and chemical modules

	Geant4-DNA		LPCHEM	
Physico-chemical stage				
Duration	From 10^{-15} to 10^{-12} seconds			
Branching ratios				
Branching ratios models	PARTRAC software ⁵³		Cobut et al. (1998), Muroya et al. (2002).	
Single event dissociation channels				
	Decay Channel	Fraction	Decay channel	Fraction
All ionization states	$H_3O^+ + \cdot OH$	100	$H_3O^+ + \cdot OH$	100
Excitation state A1B1	$\cdot OH + H\cdot$	65	$\cdot OH + H\cdot$	70
	$H_2O + \Delta E$	35	$H_2O + \Delta E$	30
Excitation state B1A1	$H_3O^+ + \cdot OH + e_{eq}^-$	55	$H_2O + e_{eq}^-$	25.00
	$\cdot OH + H\cdot$	15	H_2O	22.50
	$\cdot OH + \cdot OH + H_2$	15	$\cdot OH + H\cdot$	40.95
	$H_2O + \Delta E$	30	$O + 2H\cdot$	6.30
			$O(^1D) + H_2$	5.25
Excitation state: Rydberg, diffusion bands	$H_3O^+ + \cdot OH + e_{eq}^-$	50		
	$H_2O + \Delta E$	50		
Dissociative electron attachment	$\cdot OH + OH^- + H_2$	100	$\cdot OH + OH^- + H_2$	100
$H_2O + e^-$			H_2O	40.0
			$\cdot OH + H\cdot$	30.0
			$O + 2H\cdot$	15.6
			$O(^1D) + H_2$	14.4
Multiple event dissociation channels				
$H_2OQ^+ (q > 3)$			$H_3O^+ + H_3O^+ + OH^{(q-2)}$ $\rightarrow qH_3O^+ + (q-2)OH + O$	100
$H_2O_2^+$			$H_3O^+ + OH^+ \rightarrow 2H_3O^+ + O$	29
			$H_3O^+ + H + O^+ \rightarrow 2H_3O^+ + H + \cdot OH + O$	16
			$H_3O^+ + H + O^+ \rightarrow 2H_3O^+ + O$	55
Chemical stage				
Duration	From 10^{-12} to 10^{-6} seconds			

Number of chemical species	7	31
Number of chemical reactions	10	98
Simulation method	Step by step ⁵²	Inspired by the Independent Reaction Time method ⁸⁵
	Diffusion coefficients ($10^{-9}\text{m}^2.\text{s}^{-1}$)	
Diffusion coefficients model	PARTRAC software ⁵³	Frongillio et al., 1998 ⁸⁶
e_{aq}^-	4.9	4.9
$\cdot OH$	2.8	2.2
$H\cdot$	7.0	7.0
H_3O^+	9.0	9.46
H_2	5.0	4.8
OH^-	5.0	5.3
H_2O_2	1.4	2.3
O_2		2.4
O_2^-		1.75
HO_2		2.3
HO_2^-		1.4
$O(^3P)$		2.0
O^-		2.0
O_3^-		2.0
		Time steps (μs)
	Time step Δt	Not calculated
Until 10^{-11} seconds	0.1	
10^{-11} to 10^{-10} seconds	1	
10^{-10} to 10^{-9} seconds	3	
10^{-9} to 10^{-8} seconds	10	
Above 10^{-8} seconds	100	
Reaction rates ($10^7\text{m}^3.\text{mol}^{-1}.\text{s}^{-1}$): only the reactions modeled in Geant4-DNA are listed, LPCHEM models 98 reactions		
Reaction rates model	PARTRAC software ⁵³	Frongillio et al., 1998 ⁸⁶ , Green et al., 1990 ⁸⁷
$H_3O^+ + OH^- \rightarrow 2H_2O$	14.3	14.3
$\cdot OH + e_{aq}^- \rightarrow OH^-$	2.95	2.95
$H\cdot + e_{aq}^- + H_2O \rightarrow OH^- + H_2$	2.65	2.65
$H_3O^+ + e_{aq}^- \rightarrow H\cdot + H_2O$	2.11	2.4
$H\cdot + \cdot OH \rightarrow H_2O$	1.44	1.44
$H_2O_2 + e_{aq}^- \rightarrow OH^- \rightarrow OH^- + \cdot OH$	1.41	1.41
$H\cdot + H\cdot \rightarrow H_2$	1.20	0.503
$2e_{aq}^- + 2H_2O \rightarrow 2OH^- + H_2$	0.50	
$\cdot OH + \cdot OH \rightarrow H_2O_2$	0.44	0.44

$H_2 + \cdot OH \rightarrow H\cdot + H_2O_2$	4.17×10^{-3}	
--	-----------------------	--

Appendix 3 - predictions of α and β values for the HSG cell line in response to hydrogen, helium, carbon, oxygen and oxygen ions for the NanOx model.

HYDROGEN					
E(MeV/n)	Alpha(Gy ⁻¹)	Beta(Gy ⁻²)	E(MeV/n)	Alpha(Gy ⁻¹)	Beta(Gy ⁻²)
0,1	3,52785	0,0586794	4,25	0,436973	0,0635334
0,125	3,58379	0,0219491	4,25	0,425273	0,0644498
0,15	3,64192	0,0977552	5	0,420139	0,0625937
0,175	3,64134	0,045627	6	0,406463	0,0625907
0,2	3,59205	0,0522845	7	0,389055	0,0639294
0,225	3,48742	0,0763334	7,5	0,390886	0,0518132
0,25	3,38711	0,0486352	8	0,377757	0,0648603
0,275	3,23556	0,0140717	9	0,380409	0,0416042
0,3	3,10038	0,0564686	10	0,375543	0,0629273
0,325	2,92819	0,0736448	13	0,36375	0,0637803
0,35	2,74536	0,0440922	14	0,355133	0,0663663
0,375	2,64766	0,068873	14,5	0,363962	0,039987
0,4	2,50822	0,0519665	15	0,36261	0,0653386
0,425	2,35826	0,0598118	16	0,36199	0,0194867
0,45	2,24049	0,0523686	17	0,358723	0,0634626
0,475	2,11282	0,0327819	18,5	0,354093	0,0679557
0,5	2,00902	0,0619912	20	0,361473	0,0655274
0,525	1,90411	0,048899	22,5	0,349285	0,0663717
0,55	1,81201	0,03943	25	0,348734	0,0648933
0,6	1,64405	0,0482093	30	0,340981	0,0686984
0,625	1,5553	0,0315918	35	0,338952	0,0647853
0,65	1,50294	0,0514883	40	0,33787	0,0675714
0,675	1,42643	0,0530718	42,5	0,336445	0,0712075
0,7	1,37338	0,0520192	45	0,344386	0,0727018
0,725	1,30831	0,0516787	50	0,344973	0,0997508
0,75	1,27779	0,0520332	60	0,341337	0,0779679
0,775	1,22202	0,0610424	70	0,330335	0,0788438
0,8	1,17571	0,0540186	72,5	0,339633	0,083321
0,825	1,14052	0,0496843	75	0,341254	0,0831872
0,85	1,10919	0,0522072	80	0,343223	0,088238
0,875	1,07663	0,0538031	85	0,347429	0,0845721
0,9	1,04062	0,0541082	87,5	0,340158	0,0884021
0,925	1,0123	0,0436477	90	0,343359	0,089741
0,95	0,987964	0,0546012	100	0,3399	0,0930667
0,975	0,954701	0,052234	110	0,344508	0,0972525
0,9875	0,956628	0,0588447	115	0,341763	0,010713
1	0,931771	0,058776	120	0,33716	0,093344
1,25	0,922846	0,0596302	125	0,348853	0,096485

1,375	0,829386	0,057546	130	0,348952	0,0958178
1,4375	0,811162	0,0635889	132,5	0,342216	0,108084
1,5	0,77844	0,0576283	135	0,339428	0,109774
1,5625	0,743542	0,0617835	140	0,337172	0,0978914
1,625	0,724542	0,0590762	160	0,345544	0,101325
1,6875	0,705097	0,0629384	165	0,341937	0,0939792
1,75	0,690471	0,0610498	170	0,351141	0,0839463
1,875	0,657967	0,0689717	175	0,346595	0,0956681
2	0,630247	0,0609551	180	0,331431	0,100256
2,125	0,59985	0,0558018	190	0,334884	0,104186
2,25	0,576881	0,0605689	200	0,338724	0,105441
2,375	0,560703	0,0620355	212,5	0,333464	0,094867
2,5	0,548153	0,0558827	225	0,33002	0,129717
2,75	0,521374	0,0553158	237,5	0,342825	0,0705913
3	0,49762	0,0574269	250	0,346535	0,109787
3,25	0,487405	0,0658839	275	0,339406	0,0998982
3,5	0,467097	0,0576851	300	0,339219	0,108748
3,875	0,459079	0,0697264			

HELIUM					
E(MeV/n)	Alpha(Gy ⁻¹)	Beta(Gy ⁻²)	E(MeV/n)	Alpha(Gy ⁻¹)	Beta(Gy ⁻²)
0,1	1,35471	0,0207273	4,625	0,913462	0,074134
0,115	1,34943	0,068132	4,8	0,894276	0,0399684
0,125	1,36143	0,0561437	5	0,845962	0,0545597
0,135	1,36702	0,0479669	5,5	0,788932	0,0548308
0,15	1,40449	0,0523761	6	0,729322	0,0589305
0,175	1,46176	0,0186978	7	0,65191	0,0584992
0,2	1,52903	0,0422706	7,5	0,618191	0,0546201
0,225	1,54966	0,0685532	8	0,594936	0,0590312
0,25	1,55482	0,0423817	9	0,552776	0,0556349
0,275	1,62378	0,0624645	9,5	0,537816	0,0270089
0,3	1,69296	0,0560868	10	0,521669	0,0646037
0,325	1,75868	0,0827488	12	0,492294	0,0631951
0,35	1,82571	0,09662	13	0,471319	0,0600745
0,375	1,89151	0,0417015	14	0,457	0,0540569
0,4	1,95804	0,0406013	14,5	0,454425	0,0647896
0,425	2,01788	0,0406869	15	0,447441	0,0639881
0,45	2,07856	0,0427398	16	0,442108	0,0585427
0,475	2,13803	0,0509513	17	0,427663	0,054866
0,5	2,19514	0,0360138	18,5	0,416323	0,0629227

0,525	2,24906	0,0560736	20	0,408267	0,0635374
0,55	2,30165	0,0719733	22,5	0,405099	0,0675533
0,56	2,31162	0,0589844	25	0,390136	0,0661453
0,575	2,35233	0,0283324	30	0,377674	0,0652145
0,58	2,3359	0,0610067	35	0,375329	0,0698207
0,6	2,24179	0,0365905	37,5	0,376945	0,068874
0,625	2,27969	0,048764	40	0,370289	0,0662104
0,65	2,32832	0,0571975	42,5	0,372768	0,0683548
0,675	2,36932	0,0582657	45	0,364365	0,0703231
0,7	2,40823	0,0107764	50	0,364275	0,0681571
0,725	2,44624	0,0803496	60	0,355372	0,0747071
0,75	2,47837	0,0209884	65	0,355306	0,0760348
0,775	2,51364	0,0847122	70	0,357653	0,0778917
0,8	2,54292	0,0519947	72,5	0,351378	0,0813151
0,825	2,57208	0,0609218	75	0,354749	0,0843505
0,85	2,59087	0,0639041	80	0,356145	0,0820511
0,875	2,61384	0,0825088	85	0,351307	0,087815
0,9	2,64201	0,0602317	87,5	0,359332	0,0900896
0,925	2,65902	0,0399342	90	0,353549	0,0857066
0,95	2,67573	0,0100122	100	0,352662	0,0869735
0,975	2,68649	0,0900614	110	0,350016	0,0897816
1	2,69945	0,0460438	120	0,352662	0,0924707
1,125	2,72759	0,0649546	130	0,349242	0,0993062
1,25	2,68623	0,0592119	132,5	0,350188	0,0977779
1,3125	2,67842	0,0437095	135	0,351315	0,101791
1,375	2,72147	0,0511202	140	0,351914	0,0996269
1,4375	2,6023	0,0481748	160	0,352059	0,103381
1,5	2,55898	0,0135152	165	0,348055	0,108882
1,5625	2,51015	0,0251847	170	0,349539	0,104125
1,625	2,51876	0,0820981	175	0,349366	0,097993
1,6875	2,40387	0,0796317	180	0,350419	0,104505
1,75	2,349	0,0442119	185	0,346769	0,107044
1,8	2,30672	0,0467401	190	0,342395	0,0732676
1,875	2,28272	0,0412346	195	0,349724	0,100912
1,9	2,23023	0,0968624	200	0,346889	0,116881
2	2,12334	0,0421089	212,5	0,348807	0,116918
2,125	2,05126	0,0369635	225	0,347231	0,0997025
2,25	1,91357	0,0728045	237,5	0,353986	0,110258
2,375	1,82345	0,0653356	250	0,34613	0,112309
2,5	1,73184	0,0416488	275	0,34762	0,107218
2,75	1,562	0,0705918	300	0,347978	0,101295
3	1,43353	0,0454924	400	0,344634	0,102051
3,25	1,31698	0,0449153	500	0,34295	0,109641

3,5	1,21521	0,0409911	600	0,345637	0,10687
3,75	1,13259	0,0515363	700	0,342868	0,115623
3,875	1,09196	0,0562185	800	0,341284	0,0974119
4,25	0,99491	0,0515848	900	0,3453	0,103232
			1000	0,340597	0,103002
CARBON					
E(MeV/n)	Alpha(Gy⁻¹)	Beta(Gy⁻²)	E(MeV/n)	Alpha(Gy⁻¹)	Beta(Gy⁻²)
0,1	0,554922	0,0174572	4,625	1,37202	0,0533761
0,15	0,507327	0,0501012	5	1,41833	0,0934593
0,175	0,496762	0,0185161	6	1,53289	0,0576861
0,2	0,498712	0,0128507	7	1,6441	0,0352824
0,225	0,507064	0,0398217	7,5	1,6905	0,0484951
0,25	0,517163	0,0321235	8	1,73733	0,0206558
0,275	0,524741	0,028797	9	1,81111	0,0270153
0,3	0,527277	0,024745	10	1,86519	0,0145637
0,35	0,562364	0,0325134	13	1,9013	0,0735242
0,375	0,581553	0,04897	14	1,88	0,0524471
0,4	0,600128	0,022651	14,5	1,86598	0,0753743
0,45	0,63878	0,0493113	15	1,84803	0,0247954
0,475	0,658849	0,0709208	16	1,80727	0,0386726
0,5	0,678314	0,0311766	17	1,75589	0,127889
0,525	0,651331	0,0378454	18,5	1,6866	0,0289437
0,53	0,654257	0,0387549	20	1,59615	0,0269112
0,55	0,668569	0,0323383	22,5	1,46482	0,02547
0,575	0,685794	0,0958369	25	1,3439	0,0377534
0,6	0,698747	0,0925473	27	1,25757	0,0699588
0,625	0,71445	0,0123321	30	1,14384	0,063285
0,65	0,729095	0,018834	32	1,08349	0,0503975
0,675	0,743807	0,033274	35	0,995382	0,0563748
0,7	0,757473	0,032298	37,5	0,937827	0,0468086
0,725	0,771899	0,029902	40	0,883756	0,0536156
0,75	0,7715	0,0258204	42,5	0,843352	0,06574
0,775	0,780193	0,0222819	45	0,806053	0,060595
0,8	0,792595	0,0115817	50	0,742661	0,0559711
0,825	0,804823	0,0254497	60	0,656602	0,0738968
0,85	0,818199	0,0192019	65	0,622154	0,0275371
0,875	0,828681	0,019282	70	0,587718	0,0599057
0,9	0,838734	0,0572171	72,5	0,581034	0,0643803
0,925	0,847032	0,0501417	75	0,579367	0,0263508
0,95	0,857266	0,0462406	80	0,570936	0,0643563
0,975	0,868805	0,0614917	85	0,557118	0,0420902
0,9875	0,875099	0,0422347	87,5	0,55305	0,064244
1	0,875006	0,08374	90	0,549996	0,060972

1,125	0,918784	0,0602353	100	0,529454	0,044553
1,25	0,920182	0,0925326	110	0,514361	0,0641633
1,3125	0,937178	0,0795297	120	0,500774	0,0656887
1,375	0,949605	0,0347631	130	0,490693	0,0572786
1,4375	0,964492	0,0309748	132,5	0,486477	0,0687478
1,5	0,981289	0,0190316	135	0,484113	0,0336333
1,5625	0,993225	0,0224706	140	0,479973	0,0652569
1,625	1,00636	0,0147146	150	0,471674	0,0623355
1,6875	1,0206	0,039587	160	0,464491	0,0678329
1,75	1,0308	0,0626443	165	0,461521	0,0694929
1,875	1,03536	0,0595288	175	0,455044	0,0702457
2	1,03757	0,140597	180	0,454354	0,0690091
2,125	1,05661	0,0580031	185	0,450706	0,0807745
2,25	1,07951	0,047584	190	0,446442	0,0477704
2,5	1,11612	0,0134392	195	0,445182	0,0765487
2,75	1,15096	0,0417291	200	0,443174	0,075495
3	1,18637	0,0549517	212,5	0,436772	0,0750927
3,25	1,2192	0,0958209	225	0,432475	0,0477424
3,5	1,25362	0,034796	237,5	0,429575	0,0770921
3,875	1,27999	0,0602744	250	0,428672	0,0863672
4,25	1,3268	0,0283756	275	0,419821	0,0642036
			300	0,414074	0,0833777

OXYGEN					
E(MeV/n)	Alpha(Gy ⁻¹)	Beta(Gy ⁻²)	E(MeV/n)	Alpha(Gy ⁻¹)	Beta(Gy ⁻²)
0,1	0,413736	0,0142512	6	1,09991	0,0179879
0,2	0,389411	0,0289218	7	1,17086	0,0553748
0,25	0,390787	0,0132718	8	1,23791	0,03446
0,3	0,408917	0,0151436	10	1,36301	0,0780824
0,35	0,432501	0,0102363	13	1,53735	0,0380272
0,4	0,457564	0,0140088	15	1,63487	0,0208637
0,45	0,487057	0,0416276	20	1,77359	0,0114724
0,5	0,512859	0,029806	25	1,78011	0,0369413
0,55	0,497537	0,0513708	30	1,69153	0,0243579
0,6	0,519719	0,023812	40	1,43087	0,0687465
0,7	0,561975	0,0147102	50	1,20946	0,0680245
0,75	0,585803	0,0239479	60	1,044	0,0593522
0,8	0,608447	0,00467075	70	0,93624	0,0608797
0,85	0,618215	0,0265444	80	0,854476	0,0671706
0,9	0,636862	0,0320603	90	0,803408	0,0549333
0,95	0,65226	0,0291653	100	0,758682	0,0548792
1	0,670432	0,0378584	110	0,720772	0,0656161

1,25	0,710918	0,0462263	120	0,689713	0,0541748
1,5	0,7642	0,0888616	130	0,659153	0,0666365
1,75	0,794974	0,0780676	140	0,641074	0,0580988
2,25	0,836185	0,0696362	150	0,621408	0,0605031
2,5	0,864835	0,0403956	160	0,602909	0,0606604
2,75	0,880924	0,0148689	180	0,576667	0,0703917
3	0,894613	0,00887251	200	0,556955	0,0680523
3,5	0,941321	0,0402146	250	0,517284	0,0828523
5	1,04036	0,0320689	300	0,493476	0,0861731
			350	0,47441	0,0914356

Appendix 4 - Predictions of α and β values for the HSG cell line in response to hydrogen, helium, carbon and oxygen ions for the mMKM model.

HYDROGEN					
E(MeV/n)	Alpha(Gy ⁻¹)	Beta(Gy ⁻²)	E(MeV/n)	Alpha(Gy ⁻¹)	Beta(Gy ⁻²)
0,1	1,76015784	0,0615	4,25	0,41269852	0,0615
0,125	1,90316891	0,0615	4,625	0,39792158	0,0615
0,15	1,85167715	0,0615	5	0,37526441	0,0615
0,175	1,79620928	0,0615	6	0,3465522	0,0615
0,2	1,72047753	0,0615	7	0,32547431	0,0615
0,225	1,686197	0,0615	7,5	0,31677023	0,0615
0,25	1,63496363	0,0615	8	0,31103573	0,0615
0,275	1,55673265	0,0615	9	0,30400634	0,0615
0,3	1,50465213	0,0615	10	0,29759482	0,0615
0,325	1,45851417	0,0615	13	0,27563387	0,0615
0,35	1,40890868	0,0615	14	0,25797535	0,0615
0,375	1,37158627	0,0615	14,5	0,26592402	0,0615
0,4	1,34708463	0,0615	15	0,2607293	0,0615
0,425	1,28856167	0,0615	16	0,25896092	0,0615
0,45	1,27640762	0,0615	17	0,2597976	0,0615
0,475	1,22548674	0,0615	18,5	0,24932084	0,0615
0,5	1,20290671	0,0615	20	0,23703403	0,0615
0,525	1,16652015	0,0615	22,5	0,23584525	0,0615
0,55	1,14828801	0,0615	25	0,24512923	0,0615
0,6	1,10455273	0,0615	30	0,23253512	0,0615
0,625	1,0710152	0,0615	35	0,22953456	0,0615
0,65	1,0442441	0,0615	40	0,22510101	0,0615
0,675	1,02892927	0,0615	42,5	0,21525845	0,0615
0,7	1,01230563	0,0615	45	0,21364756	0,0615

0,725	1,00993717	0,0615	50	0,20728247	0,0615
0,75	0,99169901	0,0615	60	0,21160957	0,0615
0,775	0,9504684	0,0615	70	0,21542632	0,0615
0,8	0,93575076	0,0615	72,5	0,21168926	0,0615
0,825	0,93725789	0,0615	75	0,21454225	0,0615
0,85	0,91940491	0,0615	80	0,20557802	0,0615
0,875	0,90710971	0,0615	85	0,20915264	0,0615
0,9	0,88489348	0,0615	87,5	0,21005575	0,0615
0,925	0,85892201	0,0615	90	0,19931656	0,0615
0,95	0,84808765	0,0615	100	0,20679814	0,0615
0,975	0,82971714	0,0615	110	0,20829383	0,0615
0,988	0,85598572	0,0615	115	0,20360297	0,0615
1	0,9810095	0,0615	120	0,20592231	0,0615
1,375	0,81205418	0,0615	125	0,20449326	0,0615
1,438	0,81442601	0,0615	130	0,20444967	0,0615
1,5	0,75449721	0,0615	132,5	0,20764789	0,0615
1,562	0,75771038	0,0615	135	0,20557136	0,0615
1,625	0,73026718	0,0615	140	0,20865446	0,0615
1,688	0,69581744	0,0615	160	0,2021342	0,0615
1,75	0,69183551	0,0615	165	0,19910029	0,0615
1,875	0,66042851	0,0615	170	0,20163043	0,0615
2	0,63047876	0,0615	175	0,20342183	0,0615
2,125	0,61644836	0,0615	180	0,19935637	0,0615
2,25	0,57953347	0,0615	190	0,19497002	0,0615
2,375	0,58510633	0,0615	200	0,19964379	0,0615
2,5	0,54312614	0,0615	212,5	0,19807176	0,0615
2,75	0,52668644	0,0615	225	0,1980282	0,0615
3	0,5225944	0,0615	237,5	0,19863153	0,0615
3,25	0,47132339	0,0615	250	0,20256654	0,0615
3,5	0,45446625	0,0615	275	0,19835696	0,0615
3,875	0,42329655	0,0615	300	0,19917811	0,0615

HELIUM					
E(MeV/n)	Alpha(Gy ⁻¹)	Beta(Gy ⁻²)	E(MeV/n)	Alpha(Gy ⁻¹)	Beta(Gy ⁻²)
0,1	1,39368254	0,0615	4,625	0,96230827	0,0615
0,115	1,36937733	0,0615	4,8	0,94225563	0,0615
0,125	1,36745112	0,0615	5	0,88911444	0,0615
0,135	1,36213099	0,0615	5,5	0,83434223	0,0615
0,15	1,38439522	0,0615	6	0,82117505	0,0615
0,175	1,42048374	0,0615	7	0,72771876	0,0615
0,2	1,47155149	0,0615	7,5	0,67973888	0,0615

0,225	1,51566938	0,0615	8	0,65120626	0,0615
0,25	1,45535665	0,0615	9	0,60447989	0,0615
0,275	1,51257501	0,0615	9,5	0,59490674	0,0615
0,3	1,56460825	0,0615	12	0,517091	0,0615
0,325	1,60506986	0,0615	13	0,49108525	0,0615
0,35	1,66200317	0,0615	14	0,48217333	0,0615
0,375	1,70567852	0,0615	14,5	0,45355589	0,0615
0,4	1,75101482	0,0615	15	0,4603493	0,0615
0,425	1,78517233	0,0615	16	0,43637705	0,0615
0,45	1,82903515	0,0615	17	0,42769368	0,0615
0,475	1,86894901	0,0615	18,5	0,40850354	0,0615
0,5	1,89593537	0,0615	20	0,38354342	0,0615
0,525	1,91584789	0,0615	22,5	0,39052976	0,0615
0,55	1,9416978	0,0615	25	0,34625961	0,0615
0,56	1,95247026	0,0615	30	0,34060395	0,0615
0,575	1,96519554	0,0615	35	0,31125112	0,0615
0,58	1,97270031	0,0615	37,5	0,31120437	0,0615
0,6	1,90338008	0,0615	40	0,30110398	0,0615
0,625	1,93381438	0,0615	42,5	0,29806927	0,0615
0,65	1,94856927	0,0615	45	0,28731212	0,0615
0,675	1,96447665	0,0615	50	0,28434712	0,0615
0,7	1,99257377	0,0615	60	0,27235922	0,0615
0,725	2,004059	0,0615	65	0,27475892	0,0615
0,75	2,0092631	0,0615	70	0,25924287	0,0615
0,775	2,02168365	0,0615	72,5	0,25075129	0,0615
0,8	2,03352762	0,0615	75	0,25857623	0,0615
0,825	2,03364266	0,0615	80	0,25831101	0,0615
0,85	2,04461617	0,0615	85	0,2523552	0,0615
0,875	2,04794839	0,0615	87,5	0,23523516	0,0615
0,9	2,04944316	0,0615	90	0,24796673	0,0615
0,925	2,05383802	0,0615	100	0,24530574	0,0615
0,95	2,05227089	0,0615	110	0,23886659	0,0615
0,975	2,05360573	0,0615	120	0,23670685	0,0615
1	2,04932288	0,0615	130	0,23381593	0,0615
1,125	2,03431604	0,0615	132,5	0,23330326	0,0615
1,25	2,00341284	0,0615	135	0,22587891	0,0615
1,312	1,97632077	0,0615	140	0,22961596	0,0615
1,375	1,94453497	0,0615	160	0,22902871	0,0615
1,438	1,93463072	0,0615	165	0,23033065	0,0615
1,5	1,91692309	0,0615	170	0,22880151	0,0615
1,562	1,88227096	0,0615	175	0,22281551	0,0615
1,625	1,82822213	0,0615	180	0,22562653	0,0615
1,688	1,81990989	0,0615	185	0,2232301	0,0615
1,75	1,79166858	0,0615	190	0,21677319	0,0615
1,8	1,76094575	0,0615	195	0,22151075	0,0615

1,875	1,75294194	0,0615	200	0,22526867	0,0615
1,9	1,69542062	0,0615	212,5	0,2183769	0,0615
2	1,67302649	0,0615	225	0,22302907	0,0615
2,125	1,60603852	0,0615	237,5	0,2219778	0,0615
2,25	1,57159	0,0615	250	0,21148815	0,0615
2,375	1,5227767	0,0615	275	0,22256361	0,0615
2,5	1,49062651	0,0615	300	0,2120016	0,0615
2,75	1,37790739	0,0615	400	0,21014623	0,0615
3	1,29101377	0,0615	500	0,21069392	0,0615
3,25	1,23449549	0,0615	600	0,20814372	0,0615
3,5	1,16275574	0,0615	700	0,20445455	0,0615
3,75	1,11019208	0,0615	800	0,20849856	0,0615
3,875	1,07576636	0,0615	900	0,20332779	0,0615
4,25	1,00479394	0,0615	1000	0,20570698	0,0615

CARBON					
E(MeV/n)	Alpha(Gy⁻¹)	Beta(Gy⁻²)	E(MeV/n)	Alpha(Gy⁻¹)	Beta(Gy⁻²)
0,15	0,50339808	0,0615	5	1,55653422	0,0615
0,175	0,48454942	0,0615	6	1,75053464	0,0615
0,2	0,47487403	0,0615	7	1,90877459	0,0615
0,225	0,47187832	0,0615	7,5	1,95249266	0,0615
0,25	0,47407494	0,0615	8	1,99679369	0,0615
0,275	0,45992261	0,0615	9	2,03862693	0,0615
0,3	0,46235642	0,0615	10	2,05601166	0,0615
0,35	0,47192496	0,0615	13	1,97305347	0,0615
0,375	0,47813642	0,0615	14	1,94262411	0,0615
0,4	0,48505401	0,0615	14,5	1,90610348	0,0615
0,45	0,49879305	0,0615	15	1,89554533	0,0615
0,475	0,50483791	0,0615	16	1,85562239	0,0615
0,5	0,51322218	0,0615	17	1,77657221	0,0615
0,525	0,49146793	0,0615	18,5	1,73405714	0,0615
0,53	0,49445111	0,0615	20	1,66676365	0,0615
0,55	0,49573957	0,0615	22,5	1,54318579	0,0615
0,575	0,50445866	0,0615	25	1,46078637	0,0615
0,6	0,51250679	0,0615	27	1,40127589	0,0615
0,625	0,51767073	0,0615	30	1,32642616	0,0615
0,65	0,5256997	0,0615	32	1,27113082	0,0615
0,675	0,53160257	0,0615	35	1,1848265	0,0615
0,7	0,53863325	0,0615	37,5	1,14827529	0,0615
0,725	0,54617082	0,0615	40	1,09587716	0,0615
0,75	0,54341952	0,0615	42,5	1,03951646	0,0615

0,775	0,54739658	0,0615	45	1,01144134	0,0615
0,8	0,55725082	0,0615	50	0,95704141	0,0615
0,825	0,56183319	0,0615	60	0,84947386	0,0615
0,85	0,56804995	0,0615	65	0,79309164	0,0615
0,875	0,57653972	0,0615	70	0,76869037	0,0615
0,9	0,58180655	0,0615	72,5	0,74023123	0,0615
0,925	0,58825069	0,0615	75	0,7394691	0,0615
0,95	0,59650123	0,0615	80	0,7154438	0,0615
0,975	0,60167595	0,0615	85	0,67492106	0,0615
0,988	0,60524041	0,0615	87,5	0,6745586	0,0615
1	0,6126607	0,0615	90	0,66200055	0,0615
1,125	0,64546276	0,0615	100	0,62537666	0,0615
1,25	0,64506518	0,0615	110	0,51090028	0,0615
1,312	0,66343661	0,0615	120	0,56221711	0,0615
1,375	0,6801614	0,0615	130	0,54273609	0,0615
1,438	0,69527217	0,0615	132,5	0,53486851	0,0615
1,5	0,71570436	0,0615	135	0,53097809	0,0615
1,562	0,7343878	0,0615	140	0,52415145	0,0615
1,625	0,74580065	0,0615	150	0,50843461	0,0615
1,688	0,76131236	0,0615	160	0,49663483	0,0615
1,75	0,78269442	0,0615	165	0,48895603	0,0615
1,875	0,80061062	0,0615	175	0,47546677	0,0615
2	0,83450504	0,0615	180	0,47380211	0,0615
2,125	0,8360636	0,0615	185	0,46439192	0,0615
2,25	0,87478362	0,0615	190	0,4597621	0,0615
2,5	0,93848816	0,0615	195	0,45408332	0,0615
2,75	1,0071553	0,0615	200	0,45227578	0,0615
3	1,08229543	0,0615	212,5	0,44305794	0,0615
3,25	1,15264005	0,0615	225	0,43045946	0,0615
3,5	1,21718809	0,0615	237,5	0,42182226	0,0615
3,875	1,28441299	0,0615	250	0,40828412	0,0615
4,25	1,36850829	0,0615	275	0,40622332	0,0615
4,625	1,48784096	0,0615	300	0,39136842	0,0615

OXYGEN					
E(MeV/n)	Alpha(Gy ⁻¹)	Beta(Gy ⁻²)	E(MeV/n)	Alpha(Gy ⁻¹)	Beta(Gy ⁻²)
0,1	0,57683641	0,0615	40	1,61813083	0,0615
0,2	0,39461372	0,0615	50	1,41288483	0,0615
0,25	0,38549096	0,0615	60	1,2769869	0,0615
0,3	0,38420183	0,0615	70	1,1465992	0,0615
0,35	0,38874355	0,0615	80	1,0769192	0,0615

0,4	0,39431564	0,0615	90	0,99183267	0,0615
0,45	0,40153681	0,0615	100	0,93563608	0,0615
0,5	0,41036818	0,0615	110	0,90126161	0,0615
0,55	0,39382537	0,0615	120	0,83897904	0,0615
0,6	0,40244051	0,0615	130	0,80282571	0,0615
0,7	0,41948742	0,0615	140	0,76208427	0,0615
0,75	0,42708322	0,0615	150	0,73875254	0,0615
0,8	0,43581879	0,0615	160	0,71921426	0,0615
0,85	0,44460969	0,0615	180	0,67685998	0,0615
0,9	0,45262565	0,0615	200	0,63836255	0,0615
0,95	0,46079407	0,0615	250	0,58416082	0,0615
1	0,47074632	0,0615	300	0,53276501	0,0615
1,25	0,5008777	0,0615	350	0,50905649	0,0615
1,5	0,53970912	0,0615	400	0,48671036	0,0615
1,75	0,57550625	0,0615	0,75	0,36571457	0,0615
2,25	0,63054616	0,0615	1,5	0,43244717	0,0615
2,5	0,662315	0,0615	1,7	0,45753939	0,0615
2,75	0,69868629	0,0615	2,8	0,55556211	0,0615
3	0,74023048	0,0615	5	0,73531098	0,0615
3,5	0,82502643	0,0615	7	0,91601311	0,0615
5	1,02532216	0,0615	8	1,01432123	0,0615
6	1,17652843	0,0615	10	1,18638951	0,0615
7	1,2918773	0,0615	13	1,44146401	0,0615
8	1,42043736	0,0615	15	1,59418043	0,0615
10	1,66855287	0,0615	80	1,45976032	0,0615
13	1,92005086	0,0615	85	1,40898716	0,0615
15	2,00085691	0,0615	90	1,35830835	0,0615
20	2,04557772	0,0615	95	1,32300946	0,0615
25	1,96074999	0,0615	100	1,29277276	0,0615
30	1,85318684	0,0615			